

1700
112
193134
P-128

IMPROVEMENTS TO A METHOD FOR THE
GEOMETRICALLY NONLINEAR ANALYSIS OF
COMPRESSIVELY LOADED STIFFENED COMPOSITE PANELS

Final Technical Report
February 1991 - December 1993

F. Stoll

Department of Engineering Science and Mechanics
Virginia Polytechnic Institute and State University
Blacksburg, Virginia 24061-0219

Prepared for
NASA Langley Research Center
Hampton, Virginia 23681-0001

Prepared under
NASA Grant No. NAG-1-1215

(NASA-CR-194715) IMPROVEMENTS TO A
METHOD FOR THE GEOMETRICALLY
NONLINEAR ANALYSIS OF COMPRESSIVELY
LOADED STIFFENED COMPOSITE PANELS
Final Technical Report, Feb. 1991 -
Dec. 1993 (Virginia Polytechnic
Inst. and State Univ.) 128 p

N94-21814

Unclass

G3/39 0198154

SUMMARY

The NLPAN computer code uses a finite-strip approach to the analysis of thin-walled prismatic composite structures such as stiffened panels. The code can model in-plane axial loading, transverse pressure loading, and constant through-the-thickness thermal loading, and can account for shape imperfections. The NLPAN code represents an attempt to extend the buckling analysis of the VIPASA computer code into the geometrically nonlinear regime. Buckling mode shapes generated using VIPASA are used in NLPAN as global functions for representing displacements in the nonlinear regime. While the NLPAN analysis is approximate in nature, it is computationally economical in comparison with finite-element analysis, and is thus suitable for use in preliminary design and design optimization. This document provides a comprehensive description of the theoretical approach of NLPAN, highlighting the capabilities developed under NASA Grant NAG-1-1215. A discussion of some operational considerations for the NLPAN code is included. NLPAN is applied to several test problems in order to demonstrate new program capabilities, and to assess the accuracy of the code in modelling various types of loading and response. User instructions for the NLPAN computer program are provided, including a detailed description of the input requirements, and example input files for two stiffened-panel configurations.

CONTENTS

	Page
Summary	i
Table of Contents	ii
List of Tables	iv
List of Figures	v
List of Symbols	vi
1. Introduction	1
2. Theoretical Approach of NLPAN	3
2.1 Nonlinear Plate Theory	3
2.2 Characteristics of Multiple-Plate Configurations	5
2.3 Loading and Boundary Conditions	6
2.4 Expansion of the Displacement Functions	7
2.5 Prebuckling Solution	8
2.6 Buckling Eigensolutions	8
2.7 Second-Order Displacement Fields	11
2.8 Stationary Total Potential Energy Formulation	13
2.9 Solution of the Nonlinear Algebraic Equations	18
3. Extensions to the Method of Analysis	21
3.1 Dynamic Snap Analysis	21
3.2 Thermal Loading	24
3.3 Rotationally Elastic End Support	25
3.4 Constraint of the End Displacements	26
3.5 Solution Procedure with Thermal Loading and Displacement Constraints	30
4. Improvements in the Computation of the Second-Order Displacement Fields	36
4.1 Problems with the Second-Order Displacement Fields	36
4.2 Implications of Imposing Orthogonality Between $\{u_i\}$ and $\{u_j\}$	37
4.3 Computation of $\{u_i\}$ with Orthogonality Imposed	39
5. Miscellaneous Considerations	43
5.1 Geometric Representation of Stiffened Panels	43
5.2 Convergence Considerations	43
5.3 Computer Execution Times and Memory Requirements	45

6. Results	46
6.1 I-Stiffened Graphite/Epoxy Panel Under Axial Compression	46
6.2 Imperfection Sensitivity in a Thin-Blade-Stiffened Isotropic Panel	47
6.3 Stiffened Composite Panel Under Pressure Loading	49
6.4 Thermally Loaded Unstiffened Composite Panel	50
6.5 Panels and Columns with Constrained End-Rotation	51
7. Concluding Remarks and Recommendations	52
7.1 Concluding Remarks	52
7.2 Recommendations for Future Work	53
Appendix A: Formulae for the Linear, Unbuckled Solutions	54
Appendix B: Orthogonality of the Displacement Shape Functions	59
Appendix C: An Expansion of $\delta\pi_3$	62
Appendix D: Description of the Nonlinear Solution Strategies	64
Appendix E: User Instructions for the NLPAN Computer Program	70
References	103
Tables	105
Figures	109

LIST OF TABLES

1. Options for Control of the In-Plane Loading	105
2. Input Parameters Corresponding to Several Different Cases for In-Plane Loading.	106
3. Options Available for Specifying Conditions Along the Boundary Node-Lines.	107
4. Simplifications to the General Displacement Form for Special Cases.	107
5. Suggested Mode Sets for Analyzing Various Types of Postbuckling Response.	108

LIST OF FIGURES

1. Generalized load types modelled by NLPAN.	109
2. Labeling conventions for a representative plate strip.	110
3. Labeling conventions for a typical linked-plate analysis model.	111
4. Relative orientation of the side edge of a plate strip and its associated node line.	112
5. I-stiffened graphite/epoxy panel configuration.	113
6. Analytical and experimental results for an I-stiffened panel.	114
7. Longitudinal surface strains on an I-stiffened panel.	115
8. Results for an imperfection-sensitive thin-blade-stiffened panel loaded in compression.	116
9. Pressure-loaded panel configuration.	117
10. Skin displacements with one atmosphere pressure (14.7 psi).	118
11. Laminated composite plate subjected to thermal loading.	119

LIST OF SYMBOLS

A	Planform area of a plate strip
A_{ij}	Coefficient appearing in modified second-order displacement fields
b	Width of a plate strip (in the local y -direction)
B	Reference width of a panel or other structure (global y -direction)
B_i	Coefficient appearing in modified buckling mode shapes
cl	Indicates "clamped" boundary condition for a plate edge
e	Index number of the side edge of a plate strip: $y = 0$ for $e = 1$; $y = b$ for $e = 2$
e_x, e_y	Measures of the eccentricity of a node line relative to an associated plate-strip edge
$\{f_e\}$	Generalized force resultants at side edge no. e of a plate strip, defined w.r.t. local coordinate axes: $[f_{x_e} \ f_{y_e} \ f_{x_e} \ m_{x_e}]^T$
$\{f^a\}$	Same as $\{f_e\}$ except referred to the associated node line and global coordinate axes: $[f_x^a \ f_y^a \ f_z^a \ m^a]^T$
$\{F^a\}$	Generalized force resultants along a node line: $[F_x^a \ F_y^a \ F_z^a \ M^a]^T$
h	Plate thickness
L	Length of a structure in the longitudinal (x) direction -or- Operator acting on $\{N\}$, $\{M\}$
m_i	Number of longitudinal halfwaves for buckling mode no. i
\hat{m}	Number of longitudinal halfwaves of contribution no. α ($\alpha = 1, 2$) to second-order displacement field no. ij : $\hat{m} = m_i \pm m_j$
M	Number of buckling modes used in an analysis
$\{M\}$	Bending moment resultants in a plate strip: $[M_x \ M_y \ M_{xy}]^T$
n	Index number of a node line
n_1, n_2	Index numbers of the two boundary node-lines of a structure
\hat{n}	The in-plane unit vector normal to the edge of a plate: $\hat{n} = n_x \hat{i} + n_y \hat{j}$
N	Total number of node lines in a structure -or- Operator acting on $\{N\}$, $\{u\}$
$\{N\}$	In-plane stress resultants in a plate strip: $[N_x \ N_y \ N_{xy}]^T$
N_{xG}	Axial load on a panel or other structure (the mean tensile load in the x -direction per unit width, based on B)
N_{yG}	Edge-normal transverse load on a panel (the mean tensile load in the global y -direction per unit length, based on L)
p	Index number of a plate strip
P	Total number of plate strips in a structure
q_i	Modal amplitude for the i^{th} buckling mode
q_i^o	Modal imperfection amplitude for an imperfection in the shape of the i^{th} buckling mode
q_i^f	Modal amplitude for specifying forced end rotations
Q	Transverse pressure loading on a plate strip, $+z$ direction

$\{u\}$	Displacement components for the mid-surface of a plate strip w.r.t. the local coordinate axes: $[u(x, y) \ v(x, y) \ w(x, y)]^T$
$\{u^o\}$	Values for $\{u\}$ describing geometric shape imperfections
$\{u_e\}$	Generalized displacements along side-edge no. e of a plate strip, defined w.r.t. local coordinate axes: $[u_e \ v_e \ w_e \ \psi_e]^T$
$\{u_A\}$	Displacements $[0 \ v_A \ 0]^T$ associated with unit load N_{yGA} , $\epsilon_{xA} = 0$:
$\{u_B\}$	Displacements $[u_B \ v_B \ 0]^T$ associated with unit load N_{yGB} , $N_{xGB} = 0$:
$\{u_i\}$	Buckling eigenfunctions (or buckling "modes"): $[u_i \ v_i \ w_i]^T$
$\{u_{ij}\}$	Second-order displacement fields: $[u_{ij} \ v_{ij} \ w_{ij}]^T$
$\{u_L\}$	Displacements $[u_L \ v_L \ 0]^T$ associated with unit loads N_{xGL} and N_{yGL} :
$\{u_T\}$	Displacements $[u^T \ v^T \ 0]^T$ associated with unit thermal loads
$\{U^n\}$	Generalized displacements along a node line: $[U^n \ V^n \ W^n \ \Psi^n]^T$
y_e	The value of y (local) at edge no. e of a plate strip: $y_e = 0$ for $e = 1$; $y_e = b$ for $e = 2$
α	Index number for the two contributions to $\{u_{ij}\}$: $\alpha = 1, 2$
β	Pressure load parameter
$\{\epsilon\}$	In-plane strain components: $[\epsilon_x \ \epsilon_y \ \gamma_{xy}]^T$
$\{\epsilon^c\}$	Nominal in-plane strain components at the mid-surface of a plate
$\{\epsilon^m\}$	Mechanical (load-related) in-plane strain components at the mid-surface of a plate
γ	Thermal load parameter
Γ	Lagrange multiplier
$\{\kappa^c\}$	Nominal curvature components of the mid-surface of a plate: $[\kappa_x^c \ \kappa_y^c \ \kappa_{xy}^c]^T$
$\{\kappa^m\}$	Mechanical (load-related) curvature components of the mid-surface of a plate strip
λ	Generalized in-plane load parameter
λ_b	Reference value of λ used when computing $\{u_{ij}\}$
Λ	Generalized load parameter for combined loading
μ	Offset angle between local y - z coordinate axes and global y - z coordinate axes
ψ_e	Rotation angle of edge no. e ($e = 1, 2$) of a plate strip ($\partial w / \partial y$ at the edge)
Ψ^n	Rotation angle of node-line no. n
$\{\xi_i\}$	The y -dependent portion of buckling eigenfunction no. i : $[\xi_i(y) \ \eta_i(y) \ \phi_i(y)]^T$
$\{\xi_{\alpha ij}\}$	The y -dependent portion of contribution no. α ($\alpha=1, 2$) of the second-order displacement field no. ij : $[\xi_{\alpha ij}(y) \ \eta_{\alpha ij}(y) \ \phi_{\alpha ij}(y)]^T$

Subscripts and superscripts

$f(x) _{x=0, L}$	$f(0) + f(L)$
$f(x) _{x=0}^L$	$f(L) - f(0)$
\dot{f}	Derivative of function f with respect to time
$(-)_e$	Expression associated with side-edge no. e of a plate strip
$(-)_L$	Expression corresponding to the linear response of a perfect structure to unit global loads \hat{N}_{xG} and \hat{N}_{yG}

$(-)_A$	Expression associated with the unit displacement solution $\{\mu_A\}$
$(-)_B$	Expression associated with the unit displacement solution $\{\mu_B\}$
$(-)_n$	Expression corresponding to node line no. n
$(-)_p$	Expression corresponding to plate strip no. p
$(-)_T$	Expression corresponding to the unit thermal response $\{\mu_T\}$
$[-]^T$	Transpose of a matrix
$(-)_\alpha$	Expression corresponding to contribution no. α ($\alpha = 1, 2$) of a second-order displacement field

1. INTRODUCTION

Geometrically nonlinear analysis is generally required to accurately predict the ultimate strength of compressively loaded thin-walled structures such as stiffened panels. The nonlinear analysis of such configurations using finite elements is expensive in terms of computer resources. This has spurred the development of finite strip methods [1-11] which are less general than the finite element method, but which are computationally economical, and thus are suitable for use in iterative applications such as preliminary design and design optimization. These methods vary widely with regard to the specific plate or shell theory used, the geometric modelling flexibility, whether or not imperfections are accounted for, the types of shape functions used, the targeted modes of response, the mathematical formulation used, and the solution strategies employed. No attempt is made here to review or compare all of these methods. A discussion of some of these methods can be found in [7].

This document concerns one such method which is implemented in the computer code NLPAN. In philosophy, NLPAN represents an attempt to extend the buckling analysis of the VIPASA code [12] (the analysis code within the PASCO stiffened-panel design code [13]) into the postbuckling and geometrically nonlinear regime. NLPAN uses buckling mode shapes obtained from VIPASA as global shape functions for representing displacements in a geometrically nonlinear analysis. NLPAN uses a stationary total potential energy formulation to obtain a set of nonlinear algebraic equations governing equilibrium. These equations have load-independent coefficients and a relatively small number of variable modal amplitudes, allowing rapid exploration of the nonlinear regime. For simple rectangular plate configurations, NLPAN degenerates to an exact series solution method for the von Karman nonlinear plate equations.

NLPAN is limited to the treatment of prismatic structures which can be represented as assemblages of rigidly linked plate strips. NLPAN can model the static elastic response of a structure to in-plane normal loads, transverse pressure loads, and thermal loading which is uniform through the thickness of each plate strip. Figure 1 depicts a typical configuration with the applied loadings. Shape imperfections can be simulated. The side edges and longitudinal ends may have any of a variety of different support conditions. The individual plate strips may have orthotropic material properties, suitable for characterizing the elastic properties of some classes of laminated composite plates.

The first comprehensive description of NLPAN was given in [7]. Under NASA Grant NAG-1-1215, a number of improvements and additions to NLPAN have been developed relative to the method as described in [7]. The major developments are listed here, along with the sections in this document (if applicable) in which each is discussed:

1. Transverse pressure loading capability was added to the NLPAN code.
2. Thermal loading capability was added to the NLPAN code. Temperature is assumed to be constant through the thickness of each plate strip, but may be different from plate strip to plate strip (Sect. 3.2, 3.5).
3. Advanced nonlinear solution strategies were incorporated into the NLPAN code which enable asynchronous application of the various load types, navigation of limit points, and navigation of simple or compound solution branch points (Appendix D).
4. Methods for modelling a variety of support conditions at the longitudinal ends of a structure have been added to NLPAN. The new types of support include rotationally elastic support, eccentric load application, and clamped end support (Sect. 3.3-3.5).
5. The NLPAN code was modified to decrease both the computer memory usage and the execution times for a given problem. Memory usage was decreased through the implementation of a data storage method which sets the dimensions of large data arrays based on the actual needs of a given problem (Sect 5.2). Execution times were reduced by rewriting key subroutines to run more efficiently.

6. An automated procedure was developed which unites NLPAN and PASCO (in which VIPASA is embedded), so that buckling-mode generation requests are passed automatically from NLPAN to PASCO, and material property data and buckling mode information are passed automatically from PASCO to NLPAN. (Assistance in performing this task is noted in the last paragraph of this section.)
7. Troublesome aspects of the second-order displacement fields have been studied in detail, and suggestions for improving the method of computing the fields have been provided. Modifications were made to the method used by NLPAN in computing these fields (Sect. 4).
8. The theory was developed for performing a transient dynamic analysis in situations where unstable critical points are encountered. The analysis has not been fully implemented in the NLPAN code, in part due to time constraints, and in part because the analytical capability is deemed to have little practical value within the limits of the NLPAN code (Sect. 3.1).
9. Improvements and corrections were made to the technique used to control the relative values of the two generalized in-plane load components (Sect. 2.6, 2.7).
10. A stationary total potential energy formulation was adopted in favor of the original virtual work formulation [7]. This was necessary in order to give the governing equations certain properties necessary to permit use of the advanced nonlinear solution strategies (Sect. 2.8).

This document provides a comprehensive description of the capabilities of, and theory behind, the NLPAN computer code. Section 2 contains the details of the theory for the baseline method. Section 3 documents the theory behind some of the recent additions to the method. Section 4 contains a discussion of various issues related to the computation of the second-order displacement fields, and describes certain modifications to the original method of computing them which have been implemented. Section 5 presents a brief discussion of some operational considerations for the NLPAN code. Section 6 presents results from applications of NLPAN which demonstrate program capabilities that are not demonstrated in other documents. Appendices A-C provide background material for the main text. Appendix D contains a description of the implementation of advanced nonlinear solution strategies within NLPAN. Appendix E contains detailed user instructions for the NLPAN computer code. Other work related to NLPAN and performed under NASA Grant NAG-1-1215 is reported in [16], [23-24].

In all work reported here, access to the buckling analysis of the VIPASA code [12] is obtained through the PASCO code [13], and therefore this document contains references to both codes. Which code is referenced in a particular discussion depends on the context; it should be kept in mind that PASCO is used only for the purpose of obtaining access to the embedded VIPASA analysis.

Much of the work of linking PASCO with NLPAN was performed as a part of a separate research project by Ms. Christine Perry, graduate assistant to Professor Zafer Gurdal of Virginia Polytechnic Institute and State University. The NASA technical monitor for this project was Dr. James H. Starnes Jr. of the Aircraft Structures Branch of NASA Langley Research Center.

2. THEORETICAL APPROACH OF NLPAN

2.1 Nonlinear Plate Theory

Consider a rectangular plate strip and an associated local (x, y, z) coordinate system, where the x - y plane lies at the mid-surface of the undisplaced plate. The plate has dimensions L and b in the x - and y -directions, respectively, as shown in Figure 2. Displacements of the mid-surface are denoted by $\{u\} = [u(x, y) \ v(x, y) \ w(x, y)]^T$ where the three components correspond to the x -, y -, and z -directions, respectively. The applied loads acting on the plate strip include force and moment resultants applied at the plate edges and uniform pressure Q acting in the local z -direction.

2.1.1 Strain-displacement relations. The in-plane strain components $\{\epsilon\} = [\epsilon_x \ \epsilon_y \ \gamma_{xy}]^T$ are restricted to be small compared to unity, but rotation angles associated with out-of-plane deflections and in-plane rotations are permitted to take on moderately large amplitudes. The Kirchhoff-Love assumptions are used to determine the distribution of the in-plane strain components through the thickness of the plate. The in-plane strains are then given by

$$\{\epsilon\} = \{\epsilon^c\} + z\{\kappa^c\} \quad (2.1.1)$$

where the mid-surface strains, $\{\epsilon^c\} = [\epsilon_x^c \ \epsilon_y^c \ \gamma_{xy}^c]^T$, and the mid-surface curvatures, $\{\kappa^c\} = [\kappa_x^c \ \kappa_y^c \ \kappa_{xy}^c]^T$, are given by

$$\{\epsilon^c\} = \begin{Bmatrix} u_{,x} + .5(v_{,x}^2 + w_{,x}^2) \\ v_{,y} + .5(u_{,y}^2 + w_{,y}^2) \\ u_{,y} + v_{,x} + w_{,x}w_{,y} \end{Bmatrix}, \quad \{\kappa^c\} = - \begin{Bmatrix} w_{,xx} \\ w_{,yy} \\ 2w_{,xy} \end{Bmatrix} \quad (2.1.2)$$

The derivation of the strain-displacement relations is given in [7].

An imperfect plate is assumed to be free of internal stress resultants, and have non-zero mid-surface displacements $\{u\} = \{u^o\}$ which describe the imperfection shape. Let equation (2.1.2) define the functions $\{\epsilon^c\} = \{\epsilon^c(\{u\})\}$ and $\{\kappa^c\} = \{\kappa^c(w)\}$. Mid-surface "mechanical" strains $\{\epsilon^m\}$ and curvatures $\{\kappa^m\}$ are defined by

$$\{\epsilon^m\} = \{\epsilon^c(\{u\})\} - \{\epsilon^c(\{u^o\})\}, \quad \{\kappa^m\} = \{\kappa^c(w)\} - \{\kappa^c(w^o)\} \quad (2.1.3)$$

These are the strain and curvature measures to which stress resultants are proportional.

2.1.2 Equilibrium equations. Force resultants (forces per unit length) f_x , f_y , and f_z are assumed to act along the edges of the plate in the x -, y -, and z -directions, respectively, and distributed bending moments M_x and M_y are assumed to act along the x -normal and y -normal edges, respectively. Force resultant f_z is assumed to account for the Kirchhoff equivalent shear force due to a distributed edge twisting moment M_{xy} . Special notation is used to represent the load and displacement measures along the side (y -normal) edges. Each side edge of the strip is given an index number e ($e = 1, 2$), such that the edge station y_e and the associated y -normal unit-vector component n_y are given by

$$[y_e, n_y] = \begin{cases} [0, -1] & \text{for } e = 1 \\ [b, 1] & \text{for } e = 2 \end{cases} \quad (2.1.4)$$

The generalized displacements and generalized force resultants along edge number e are denoted as $\{u_e\} = [u_e \ v_e \ w_e \ \psi_e]^T$ and $\{f_e\} = [f_{ex} \ f_{ey} \ f_{ez} \ m_e]^T$, respectively. The conventions for these parameters are shown in Figure 2. The edge rotation angle ψ_e is the derivative of w with respect to y .

In addition to the edge loads, a pressure load Q , acting in the z -direction, may be present. The plate material is assumed to be linearly elastic. The transverse shear strains, γ_{xz} and γ_{yz} , are neglected,

consistent with the Kirchhoff-Love assumptions, and the transverse normal stress, σ_z , is neglected. The total potential energy π is given by

$$\begin{aligned}\pi = & \int_A \frac{1}{2} (\{N\}^T \{\epsilon^m\} + \{M\}^T \{\kappa^m\}) dA \\ & - \int_A Q w dA - \int_0^b [\hat{f}_x u + \hat{f}_y v + \hat{f}_z w - n_x \hat{M}_x w_{,x}]|_{x=0,L} dy \\ & - \int_0^L [\hat{f}_{xe} u_e + \hat{f}_{ye} v_e + \hat{f}_{ze} w_e + \hat{m}_e \Psi_e]|_{e=1,2} dx\end{aligned}\quad (2.1.5)$$

where A is the planform area of the plate strip, hats denote specified edge-loads, and stress resultants $\{N\} = [N_x, N_y, N_{xy}]^T$ and $\{M\} = [M_x, M_y, M_{xy}]^T$ are defined by

$$\begin{Bmatrix} N_x, M_x \\ N_y, M_y \\ N_{xy}, M_{xy} \end{Bmatrix} = \int_{-\frac{h}{2}}^{\frac{h}{2}} \begin{Bmatrix} \sigma_x \\ \sigma_y \\ \sigma_{xy} \end{Bmatrix} (1, z) dz \quad (2.1.6)$$

Equations governing equilibrium are obtained by requiring stationary total potential energy:

$$\delta\pi = 0 \quad (2.1.7)$$

By evaluating equation (2.1.7) and applying Green's Theorem, the field equations governing plate equilibrium are found to be [7]

$$N_{x,x} + N_{xy,y} + (N_y u_{,y})_{,y} = 0 \quad (2.1.8a)$$

$$N_{xy,x} + N_{yy} + (N_x v_{,x})_{,x} = 0 \quad (2.1.8b)$$

$$M_{x,xx} + 2M_{xy,xy} + M_{y,yy} + (N_x w_{,x} + N_{xy} w_{,y})_{,x} + (N_{xy} w_{,x} + N_y w_{,y})_{,y} + Q = 0 \quad (2.1.8c)$$

On the x -normal edges, where $n_x = \pm 1$, the expressions for the edge force resultants in terms of plate stress resultants are found to have the form

$$\begin{aligned}f_x &= n_x N_x \\ f_y &= n_x (N_{xy} + N_x v_{,x}) \\ f_z &= n_x (M_{x,x} + 2M_{xy,y} + N_x w_{,x} + N_{xy} w_{,y})\end{aligned} \quad (2.1.9)$$

Along y -normal edges, the generalized force resultants are given by

$$\begin{aligned}f_{x_e} &= n_y (N_{xy} + N_y u_{,y}) \\ f_{y_e} &= n_y N_y \\ f_{z_e} &= n_y (2M_{xy,x} + M_{y,y} + N_{xy} w_{,x} + N_y w_{,y}) \\ m_e &= -n_y M_y\end{aligned} \quad e = 1, 2 \quad (2.1.10)$$

where the value n_e corresponding to e is given in equation (2.1.4).

2.1.3 Plate constitutive equations. The plate elastic properties are assumed to be those of a balanced, symmetric laminated composite plate, with the additional limitation that the bending/twisting coupling terms are neglected. The bending/twisting coupling terms become small in significance if each balanced pair of angle plies in a laminate span a portion of the laminate thickness which is small compared to the thickness of the laminate. The following plate constitutive equations then relate the plate stress resultants to the mid-surface mechanical strains and curvatures:

$$\{N\} = [A] \{\epsilon^m\}, \quad \{M\} = [D] \{\kappa^m\} \quad (2.1.11)$$

where

$$[A] = \begin{bmatrix} A_{11} & A_{12} & 0 \\ A_{12} & A_{22} & 0 \\ 0 & 0 & A_{66} \end{bmatrix}, \quad [D] = \begin{bmatrix} D_{11} & D_{12} & 0 \\ D_{12} & D_{22} & 0 \\ 0 & 0 & D_{66} \end{bmatrix} \quad (2.1.12)$$

2.2 Characteristics of Multiple-Plate Configurations

A linked-plate structure has an associated global coordinate system, as shown for a sample configuration in Figure 3. The global and local coordinate systems share a common x -axis. The overall width in the global y -direction is B . A set of "node lines" are defined which are analogous to nodes in a finite element model. The generalized displacements $\{u_e\}$ along the side edges of a plate strip are rigidly linked to the generalized displacements $\{U^n\} = [U^n \ V^n \ W^n \ \Psi^n]^T$ of one of the node lines. The latter displacements are defined with respect to the global coordinate directions. The configuration shown in Figure 3 has four node lines, which are labeled in the figure with circled numbers.

The most general orientation of the side-edge of a plate strip relative to the associated node line is shown in Figure 4(a). There is an angle μ between the local and global y - z coordinate directions, and offset measures e_y and e_z . Using offsets allows an accurate representation of complex cross sections, as can be seen in the example shown in Figure 4(b). The generalized displacements $\{u_e\}$ can be expressed in terms of $\{U^n\}$ by applying sequential transformations accounting for rotation, and eccentricity, respectively (Wittrick and Williams [12]):

$$\begin{aligned} \tilde{u}_e &= U^n \\ \tilde{v}_e &= V^n \cos \mu - W^n \sin \mu \\ \tilde{w}_e &= V^n \sin \mu + W^n \cos \mu \\ \tilde{\psi}_e &= \Psi^n \end{aligned} \quad (2.2.1)$$

$$\begin{aligned} u_e &= \tilde{u}_e + e_z \tilde{w}_{e,x} + e_y \tilde{v}_{e,x} \\ v_e &= \tilde{v}_e + e_z \tilde{\psi}_e \\ w_e &= \tilde{w}_e - e_y \tilde{\psi}_e \\ \psi_e &= \tilde{\psi}_e \end{aligned} \quad (2.2.2)$$

The second transformation above must be evaluated after the functional form of the displacements has been specified.

The generalized force resultants $\{f_e\}$ acting along the side edge of a plate strip can be transformed to statically equivalent generalized force resultants $\{f^n\} = [f_x^n \ f_y^n \ f_z^n \ m^n]^T$ which act at the corresponding node line and which are defined with respect to the global coordinate directions. The transformation which relates $\{f_e\}$ and $\{f^n\}$ is obtained by equating the virtual work due to $\{f_e\}$ acting through the virtual displacements $\{\delta u_e\}$ with the virtual due to $\{f^n\}$ acting through the virtual displacements $\{\delta U^n\}$. The vector of generalized force resultants along a node line $\{F^n\} = [F_x^n \ F_y^n \ F_z^n \ M^n]^T$ equals the sum of the contributions $\{f^n\}$ from all plate edges terminating at the node line. Externally applied loads acting along a boundary node line are not included in $\{F^n\}$.

Along the boundaries of the panel, it is assumed that the only non-zero specified loads are the in-plane normal components. The total potential energy for the entire structure can then be expressed as

$$\pi = \sum_{p=1}^P \left(\int_A \frac{1}{2} (\{N\}^T \{\epsilon^e\} + \{M\}^T \{\kappa^e\}) dA - \int_A Q w dA - \int_0^b \hat{f}_x u|_{x=0,L} dy \right)_p - \int_0^L \hat{F}_y^n V^n|_{n_1, n_2} dx \quad (2.2.3)$$

where p is the index number of a plate strip, P is the total number of plate strips in the structure, and n_1 and n_2 are the two designated boundary node-lines. The practical details of specifying the imposed loads are described in Section 2.8.2.

2.3 Loading and Boundary Conditions

2.3.1 Global loads. N_{xG} is the total x -normal end load divided by the width B . N_{yG} is the total y -normal edge load divided by the length L . These global load measures are defined to be positive for tension. A non-zero load N_{yG} may only be applied across a continuous, flat skin, because the initial response to in-plane loading is assumed to be free of plate bending. The effective changes in the panel length and width associated with applied loads are denoted Δu and Δv , respectively, where Δv is measured between two designated boundary node lines. (In cases where the boundary node-lines deform, Δv is a mean value.)

In a nonlinear analysis, the generalized in-plane load parameter λ controls either Δu or N_{xG} , depending on whether input parameter CONTRL is specified as 'D' or 'L', respectively (displacement control or load control). For configurations which admit biaxial loading, two options are available for controlling the second load component. Table 1 summarizes these options. In the table, Δu_L , Δv_L , N_{xGL} , and N_{yGL} , form a set of self-consistent parameter values corresponding to a unit solution for linear, unbuckled response. A unit load system is specified in terms of two parameters, one from the pair Δu_L and N_{xGL} , and one from the pair Δv_L and N_{yGL} . The two unspecified parameter values can be computed as described in Section 2.5. The option selected for control of the generalized in-plane loading (Table 1) determines which two parameters should be specified.

Illustrations of how the control options of Table 1 are used to simulate a variety of different scenarios for generalized in-plane loading are provided in Table 2. The four different cases illustrated in Table 2 are: A) loading at a constant ratio N_{yG}/N_{xG} , B) control of load component N_{xG} while holding Δv to zero, C) loading at a constant ratio $\Delta v/\Delta u$, and D) uniaxial loading for configurations which do not admit biaxial loading. For Case D, N_{yG} is zero in prebuckling response, but a non-zero load N_{yG} may arise in the nonlinear regime if the boundary node-lines are restrained.

Transverse pressure loading is permitted. The loading Q is assumed to be uniform over any given plate strip, but may be applied selectively to plate strips as necessary to simulate the desired loading. A load parameter β controls the amplitude of the pressure loading independently of the in-plane loading, as discussed in Section 2.8.3.

2.3.2 End-support conditions. The effective boundary support condition at the panel ends is determined by the harmonic form of the buckling mode shapes (obtained from the buckling analysis of VIPASA) used as global shape functions. The transverse displacements v and w have a sinusoidal dependence on x (see Section 2.6), and thus the buckling modes are actually those of an infinite-length structure which is supported against transverse displacements at uniform intervals. Axial displacement u has a cosine dependence on x . When the buckling results are applied to a finite-length structure, the ends of some panels may both rotate and warp during buckling (and postbuckling). This makes the concept of a neutral bending axis somewhat ill-defined; nonetheless a generalized neutral axis can be considered to exist, as determined by the points of zero-axial-displacement (for a buckling mode) at the longitudinal ends of the panel. The interpretation offered here is that each longitudinal end is loaded by a generalized knife-edge support which acts along the generalized neutral axis. The effective axial displacement of the panel end is then the axial displacement of the knife-edge. This issue is discussed further in Section 2.8.2.

The transverse displacements v and w of the buckling eigenfunctions are zero at the ends of the panel; in addition, the local bending moment M_x is uniformly zero at the panel ends, implying a simple support condition for each plate strip. In general, however, the local edge shear-force resultant N_y is non-zero, and can not be independently controlled.

2.3.3 Boundary conditions along the node-lines. Two of the node lines are designated as boundary node-lines. The index numbers of these two node lines are denoted n_1 and n_2 corresponding to the panel edges which have edge-normal unit vector components $n_y = -1$ and $n_y = 1$, respectively, with reference to the global coordinate axes. Along each of the boundary node-lines, four boundary conditions are specified corresponding to the four degrees of freedom along a node line. In general terms, either a displacement condition (BCVEC=1) or a load condition (BCVEC=2) can be specified for each of the degrees of freedom. For the degrees of freedom corresponding to U^n , W^n , and Ψ^n , only homogeneous boundary conditions can be specified (zero generalized displacement or zero generalized load). For the degree of freedom corresponding to V^n , non-homogeneous boundary conditions may be imposed consistent with the limitations given in Table 1.

The choices for boundary conditions are expressed mathematically in Table 3. The term V_L^n represents the node-line displacement associated with the linear response of an imperfection-free structure to the unit in-plane loads. A third boundary-condition option (BCVEC=3) is available for the degree of freedom corresponding to V^n (Component 2). The symbol \bar{F}_y^n appearing in the table is the mean value of the force resultant F_y^n over the length L . With this third boundary condition option, the net edge-normal load is controlled while the edge is constrained to remain straight with respect to in-plane displacements. The option is useful in modelling symmetry conditions, or in modelling an edge which is reinforced so as to remain straight.

For the non-boundary node-lines to be in equilibrium, the generalized force-resultants must vanish:

$$\{F^n\} = \{0\} \quad \begin{array}{l} n = 1, 2, \dots, N \\ n \neq n_1, n_2 \end{array} \quad (2.3.1)$$

2.4 Expansion of the Displacement Functions

Displacements are assumed to have the following general form on each plate strip:

$$\{u\} = \lambda \{u_L\} + q_i \{u_i\} + q_i q_j \{u_{ij}\} \quad (i, j = 1, 2, \dots) \quad (2.4.1)$$

where summation over repeated indices is implied. Symbol λ is the generalized in-plane load parameter, and $\{u_L\} = [u_L \ v_L \ 0]^T$ is the displacement solution for linear, unbuckled response to specified unit, global, in-plane loads. The i^{th} buckling mode shape is $\{u_i\} = [u_i \ v_i \ w_i]^T$, and the associated "modal amplitude" is q_i . Shape functions $\{u_{ij}\} = [u_{ij} \ v_{ij} \ w_{ij}]^T$ are referred to as the second-order displacement fields. The imperfection shape is expressed as

$$\{u^o\} = q_i^o \{u_i\} + q_i^o q_j^o \{u_{ij}\} \quad (i, j = 1, 2, \dots) \quad (2.4.2)$$

where q_i^o is the "modal imperfection amplitude" for an imperfection in the shape of $\{u_i\}$.

The boundary value problems governing the three families of shape functions are obtained by expanding the equilibrium equations and boundary condition expressions in terms of the expanded forms of the displacements, grouping terms based on their order in the modal amplitudes, and setting to zero the imperfections and pressure. The resulting expressions of order 0, 1, and 2 provide the boundary value problems governing $\{u_L\}$, $\{u_i\}$, and $\{u_{ij}\}$, respectively. Function $\{u_L\}$ satisfies the non-homogeneous in-plane boundary conditions, whereas functions $\{u_i\}$ and $\{u_{ij}\}$ satisfy homogeneous in-plane boundary conditions. Each of the three sets of shape functions is discussed in a following section.

2.5 Prebuckling Solutions

A unit load system for the prebuckling response is prescribed as part of the problem definition (Section 2.3.1). The unit load system consists of some combination of unit global in-plane loads N_{xGL} and N_{yGL} , and unit global length- and width-change measures Δu_L and Δv_L , consistent with the desired form of in-plane loading selected from Tables 1-3. The unit loads are distributed so as to produce uniform normal displacement of both the longitudinal ends and the side edges. It is assumed that the prebuckling response involves only uniform in-plane normal strains in the component plate strips (no plate bending). Thus, neglecting rigid-body displacement of the plate strips, the prebuckling solution $\{u_L\}$ involves only in-plane displacements:

$$\{u_L\} = [u_L \ v_L \ 0]^T \quad (2.5.1)$$

The nature of the loading and elastic properties of the component plate strips are such that neither shear strains nor shear stress resultants are induced, so that

$$\{\epsilon_L\} = \left\{ \begin{matrix} u_{L,x} \\ v_{L,y} \\ 0 \end{matrix} \right\} \quad (2.5.2)$$

and

$$\{N_L\} = [A]\{\epsilon_L\} = \left\{ \begin{matrix} N_{xL} \\ N_{yL} \\ 0 \end{matrix} \right\} \quad (2.5.3)$$

The quantities $\{\epsilon_L\}$ and $\{N_L\}$ are uniform over each plate strip, and this unit solution satisfies the equilibrium equations (2.1.8). The detailed formulae used for computing the prebuckling solution are given in Appendix A. The formulae are compatible with those used in PASCO [13] for determining the prebuckling response, but additional equations are included for determining the unit global loads N_{xGL} and N_{yGL} (required as input to PASCO) corresponding to specified values of Δu_L and/or Δv_L .

NLPAN, like VIPASA, requires the strains $\{\epsilon_L\}$ but not the displacements $\{u_L\}$. For some doubly connected plate-strip configurations, the method used in PASCO to compute $\{u_L\}$ results in a violation of displacement compatibility between adjoining plate strips. This is because the method only enforces compatibility of the longitudinal axial strain ϵ_x between the various plate strips. The NLPAN code includes an option to enforce displacement compatibility for cases where stiffener flanges are modelled as plate strips which are offset from the skin of a panel. In the linear solution, the plate strips are confined to pure in-plane response. Used in a pre-processor mode, NLPAN provides PASCO input parameters NX(1), NY(1), and FNY(I) [14] which distribute the in-plane loads among the individual plate strips so as to satisfy the displacement compatibility condition. When the prebuckling solution is computed with the enforcement of displacement compatibility and zero plate bending, there will in general be non-zero values for the associated node-line moment resultant contributions M_L^* .

2.6 Buckling Eigensolutions

The buckling equations obtained in the manner described in Section (2.4) are given by

$$N_{x_i,xx} + N_{x_i,yy} + \lambda_i N_{y_i} u_{i,yy} = 0 \quad (2.6.1a)$$

$$N_{x_i,xy} + N_{y_i,xy} + \lambda_i N_{x_i} v_{i,xx} = 0 \quad (2.6.1b)$$

$$M_{x_i,xx} + 2M_{x_i,xy} + M_{y_i,yy} + \lambda_i (N_{x_i} w_{i,xx} + N_{y_i} w_{i,yy}) = 0 \quad (2.6.1c)$$

where λ_i is the i^{th} buckling eigenvalue, and functions $\{N_i\} = [N_{x_i} \ N_{y_i} \ N_{xy_i}]^T$ and $\{M_i\} = [M_{x_i} \ M_{y_i} \ M_{xy_i}]^T$ are given by

$$\{N_i\} = [A]\{\epsilon_i\} \quad \{M_i\} = [D]\{\kappa_i\} \quad (2.6.2)$$

where

$$\{\varepsilon_i\} = \begin{Bmatrix} u_{i,x} \\ v_{i,y} \\ u_{i,y} + v_{i,x} \end{Bmatrix} \quad \{\kappa_i\} = - \begin{Bmatrix} w_{i,xx} \\ w_{i,yy} \\ 2w_{i,xy} \end{Bmatrix} \quad (2.6.3)$$

The eigenvalues λ_i are generally negative, corresponding to a compressive end load on the panel.

Equation (2.5.1a) differs from the corresponding equation used in the VIPASA analysis [12], the latter equation being

$$N_{x,x} + N_{xy,y} + \lambda_i N_{xL} u_{i,xx} = 0 \quad (2.6.4)$$

The third term of each of the disputed equations is assumed here to be negligible, based on arguments given in Ref. [7], and so equation (2.6.1a) is replaced by

$$N_{x,x} + N_{xy,y} = 0 \quad (2.6.5)$$

The generalized side-edge force resultants $\{f_i\} = [f_{ix} f_{iy} f_{iz} m_i]^T$ of equation (2.1.10) have contributions $\{f_{ie}\} = [f_{xie} f_{yie} f_{zie} m_{ie}]^T$ associated with the buckling eigensolutions, given by

$$\{f_{ie}\} = \begin{Bmatrix} n_y N_{xy_i} |_{y_e} \\ n_y N_{yi} |_{y_e} \\ n_y (2M_{xy_i,x} + M_{y,y} + \lambda_i N_{yL} \phi_{i,y}) |_{y_e} \\ - n_y M_{yi} |_{y_e} \end{Bmatrix} \quad (2.6.6)$$

These quantities are used to express the node-line boundary conditions (Section 2.3.3) to complete the boundary-value problem specification for the buckling mode shapes.

The solution of the buckling equations for a linked-plate configuration is performed by the VIPASA buckling and vibration analysis code [12]. The i^{th} eigenfunction has the following assumed form on each plate strip (where a phase shift in the x -direction has been applied relative to the conventions of VIPASA to provide that $w_i(0, y) = w_i(L, y) \equiv 0$):

$$\{u_i\} = \begin{Bmatrix} u_i \\ v_i \\ w_i \end{Bmatrix} = \begin{Bmatrix} \xi_i(y) \cos m_i \pi x / L \\ \eta_i(y) \sin m_i \pi x / L \\ \phi_i(y) \sin m_i \pi x / L \end{Bmatrix} \quad (2.6.7)$$

where m_i is the integer number of buckling half-waves along the length of the panel for the i^{th} buckling eigensolution. When the buckling equations (2.6.1) are expressed in terms of the displacement forms given above, the former equations can be reduced to two coupled homogeneous linear second order ordinary differential equations in the functions $\xi_i(y)$ and $\eta_i(y)$, and one homogeneous linear fourth order ordinary differential equation in the function $\phi_i(y)$.

For specified values of the longitudinal halfwave number m_i , the VIPASA program returns buckling eigensolutions in the form of an eigenvalue λ_i and a set of generalized node-line displacement amplitudes. Using this information along with the general forms of the solutions to the governing ordinary differential equations, the functions $\{\xi_i(y)\} = [\xi_i(y) \eta_i(y) \phi_i(y)]^T$ are obtained in analytic form. Details of the procedure are described in Ref. [7] Appendix B. (The following error in [7] is noted. Parameter L in equation (B10) should be given by

$$L = \frac{1}{D_{22}} \left(-\lambda \frac{L^2 N_{x_L}}{m^2 \pi^2} + D_{22} T^2 - D_{11} \right)$$

Furthermore, the term L^2 appearing in the definitions for L and T of equation (B10) refers to the length squared, and not the parameter L defined in the equation above.) For an infinite-length structure supported at uniform intervals L along the length, the eigenfunctions satisfy (to the first order) the homogeneous form of the boundary conditions along the boundary node-lines which have been selected from Table 2. However, these boundary conditions may not be satisfied for a finite-length structure, in which case a correction, described below, is applied to the buckling eigensolution.

If boundary condition Option 3 for Component 2 in Table 3 (BCVEC(2,IB)=3) is chosen, the corresponding homogeneous boundary condition is given by $V_{i,2} = 0$ and $\bar{F}_{y_i} = 0$ where $V_{i,2}$ and \bar{F}_{y_i} are the contributions of the buckling mode to V_i^* and \bar{F}_i of Table 3. The condition $\bar{F}_{y_i} = 0$ is satisfied automatically only if the average value \bar{F}_{y_i} is evaluated over an even number of halfwaves (i.e. m_i of equation (2.6.7) is even). If m_i is odd, the condition $\bar{F}_{y_i} = 0$ may be violated, which indicates that a spurious contribution to the global load component N_{yG} may be present. Thus, a compensating contribution must be added. The amplitude of $\bar{F}_{y_i}^*$ (the first-order contribution to the load \bar{F}_i^* appearing in Table 2) is determined from the mean value of the stress resultant N_{y_i} in the panel skin along one of the two boundary node-lines:

$$\bar{F}_{y_i}^* = n_{y_i} \bar{N}_{y_i} |_{n_1} \quad (2.6.8)$$

where

$$\bar{N}_{y_i} |_{n_1} = \frac{1}{L} \int_0^L N_{y_i} |_{n_1} dx \quad (2.6.9)$$

and n_1 designates a boundary node-line location. The global load contributions N_{yGi} is then defined as

$$N_{yGi} = \bar{N}_{y_i} |_{n_1} \quad (2.6.10)$$

The associated load component in the x -normal direction is denoted N_{xGi} , and this component is zero by virtue of the harmonic form of N_{x_i} ($N_{x_i} \equiv 0$ at $x = 0, L$):

$$N_{xGi} = \frac{1}{B} \sum_{p=1}^P \left(\int_0^b N_{x_i} |_{x=0} dx \right)_p \quad (2.6.11)$$

$$\equiv 0$$

A modified buckling eigenfunction $\{\tilde{u}_i\}$ is defined, having the form

$$\{\tilde{u}_i\} = \{u_i\} + B_i \{u_B\} \quad (2.6.12)$$

where the shape function $\{u_B\}$ has the same general characteristics as the unit linear unbuckled solution $\{u_L\}$ (see Section 2.5), except that the former corresponds to a unit load system

$$N_{yG} = N_{yGb} \quad , \quad N_{xG} = N_{xGb} = 0 \quad (2.6.13)$$

Modified global load contributions, \tilde{N}_{yGi} and \tilde{N}_{xGi} , are defined, corresponding to the modified eigenfunction $\{\tilde{u}_i\}$. In view of equations (2.6.11) and (2.6.13),

$$\tilde{N}_{xGi} = 0 \quad (2.6.14)$$

Parameter B_i is chosen so that the following homogeneous boundary condition is satisfied:

$$\begin{aligned}\tilde{N}_{yG_i} &= N_{yG_i} + B_i N_{yG_B} \\ &= 0\end{aligned}\quad (2.6.15)$$

with the result is that

$$B_i = -N_{yG_i}/N_{yG_B} \quad (2.6.16)$$

For modes which have non-zero values B_i , the eigenvalue $\tilde{\lambda}_i$ associated with $\{\tilde{u}_i\}$ will be slightly different from the original eigenvalue λ_i . NLPAN computes and prints the values $\tilde{\lambda}_i$.

If the value of BCVEC(2,IB) is 3 for one boundary and 2 for the other (see Table 3), then N_{yG_i} may be non-zero on one boundary and zero on the other. This discrepancy is the result of the nature of VIPASA buckling mode shapes. In NLPAN, the modified eigenfunction $\{\tilde{u}_i\}$ is used only if BCVEC(2,IB)=3 for IB=1 and IB=2 (both y-normal boundaries).

2.7 Second-Order Displacement Fields

The equations governing the second-order displacement fields, obtained in the manner described in Section (2.4), are given by

$$N_{x_{ij},xx} + N_{xy_{ij},yy} + \frac{1}{2} [(N_{y_i} u_{j,y})_{,y} + (N_{y_j} u_{i,y})_{,y}] = 0 \quad (2.7.1a)$$

$$N_{xy_{ij},xx} + N_{y_{ij},yy} + \lambda_b N_{x_L} v_{ij,xx} + \frac{1}{2} [(N_{x_i} v_{j,x})_{,x} + (N_{x_j} v_{i,x})_{,x}] = 0 \quad (2.7.1b)$$

$$\begin{aligned}M_{x_{ij},xx} + 2M_{xy_{ij},xy} + M_{y_{ij},yy} + \lambda_b (N_{x_L} w_{ij,xx} + N_{y_L} w_{ij,yy}) \\ + \frac{1}{2} [(N_{x_i} w_{j,x} + N_{xy_i} w_{j,y})_{,x} + (N_{xy_j} w_{i,x} + N_{y_i} w_{j,y})_{,y} \\ + (N_{x_j} w_{i,x} + N_{xy_j} w_{i,y})_{,x} + (N_{xy_i} w_{j,x} + N_{y_j} w_{i,y})_{,y}] = 0\end{aligned} \quad (2.7.1c)$$

where $\{N_{ij}\} = [N_{xij} \ N_{yij} \ N_{xyij}]^T$ and $\{M_{ij}\} = [M_{xij} \ M_{yij} \ M_{xyij}]^T$ are given by

$$\{N_{ij}\} = [A]\{\epsilon_{ij}\}, \quad \{M_{ij}\} = [D]\{\kappa_{ij}\} \quad (2.7.2)$$

where

$$\{\epsilon_{ij}\} = \left\{ \begin{array}{c} u_{ij,xx} + .5(v_{i,x}v_{j,x} + w_{i,x}w_{j,x}) \\ v_{ij,yy} + .5(u_{i,y}u_{j,y} + w_{i,y}w_{j,y}) \\ u_{ij,y} + v_{ij,x} + .5(w_{i,x}w_{j,y} + w_{i,y}w_{j,x}) \end{array} \right\}, \quad \{\kappa_{ij}\} = - \left\{ \begin{array}{c} w_{ij,xx} \\ w_{ij,yy} \\ 2w_{ij,xy} \end{array} \right\} \quad (2.7.3)$$

The in-plane load parameter λ has been replaced in the above equations by a fixed reference value λ_b , consistent with the desire to obtain a load-independent set of shape functions $\{u_{ij}\}$. In Section 4, it is argued that the load-dependent terms can be eliminated from the above equations, so in the implementation of NLPAN, λ_b is set to zero. (The term $\lambda_b N_{y_L} u_{ij,yy}$ which naturally arises in deriving equation (2.7.1a) has been omitted, consistent with the deletion of the related term from equation (2.6.1a).)

Equations (2.7.1) involve known eigenfunctions $\{u_i\}$ and $\{u_j\}$, and unknown function $\{u_{ij}\}$. Let m_x and m_y denote the number of buckling halfwaves in the x -direction for eigenfunctions $\{u_i\}$ and $\{u_j\}$, respectively. Separation of variables can be used to convert the trio of partial differential equations (2.7.1) into two trios of ordinary differential equations in the variable y , by assuming the following functional form for $\{u_{ij}\}$ [15]:

$$\{u_{ij}\} = \begin{Bmatrix} u_{ij} \\ v_{ij} \\ w_{ij} \end{Bmatrix} = \sum_{\alpha=1}^2 \begin{Bmatrix} \xi_{\alpha ij}(y) \sin \hat{m}\pi x/L \\ \eta_{\alpha ij}(y) \cos \hat{m}\pi x/L \\ \phi_{\alpha ij}(y) \cos \hat{m}\pi x/L \end{Bmatrix} \quad (2.7.4)$$

where

$$\hat{m} = \begin{cases} m_i + m_j & \alpha = 1 \\ m_i - m_j & \alpha = 2 \end{cases} \quad (2.7.5)$$

The transverse displacements v_{ij} and w_{ij} do not satisfy the same boundary conditions as v_i and w_i at $x=0, L$. This issue is discussed in detail in Section 4.

Using the assumed forms for $\{u_{ij}\}$ and $\{u_i\}$ along with trigonometric identities, the partial differential equations (2.7.1) are converted into two uncoupled trios of non-homogeneous ordinary differential equations, one trio governing $\{\xi_{1ij}\} = [\xi_{1ij} \eta_{1ij} \phi_{1ij}]^T$, the second trio governing $\{\xi_{2ij}\} = [\xi_{2ij} \eta_{2ij} \phi_{2ij}]^T$. Both equation trios have the following general form, where the subscripts α and ij are omitted:

$$C_1 \xi'' + C_2 \xi + C_3 \eta' = F(y) \quad (2.7.6a)$$

$$D_1 \xi' + D_2 \eta'' + D_3 \eta = G(y) \quad (2.7.6b)$$

$$E_1 \phi'''' + E_2 \phi'' + E_3 \phi = H(y) \quad (2.7.6c)$$

where the subscripted C 's, D 's and E 's are constant coefficients, and the functions $F(y)$, $G(y)$, and $H(y)$ have a quadratic dependence on the components of functions $\{\xi_i(y)\}$ and $\{\xi_j(y)\}$ and their derivatives. For general configurations, all three equations are coupled through the boundary conditions along node-lines where non-coplanar plate strips join. The expressions for the coefficients and nonhomogeneous terms in equations (2.7.6) are presented in Section 3.5 of Ref. [7].

The homogeneous form of the boundary conditions discussed in Section 2.3 are applied to the second-order displacements and the associated generalized node-line force resultants. These boundary conditions complete the specification of the boundary-value problem governing the functions $\{\xi_{\alpha ij}(y)\}$. Detailed boundary condition expressions are presented in Section 3.5 of Ref. [7]. Because of the complexity of the expressions found in $[F_{\alpha ij}(y) G_{\alpha ij}(y) H_{\alpha ij}(y)]$ of equations (2.7.6), a finite difference analysis is employed to obtain values of the functions $\{\xi_{\alpha ij}(y)\}$ at a finite number of evenly spaced points across the y -domain of each plate strip. The finite-difference solution procedure is presented in detail in Appendix C of Ref. [7].

The functions $\{u_{ij}\}$ satisfy the homogeneous form of the conditions along the boundary node-lines which have been selected from Table 3. At the ends of the structure ($x=0, L$), $\{u_{ij}\}$ satisfies the homogeneous form of the displacement-control (CONTRL='D' in Table 1) boundary conditions. If load control (CONTRL='L' in Table 1) is used, modified second-order displacement fields $\{\tilde{u}_{ij}\}$ are computed which satisfy homogeneous force boundary conditions at the longitudinal ends. The modified function has the form

$$\{\tilde{u}_{ij}\} = \{u_{ij}\} + A_{ij}(\{u_A\} - \{u_L\}) \quad (2.7.7)$$

where $\{u_L\} = [u_L \ v_L \ 0]^T$ is the unit prebuckling solution discussed earlier, $\{u_A\} = [0 \ v_A \ 0]^T$ is a unit unbuckled solution of the same nature as $\{u_L\}$ except that it corresponds to a unit global load N_{yGA} where the corresponding longitudinal strain ϵ_{xA} , is held to zero throughout the structure, and A_{ij} is a constant coefficient to be determined. The source and significance of the modifying terms are discussed below.

The second-order displacement fields give rise to associated second-order contributions to the global loads N_{xG} and N_{yG} , according to the relationships

$$N_{xG_{ij}} = \frac{1}{B} \sum_{p=1}^P \left(\int_0^b N_{x_{ij}}|_{x=0} dy \right)_p \quad (2.7.8)$$

$$N_{yG_{ij}} = \frac{1}{L} \int_0^L (N_{y_{ij}}|_{n_1}) dx \quad (2.7.9)$$

where the quantity inside the parentheses in equations (2.7.9) is the value of $N_{y_{ij}}$ in the skin at one of the boundary node-lines. For the case of bi-axial loading (Load Case A, Table 2), the homogeneous form of the boundary condition which is satisfied is that of Option 2 or 3 for Component 2 in Table 3, so that

$$N_{yG_{ij}} = 0 \quad (2.7.10)$$

The modified field $\{\tilde{u}_{ij}\}$ must contribute nothing to either N_{xG} or N_{yG} , so the following conditions are imposed:

$$\begin{aligned} \tilde{N}_{xG_{ij}} &= 0 \\ \tilde{N}_{yG_{ij}} &= 0 \end{aligned} \quad (2.7.11)$$

With substitutions, the above two equations take the form

$$\begin{aligned} N_{xG_{ij}} + A_{ij}(N_{xG_A} - N_{xG_L}) &= 0 \\ A_{ij}(N_{yG_A} - N_{yG_L}) &= 0 \end{aligned} \quad (2.7.12)$$

The value of N_{yG_A} is selected such that

$$N_{yG_A} = N_{yG_L} \quad (2.7.13)$$

and A_{ij} is then given by

$$A_{ij} = N_{xG_{ij}} / (N_{xG_L} - N_{xG_A}) \quad (2.7.14)$$

For load-control cases in which the desired node-line boundary condition given by Option 1 for Component 2 in Table 3, the condition $V_{ij}^n = 0$ along the boundary node-lines is automatically satisfied, but it is still necessary to use the modified function $\{\tilde{u}_{ij}\}$ satisfying

$$\tilde{N}_{xG_{ij}} = 0 \quad (2.7.15)$$

This is accomplished by using the expressions for $\{\tilde{u}_{ij}\}$ and A_{ij} given in equations (2.7.7) and (2.7.14), respectively, but setting to zero the quantities $\{u_A\}$, N_{yG_A} , and N_{xG_A} .

2.8 Stationary Total Potential Energy Formulation

2.8.1 Expansion of the strains, curvatures, and stress resultants. The form of the displacements presented in equation (2.4.1) is restated with the modified functions $\{\tilde{u}_i\}$ and $\{\tilde{u}_{ij}\}$ of equations (2.6.12) and (2.7.7), respectively, replacing the functions $\{u_i\}$ and $\{u_{ij}\}$:

$$\{u\} = \lambda\{u_L\} + q_i\{\tilde{u}_i\} + q_i q_j\{\tilde{u}_{ij}\} \quad i, j = 1, 2, 3, \dots \quad (2.8.1)$$

where

$$\begin{aligned} \{\tilde{u}_i\} &= \{u_i\} + B_i\{u_B\} \\ \{\tilde{u}_{ij}\} &= \{u_{ij}\} + A_{ij}(\{u_A\} - \{u_L\}) \end{aligned} \quad (2.8.2)$$

The generalized in-plane load parameter λ controls either end displacement or end load, consistent with the selection of parameter CONTRL from Table 1. Simplifications to equations (2.8.2) which arise in some situations are summarized in Table 4.

The mid-surface strains and curvatures of equation (2.1.3) are expanded by using the expanded form of the displacements given in equations (2.8.1-2), giving rise to the following forms:

$$\{\epsilon^m\} = \lambda\{\epsilon_L\} + (q_i - q_i^\circ)\{\tilde{\epsilon}_i\} + (q_i q_j - q_i^\circ q_j^\circ)\{\tilde{\epsilon}_{ij}\} + (q_i q_j q_k - q_i^\circ q_j^\circ q_k^\circ)\{\epsilon_{ijk}\} + (q_i q_j q_k q_l - q_i^\circ q_j^\circ q_k^\circ q_l^\circ)\{\epsilon_{ijkl}\} \quad (2.8.3)$$

$$\{\kappa^m\} = (q_i - q_i^\circ)\{\kappa_i\} + (q_i q_j - q_i^\circ q_j^\circ)\{\kappa_{ij}\} \quad (2.8.4)$$

where

$$\begin{aligned} \{\tilde{\epsilon}_i\} &= \{\epsilon_i\} + B_i\{\epsilon_B\} \\ \{\tilde{\epsilon}_{ij}\} &= \{\epsilon_{ij}\} + A_{ij}(\{\epsilon_A\} - \{\epsilon_L\}) \end{aligned} \quad (2.8.5)$$

The terms $\{\epsilon_L\}$, $\{\epsilon_i\}$, $\{\epsilon_{ij}\}$, $\{\kappa_i\}$, and $\{\kappa_{ij}\}$ appearing in equations (2.8.3)-(2.8.5) have been presented in terms of displacement functions in equations (2.5.2), (2.6.3), and (2.7.3). The remaining terms are defined by

$$\begin{aligned} \{\epsilon_B\} &= \begin{Bmatrix} u_{B,x} \\ v_{B,y} \\ 0 \end{Bmatrix} & \{\epsilon_A\} &= \begin{Bmatrix} 0 \\ v_{A,y} \\ 0 \end{Bmatrix} \\ \{\epsilon_{ijk}\} &= \begin{Bmatrix} v_{i,x}v_{j,k,x} + w_{i,x}w_{j,k,x} \\ u_{i,y}u_{j,k,y} + w_{i,y}w_{j,k,y} \\ w_{i,x}w_{j,k,y} + w_{i,y}w_{j,k,x} \end{Bmatrix} & \{\epsilon_{ijkl}\} &= \begin{Bmatrix} .5(v_{i,x}v_{j,k,x} + w_{i,x}w_{j,k,x}) \\ .5(u_{i,y}u_{j,k,y} + w_{i,y}w_{j,k,y}) \\ .5(w_{i,x}w_{j,k,y} + w_{i,y}w_{j,k,x}) \end{Bmatrix} \end{aligned} \quad (2.8.6)$$

Stress resultants $\{N\}$ and $\{M\}$ are linearly related to the mid-surface mechanical strains and curvatures, respectively, through equations (2.1.11), and thus have the same expanded forms:

$$\{N\} = \lambda\{N_L\} + (q_i - q_i^\circ)\{\tilde{N}_i\} + (q_i q_j - q_i^\circ q_j^\circ)\{\tilde{N}_{ij}\} + (q_i q_j q_k - q_i^\circ q_j^\circ q_k^\circ)\{N_{ijk}\} + (q_i q_j q_k q_l - q_i^\circ q_j^\circ q_k^\circ q_l^\circ)\{N_{ijkl}\} \quad (2.8.7)$$

$$\{M\} = (q_i - q_i^\circ)\{M_i\} + (q_i q_j - q_i^\circ q_j^\circ)\{M_{ij}\} \quad (2.8.8)$$

2.8.2 Edge-load contributions to the total potential energy. Global load and displacement quantities are used to express the contributions of the in-plane loads to the total potential energy. Consider the in-plane displacements, which have the expanded form

$$\begin{Bmatrix} u \\ v \end{Bmatrix} = \lambda \begin{Bmatrix} u_L \\ v_L \end{Bmatrix} + q_i \begin{Bmatrix} u_i + B_i u_B \\ v_i + B_i v_B \end{Bmatrix} + q_i q_j \begin{Bmatrix} u_{ij} + A_{ij}(0 - u_L) \\ v_{ij} + A_{ij}(v_A - v_L) \end{Bmatrix} \quad (2.8.9)$$

At the longitudinal ends of the structure, u_i is identically zero. It is also assumed that non-zero values of the axial buckling displacements $\tilde{u}_i = u_i + B_i u_B$ at the ends of the structure are due to rotation of the ends about the generalized neutral axis without any associated change in length. The effective change in panel length, Δu , is then

$$\begin{aligned} \Delta u &= u|_{x=L} - u|_{x=0} \\ &= (\lambda - q_i q_j A_{ij}) \Delta u_L \end{aligned} \quad (2.8.10)$$

The mean change in panel width, $\overline{\Delta v}$, is given by

$$\begin{aligned}\overline{\Delta v} &= \frac{1}{L} \int_0^L (V^{n_2} - V^{n_1}) dx \\ &= \lambda \Delta v_L + q_i (\overline{\Delta v}_i + B_i \Delta v_B) + q_i q_j [\overline{\Delta v}_{ij} + A_{ij} (\Delta v_A - \Delta v_L)]\end{aligned}\quad (2.8.11)$$

where over-bars denote the mean quantities taken over the length of the panel, and V^{n_1} and V^{n_2} are the displacements of the two boundary node-lines in the global y-direction.

The global in-plane load components N_{xG} and N_{yG} are defined by

$$N_{xG} = \frac{1}{B} \sum_{p=1}^P \left(\int_0^b N_x|_{x=0} dy \right)_p \quad (2.8.12)$$

$$N_{yG} = \frac{1}{L} \int_0^L N_y|_{n_1} dx \quad (2.8.13)$$

where n_1 is a boundary node-line, and N_y is measured in the panel skin (if present) at the boundary node-line. The expanded form for $\{N\}$ of equation (2.8.7) is inserted into the above two equations to obtain the following expanded form for the global in-plane loads:

$$\begin{aligned}\begin{Bmatrix} N_{xG} \\ N_{yG} \end{Bmatrix} &= \lambda \begin{Bmatrix} N_{xGL} \\ N_{yGL} \end{Bmatrix} + (q_i + q_i^o) \begin{Bmatrix} 0 \\ N_{yGi} + B_i N_{yGb} \end{Bmatrix} \\ &+ (q_i q_j - q_i^o q_j^o) \begin{Bmatrix} N_{xGij} + A_{ij} (N_{xGA} - N_{xGL}) \\ N_{yGij} + A_{ij} (N_{yGA} - N_{yGL}) \end{Bmatrix} + \begin{Bmatrix} O(q_i^4) \\ O(q_i^3) \end{Bmatrix}\end{aligned}\quad (2.8.14)$$

The higher order contributions inside the last set of braces are neglected.

For the case where load control is used for the in-plane loads (CONTRL='L' in Table 1) the contributions of the in-plane loads to the total potential energy (see equation (2.2.3)) are now expressed in terms of the global parameters as

$$-B \hat{N}_{xG} \Delta u - \int_0^L \hat{N}_{yG} \Delta v dy \quad (2.8.15)$$

Simplifications apply to the expanded forms of the terms appearing in the above expression because load control is in effect. Load component N_{xG} becomes

$$\hat{N}_{xG} = \lambda N_{xGL} \quad (2.8.16)$$

so that

$$-B \hat{N}_{xG} \Delta u = (-\lambda^2 + q_i q_j \lambda A_{ij}) E_L^L \quad (2.8.17)$$

where

$$E_L^L = B N_{xGL} \Delta u_L \quad (2.8.18)$$

For Option 2 of Table 1 (CONTRL='L') the load \hat{N}_{yG} is given by

$$\hat{N}_{yG} = \lambda N_{yGL} \quad (2.8.19)$$

$$-\int_0^L \hat{N}_{yG} \Delta v dy = -\lambda D_L^L - q_i \lambda (D_i^L + B_i D_B^L) - q_i q_j \lambda [D_{ij}^L + A_{ij} (D_A^L - D_L^L)] \quad (2.8.20)$$

where

$$\begin{aligned} D_L^L &= L N_{yG_L} \Delta v_L \\ D_B^L &= L N_{yG_L} \Delta v_B \\ D_A^L &= L N_{yG_L} \Delta v_A \\ D_i^L &= L N_{yG_L} \overline{\Delta v}_i \\ D_{ij}^L &= L N_{yG_L} \overline{\Delta v}_{ij} \end{aligned} \quad (2.8.21)$$

For Option 1 of Table 1 (CTRL='L'), Δv is zero, so that the second term of expression (2.8.15) contributes nothing.

2.8.3 Expansion of the total potential energy. The total potential energy expression, equation (2.2.3), is rewritten here, reflecting the use of the global load and displacement parameters to represent the contributions due to applied edge loads:

$$\begin{aligned} \pi = \sum_{p=1}^P \left(\int_A \frac{1}{2} (\{N\}^T \{\epsilon^e\} + \{M\}^T \{\kappa^e\}) dA - \int_A Q w dA \right)_p \\ - B \hat{N}_{xG} \Delta u - \int_0^L \hat{N}_{yG} \Delta v dy \end{aligned} \quad (2.8.22)$$

The pressure load Q_p acting on plate strip p is proportional to a global pressure load parameter β , such that

$$Q_p = \beta \hat{Q}_p \quad (2.8.23)$$

where \hat{Q}_p is a specified unit value for Q_p . The total potential energy is now evaluated in terms of the expanded forms of the displacements (equation (2.8.1)), the mid-surface mechanical strains and curvatures (equations (2.8.3,4)) and the stress resultants (equations (2.8.7,8)) and the substitutions of equations (2.8.17) and (2.8.20) are made. The following equation is obtained:

$$\begin{aligned} \pi = \text{Constant} \\ + \{ q_i \lambda \overline{C}_i^L - \beta C_i^Q - q_j^o \overline{C}_i^j - q_j^o q_k^o \overline{C}_{jk}^i - q_j^o q_k^o q_l^o \overline{C}_{jkl}^i \\ + q_i q_j \lambda \overline{C}_{ij}^L - \beta C_{ij}^Q + \frac{1}{2} \overline{C}_i^j - q_k^o \overline{C}_{ij}^k - q_k^o q_l^o \overline{C}_{ij}^{kl} \\ + q_i q_j q_k (\lambda C_{ijk}^L + \overline{C}_{ij}^k - q_l^o \overline{C}_{ijk}^l) \\ + q_i q_j q_k q_l (\lambda C_{ijkl}^L + \overline{C}_{ijk}^l + \frac{1}{2} \overline{C}_{ij}^{kl}) \} + O(q_i^5) \end{aligned} \quad (2.8.24)$$

where the "Constant" terms are those which do not depend on the modal amplitudes. The coefficients with over-bars are given by

$$\begin{aligned} \overline{C}_i^L &= (C_i^L + B_i C_B^L) - (D_i^L + B_i D_B^L) \\ \overline{C}_i^j &= C_i^j + B_i C_j^B + B_j C_i^B + B_i B_j C_B^B \\ \overline{C}_{ij}^L &= [C_{ij}^L + A_{ij} (C_A^L - C_L^L)] - [D_{ij}^L + A_{ij} (D_A^L - (D_L^L + E_L^L))] \\ \overline{C}_{ij}^k &= C_{ij}^k + A_{ij} (C_k^A - C_k^L) + B_k C_{ij}^B + A_{ij} B_k (C_A^B - C_B^L) \\ \overline{C}_{ijk}^l &= C_{ijk}^l + B_l C_{ijk}^B \\ \overline{C}_{ij}^{kl} &= C_{ij}^{kl} - A_{kl} C_{ij}^L - A_{ij} C_{kl}^L + A_{ij} A_{kl} (C_A^A - 2C_A^L + C_L^L) \end{aligned} \quad (2.8.25)$$

The unbarred coefficients are "primitive" coefficients. Coefficient E_L^L is defined in equation (2.8.18), D_L^L , D_B^L , D_A^L , D_i^L , and D_{ij}^L are defined in equations (2.8.21), the pressure-related coefficients are defined by

$$\begin{aligned} C_i^Q &= \sum_{p=1}^P \left(\int_A \hat{Q} w_i dA \right)_p \\ C_{ij}^Q &= \sum_{p=1}^P \left(\int_A \hat{Q} w_{ij} dA \right)_p \end{aligned} \quad (2.8.26)$$

and the remaining primitive coefficients are defined as illustrated here by two examples:

$$\begin{aligned} C_i^L &= \sum_{p=1}^P \left(\int_A \{N_L\}^T \{\epsilon_i\} dA \right)_p \\ C_{ij}^k &= \sum_{p=1}^P \left(\int_A (\{N_k\}^T \{\epsilon_{ij}\} + \{M_k\}^T \{\kappa_{ij}\}) dA \right)_p \end{aligned} \quad (2.8.27)$$

The primitive coefficient C_{ij}^A which arises in determining equation (2.8.24) is omitted because it is identically zero. Contributions to π which are of order five or greater in the modal amplitudes are henceforth neglected.

The displacement shape functions and their derivatives are known analytically in the x -direction, and are known at discrete points across the y -domain of each plate strip. Thus, in evaluating the various integrals which define the primitive coefficients, analytical integration is performed in the x -direction, and numerical integration (using Simpson's rule) is performed in the y -direction. Numerical integration is performed using quantities evaluated at the discrete points in the transverse plane used for computing the finite-difference solution for the second-order displacement field.

A stationary total potential energy condition is imposed in order to obtain expressions governing equilibrium:

$$\begin{aligned} \delta\pi &= \delta q_i \left(\frac{\partial\pi}{\partial q_i} \right) \\ &= 0 \end{aligned} \quad (2.8.28)$$

Each of the "virtual modal amplitudes," δq_i ($i = 1, 2, \dots$), appearing in equation (2.8.28), is both arbitrary and independent, and thus, in order to satisfy the equation, each expression $\partial\pi/\partial q_i$ must independently be zero. With the selection of a finite basis of M buckling mode shapes for use in the analysis, the following set of simultaneous algebraic equations is obtained:

$$\begin{aligned} \frac{\partial\pi}{\partial q_i} &= (\lambda \hat{C}_i^L + \beta \hat{C}_i^Q - q_j^o \hat{C}_i^j - q_j^o q_k^o \hat{C}_i^{jk} - q_j^o q_k^o q_l^o \hat{C}_i^{jkl}) \\ &\quad + q_j (\lambda \hat{C}_{ij}^L + \beta \hat{C}_{ij}^Q + \hat{C}_{ij} - q_k^o \hat{C}_{ij}^k - q_k^o q_l^o \hat{C}_{ij}^{kl}) \\ &\quad + q_j q_k (\lambda \hat{C}_{ijk}^L + \hat{C}_{ijk} - q_l^o \hat{C}_{ijk}^l) \\ &\quad + q_j q_k q_l (\lambda \hat{C}_{ijkl}^L + \hat{C}_{ijkl}) \\ &= 0 \quad (i = 1, 2, \dots, M) \end{aligned} \quad (2.8.29)$$

where the modified coefficients which appear are given by

$$\begin{aligned}
\hat{C}_i^{jk} &= \bar{C}_{jk}^i \\
\hat{C}_i^{jkl} &= \bar{C}_{jkl}^i \\
\hat{C}_{ij}^k &= 2\bar{C}_{ij}^k \\
\hat{C}_{ij}^{kl} &= 2\bar{C}_{ij}^{kl} \\
\hat{C}_{ijk} &= 2\bar{C}_{ij}^k + \bar{C}_{jk}^i \\
\hat{C}_{ijk}^l &= \bar{C}_{ijk}^l + 2\bar{C}_{jik}^l \\
\hat{C}_{ijkl}^L &= 2(\bar{C}_{ijkl}^L + \bar{C}_{jikl}^L) \\
\hat{C}_{ijkl} &= \bar{C}_{ijk}^l + 2\bar{C}_{jik}^l + \bar{C}_{kl}^i + \bar{C}_{ij}^{kl} + \bar{C}_{jk}^{il} \\
\hat{C}_{ij}^L &= 2\bar{C}_{ij}^L \\
\hat{C}_{ij} &= \bar{C}_i^j \\
\hat{C}_i^L &= \bar{C}_i^L \\
\hat{C}_i^j &= \bar{C}_i^j \\
\hat{C}_{ijk}^L &= \bar{C}_{ijk}^L + 2\bar{C}_{jik}^L \\
\hat{C}_i^Q &= -\bar{C}_i^Q \\
\hat{C}_{ij}^Q &= -2\bar{C}_{ij}^Q
\end{aligned} \tag{2.8.30}$$

Equations (2.8.29) are nonlinear in the modal amplitudes q_j ($j = 1, 2, \dots, M$) and linear in the two load parameters λ and β . The algebraic equations have been derived for general values of the modal imperfection amplitudes q_i^0 ($i = 1, 2, \dots, M$), and thus the equations can be used to explore the structural response in the presence of a variety of imperfection shapes and amplitudes.

2.9 Solution of the Nonlinear Algebraic Equations

2.9.1 Normalization of the variable parameters. Before applying solutions strategies to the set of nonlinear algebraic equations (2.8.29), the variable parameters are normalized so that they take on values of order of magnitude unity. The parameters to be normalized include the set of modal amplitudes $\{q\}$, and the in-plane and pressure load parameters, λ and β , respectively. Each of these is discussed below.

The buckling modes $\{u_i\}$ are normalized before their subsequent use in other parts of the NLPAN analysis, such that the maximum displacement for each mode anywhere in the structure is equal to a specified reference thickness h_{ref} . Thus, the modal amplitudes appearing in equations (2.8.29) are considered to be normalized.

The in-plane load parameter λ is normalized by its critical value associated with primary buckling, λ_1 . Therefore, the normalized in-plane load parameter $\bar{\lambda}$ is given by

$$\bar{\lambda} = \lambda / \lambda_1 \tag{2.9.1}$$

The pressure load parameter β is normalized by a reference value β_{ref} so that the normalized pressure load parameter $\bar{\beta}$ is given by

$$\bar{\beta} = \beta / \beta_{ref} \tag{2.9.2}$$

The reference value is selected to be the value of β which produces a deflection response, in a single-mode NLPAN analysis, having a maximum amplitude in the structure equal to the reference thickness h_{ref} . Thus, in a single mode analysis of the perfect structure using mode number r , if β is set to β_{ref} and λ is set to zero, then the modal response is $|q_r| = 1$. Applying equations (2.8.29), it can be determined that

$$\beta_{ref} = \left| \frac{1}{C_r^Q} (C_{rr} + C_{rrr} + C_{rrrr}) \right| \tag{2.9.3}$$

where the coefficients shown are those defined in equations (2.8.30) with the hats omitted, and where coefficient C_r^Q which would generally appear has been assumed to be negligible compared to coefficient C_r^Q . The mode number r is selected to correspond to the mode which, among those in use, has the coefficient C_r^Q of largest magnitude.

Equations (2.8.29) can now be expressed in terms of the normalized parameters $\bar{\lambda}$ and $\bar{\beta}$. The resulting equations are identical in form to equations (2.8.29) except that $\bar{\lambda}$ and $\bar{\beta}$ replace λ and β , and the

constant coefficients have been transformed in the obvious manner to account for the definitions of $\bar{\lambda}$ and $\bar{\beta}$.

2.9.2 Specification of shape imperfections. After the normalization of the variable parameters is completed, the general form of the nonlinear algebraic equations is unchanged from the original form given in equations (2.8.29). To simplify notation, the notation of equations (2.8.29) is used in this section, where it is understood that the parameters and coefficients which appear are the normalized ones. Once the values for the modal imperfection amplitudes, $\{q^o\}$, are specified, equations (2.8.29) can be written as

$$(C_i^o + \lambda C_i^L + \beta C_i^Q) + q_j(C_{ij}^o + \lambda C_{ij}^L + \beta C_{ij}^Q) + q_j q_k (C_{ijk}^o + \lambda C_{ijk}^L) + q_j q_k q_l (C_{ijkl}^o + \lambda C_{ijkl}^L) = 0 \quad (i = 1, 2, \dots, M) \quad (2.9.4)$$

where

$$\begin{aligned} C_i^o &= -q_j^o C_i^j - q_j^o q_k^o C_i^{jk} - q_j^o q_k^o q_l^o C_i^{jkl} \\ C_{ij}^o &= C_{ij} - q_k^o C_{ij}^k - q_k^o q_l^o C_{ij}^{kl} \\ C_{ijk}^o &= C_{ijk} - q_l^o C_{ijk}^l \end{aligned} \quad (2.9.5)$$

and where the hat symbol ($\hat{}$), appearing over the coefficients in equation (2.8.29), has been dropped here.

Given the shape-imperfection field $\{u^o\}$ the effective modal imperfection amplitudes can be determined by making use of the orthogonality condition for the buckling mode shapes. With the i^{th} buckling mode shape denoted by $\{u_i\} = [u_i \ v_i \ w_i]^T$, this orthogonality condition is given by (see Appendix B equation (B10))

$$\langle \{u_j\}, L(\{u_i\}) \rangle = \begin{cases} b_i, & i = j \\ 0, & i \neq j \end{cases} \quad (2.9.6)$$

where the inner product on the left-hand side of the above equation is given by

$$\langle \{u_j\}, L(\{u_i\}) \rangle = \sum_{p=1}^P \left(\int_A [v_j N_{xL} v_{i,xx} + w_j (N_{xL} w_{i,xx} + N_{yL} w_{i,yy})] dA \right)_p \quad (2.9.7)$$

where p is the plate strip index number, P is the total number of plate strips, A is the planform area of a plate strip, and N_{xL} and N_{yL} are the in-plane stress resultants corresponding to the unit pre-buckling solution. Express $\{u^o\}$ as a series in the buckling mode shapes,

$$\{u^o\} = \sum_{i=1}^M q_i^o \{u_i\} \quad (2.9.8)$$

and evaluate the following inner product with consideration of the orthogonality condition:

$$\begin{aligned} \langle \{u^o\}, L(\{u_i\}) \rangle &= \sum_{j=1}^M q_j^o \langle \{u_j\}, L(\{u_i\}) \rangle \\ &= q_i^o b_i \quad (i = 1, 2, \dots, M) \end{aligned} \quad (2.9.9)$$

where no summation over i is intended. Hence, the modal imperfection amplitudes are given by

$$q_i^o = \frac{1}{b_i} \langle \{u^o\}, L(\{u_i\}) \rangle \quad (i = 1, 2, \dots, M) \quad (2.9.10)$$

The computation of the coefficient b_i is performed in the NLPAN program for all modes. The evaluation of the inner product of equation (2.9.10) is more challenging, since the shape-imperfection field is not generally known as a continuous function, but is more likely known as a set of values at discrete points,

or is known along a set of discrete lines on the surface of the structure. No attempt has been made in NLPAN to automate the computation of q^* based on a measured imperfection field.

2.9.3 Asynchronous control of in-plane and pressure loads. For the general case of combined in-plane and pressure loading, the nonlinear algebraic equations governing equilibrium (equations (2.9.4)) contain the two load parameters λ and β . A single load parameter, Λ , is used when applying the nonlinear solution strategies discussed in the next section. This section describes a procedure for relating λ and β to Λ in a way which permits the modelling of asynchronous application of the two types of loading.

A series of load ranges is specified in terms of target values for λ and β : $(0, 0)$, (λ_1, β_1) , (λ_2, β_2) , Over the k^{th} load range, λ and β vary linearly with Λ as Λ varies from 0 to 1:

$$\begin{pmatrix} \lambda \\ \beta \end{pmatrix} = \begin{pmatrix} \lambda_{k-1} \\ \beta_{k-1} \end{pmatrix} + \Lambda \begin{pmatrix} \lambda_k - \lambda_{k-1} \\ \beta_k - \beta_{k-1} \end{pmatrix} \quad 0 \leq \Lambda \leq 1 \quad (2.9.11)$$

Equation (2.9.11) is used to express λ and β in equation (2.9.4) in terms of Λ , and terms are regrouped to obtain equations with the following form which governing equilibrium over the k^{th} load range:

$$\begin{aligned} (\bar{C}_i + \Lambda \bar{C}_i^L) + q_j(\bar{C}_{ij} + \Lambda \bar{C}_{ij}^L) + q_j q_k(\bar{C}_{ijk} + \Lambda \bar{C}_{ijk}^L) \\ + q_j q_k q_l(\bar{C}_{ijkl} + \Lambda \bar{C}_{ijkl}^L) = 0 \quad (i = 1, 2, \dots, M) \end{aligned} \quad (2.9.12)$$

Details of this procedure are given in Appendix D Section D.1, where it is noted that there are some obvious differences in notation. Equations (D3), (D5), and (D6) of Appendix D correspond to equations (2.9.4), (2.9.11), and (2.9.12), respectively.

2.9.4 Nonlinear solution strategies. The solution of the system of nonlinear algebraic equations governing equilibrium (equations (2.9.4)) can in many cases be performed using Newton-Raphson iteration. In some important cases, however, limit-point behavior or solution branching is encountered, and Newton-Raphson iteration breaks down in the vicinity of associated critical-stability points. Consequently, advanced solutions strategies for the analysis of nonlinear equilibrium behavior have been implemented in NLPAN. The implementation of the strategies is the subject of Appendix D, which was extracted from [16]. The two basic strategies incorporated are the arc-length control method popularized by Riks [17] and the equivalence transformation method developed by Thurston [18]. An integrated procedure is obtained which allows equilibrium solution paths to be followed past limit points, and through regions of complex solution branching involving modal interaction.

The implementation of the solution strategies has been found to be fairly robust, with a few qualifications mentioned here. The solution strategies require the specification of several parameter values which, for example, control the solution step size, and determine cutoff values used for determining the proximity and classification of critical stability points. On occasion, the solution strategies are "fooled" into making an improper diagnosis, and the solution stepping will proceed along an inappropriate solution path. An adjustment of the input parameter values will generally fix this problem. This type of difficulty arises when very small modal imperfection amplitudes are used, or when there are very small effective imperfection values arising due to numerical error. The use of significant modal imperfection amplitudes ($q^* \geq .01$) tends to improve the reliability of the solution procedures.

It has also been found on occasion that a solution path will lead into a web of unstable equilibrium paths from which the solution strategies are unable to guide the analysis. This behavior occurs in the highly nonlinear regime (such as deep postbuckling), and is believed to be associated with the use of an insufficient set of buckling modes as shape functions. If the tangent stiffness matrix becomes singular for the second eigenvalue (indicating that this troublesome behavior is being encountered), the NLPAN analysis is terminated, and a warning message is issued.

3. EXTENSIONS TO THE METHOD OF ANALYSIS

3.1 Dynamic Snap Analysis

The nonlinear analysis of NLPAN is designed to predict the equilibrium response of a structure which is subjected to a varying load level, and thus there is an assumption made that the time rate of loading is sufficiently small so that inertial effects are negligible. The methods of Riks [17] and Thurston [18] have been implemented for following the equilibrium solution paths past limit points and bifurcation points, and the ability to track unstable equilibrium paths has been achieved (see Appendix D). While a physical structure will not follow an unstable equilibrium path, following such a path with the analysis will sometimes reveal a second path or path segment exhibiting stable equilibrium. In this situation, the physical structure is assumed to exhibit a dynamic snap from the original stable path to the second stable path, departing the original path at the point where the equilibrium becomes unstable.

In some test cases modelled using NLPAN, the analysis follows an unstable equilibrium path to secondary limit points or bifurcation points where there is no transition back to solutions of stable equilibrium. This situation is detected when the second eigenvalue of the tangent stiffness matrix goes to zero. The process of trying to navigate through such a complex regime of solution paths (in search of the desired path of stable equilibrium) is difficult to automate, and is also of questionable wisdom since the solution paths represent structural behavior which will never be encountered. The snap phenomenon is a dynamic event, and by analyzing it as such, the difficulties encountered in following equilibrium paths are avoided. This reasoning provided the motivation for incorporating a dynamic analysis capability along with the static analysis capabilities already in place.

In the time since this undertaking was proposed and initiated, a change in thinking has taken place in the mind of this investigator. The primary mode of response for which the dynamic solution capability was desired is that of the change in waveform which occurs in structures dominated by local-buckling behavior (as opposed to global column- or wide-column-type buckling). A study of the literature has shown that the accurate representation of secondary instability behavior generally requires the use of a relatively large number of appropriately selected mode shapes as global shape functions (see, for example, [19]). While NLPAN employs rigorous criteria for determining critical stability points, it incorporates no strategy for selecting the crucial modes required for accuracy, and NLPAN is also limited to a relatively small number of included modes. For these reasons, a dynamic analysis capability has been judged to have relatively little practical value in the NLPAN code. The dynamic analysis capability detailed in this section has been coded in NLPAN to the extent of computing the generalized mass and damping coefficients, but the full solution procedure has not been implemented.

The theory for the dynamic snap analysis is presented here. The goal of the dynamic analysis is to locate the new equilibrium position sought by the structure during the snap, so the accuracy of the dynamic analysis is not considered to be of extreme importance, and some simplifying assumptions are thus made. The dynamic analysis is performed at a fixed value of the generalized load parameter Λ (defined in Section 2.9.3), namely the value at which the equilibrium path becomes unstable. Motion-damping forces are incorporated. In the following sections, the equations of motion are first developed, and then a solution procedure is described.

3.1.1 Equations of motion. Hamilton's principle (as it is presented in [20]) is applied to obtain the equations of motion. Let T be the kinetic energy of the system, and let δW be the external virtual work done on the system, which is broken down as follows:

$$\delta W = -\delta\pi + \delta W_{nc} \quad (3.1.1)$$

where $\delta\pi$ is the first variation of the total potential energy for the conservative elastic system and the specified loads (see equation (2.8.28)), and δW_{nc} is the external virtual work of non-conservative forces, which in this situation are the motion-damping forces. Hamilton's principle can then be stated as

$$\int_{t_1}^{t_2} (\delta T + \delta W) dt = 0 \quad \text{subject to} \quad \{\delta u\} = 0 \quad \text{at} \quad t = t_1, t_2 \quad (3.1.2)$$

where t_1 and t_2 are two reference times, $t_1 < t_2$. Using equations (3.1.1) and (3.1.2), Hamilton's principle is re-expressed in its negative form as

$$\int_{t_1}^{t_2} (\delta \pi - \delta W_{nc} - \delta T) dt = 0 \quad \text{subject to} \quad \{\delta u\} = 0 \quad \text{at} \quad t = t_1, t_2 \quad (3.1.3)$$

The kinetic energy is taken to be that associated with motion of the mid-surfaces of the plate strips in the transverse (y- and z-) directions. This is written as

$$T = \sum_{p=1}^P \left(\int_A \frac{1}{2} m (\dot{v}^2 + \dot{w}^2) dA \right)_p \quad (3.1.4)$$

where m is the mass per unit area of a plate strip, p is the index number of a plate strip, P is the total number of plate strips, and \dot{f} denotes the derivative of function f with respect to time. Using integration by parts and imposing the constraints $\{\delta u\} = 0$ at $t = t_1$ and $t = t_2$, the following expression is obtained:

$$\int_{t_1}^{t_2} (\delta T) = - \int_{t_1}^{t_2} \sum_{p=1}^P \left(\int_A m (\ddot{v} \delta v + \ddot{w} \delta w) dA \right)_p dt \quad (3.1.5)$$

In evaluating the right-hand side of the above equation, only the first-order contributions to the displacements v and w (see equation (2.4.1)) are taken into account, to arrive at

$$\int_{t_1}^{t_2} (\delta T) = - \int_{t_1}^{t_2} \left(\sum_{i=1}^M \delta q_i \sum_{j=1}^M \ddot{q}_j \ddot{C}_{ij} \right) dt \quad (3.1.6)$$

where

$$\ddot{C}_{ij} = \sum_{p=1}^P \left(\int_A m (v_i v_j + w_i w_j) dA \right)_p \quad (3.1.7)$$

A non-conservative motion damping force is assumed to act normal to a plate surface in the direction opposite its normal velocity. The force per unit area is assumed to equal the normal velocity, \dot{w} , times a damping coefficient, μ , which has the units of force per unit area per unit velocity. The non-conservative virtual work is thus given by

$$\delta W_{nc} = - \sum_{p=1}^P \left(\int_A \mu \dot{w} \delta w dA \right)_p \quad (3.1.8)$$

In evaluating the right-hand side of the above equation, only the first-order contributions to the displacement w are taken into account, to arrive at

$$\delta W_{nc} = - \sum_{i=1}^M \delta q_i \sum_{j=1}^M \dot{q}_j \dot{C}_{ij} \quad (3.1.9)$$

where

$$\dot{C}_{ij} = \sum_{p=1}^P \left(\int_A \mu w_i w_j dA \right)_p \quad (3.1.10)$$

With the generalized load Λ held constant at the critical value Λ^* (the value at which equilibrium becomes unstable), $\delta\pi$ can be written as

$$\delta\pi = \delta q_i (C_i + q_j C_{ij} + q_j q_k C_{ijk} + q_j q_k q_l C_{ijkl}) \quad (3.1.11)$$

where summation over repeated indices is implied, and the coefficients appearing in equation (3.1.11) are related to the coefficients defined in equations (2.9.12) by

$$\begin{aligned} C_i &= (\Lambda^* \tilde{C}_i^L + \tilde{C}_i^o) & C_{ijk} &= (\Lambda^* \tilde{C}_{ijk}^L + \tilde{C}_{ijk}^o) \\ C_{ij} &= (\Lambda^* \tilde{C}_{ij}^L + \tilde{C}_{ij}^o) & C_{ijkl} &= (\Lambda^* \tilde{C}_{ijkl}^L + \tilde{C}_{ijkl}^o) \end{aligned} \quad (3.1.12)$$

Equations (3.1.6), (3.1.9), and (3.1.11) are now substituted into equation (3.1.3):

$$\int_{t_1}^{t_2} \delta q_i (C_i + q_j C_{ij} + q_j q_k C_{ijk} + q_j q_k q_l C_{ijkl} + \ddot{q}_j \tilde{C}_{ij} + \dot{q}_j \dot{C}_{ij}) dt = 0, \text{ subject to } \{\delta u\} = 0 \text{ at } t = t_1, t_2 \quad (3.1.13)$$

The time interval $[t_1, t_2]$ of equation (3.1.13) is arbitrary, and each of the virtual modal amplitudes δq_i ($i = 1, 2, \dots$) is both arbitrary and independent, so that the equations governing motion at a fixed level of the generalized load can be reduced to

$$\begin{aligned} \ddot{q}_j \tilde{C}_{ij} + \dot{q}_j \dot{C}_{ij} + q_j C_{ij} + q_j q_k C_{ijk} + q_j q_k q_l C_{ijkl} + C_i &= 0 \\ (i = 1, 2, \dots, M) \end{aligned} \quad (3.1.14)$$

Initial values of the generalized coordinates and their time derivatives, $\{q\}_{t=0}$ and $\{\dot{q}\}_{t=0}$, respectively, must accompany the equations of motion. One approach is to set the former equal to the critical stability solution $\{q^*\}$ and set the later to

$$\{\dot{q}\}_{t=0} = \varepsilon \{\phi^1\} \quad (3.1.15)$$

where $\{\phi^1\}$ is the eigenvector corresponding to the zero eigenvalue of the tangent stiffness matrix, and ε is a small non-zero number.

3.1.2 Solution of the equations of motion. The Newmark direct integration procedure, as presented in Ref. [21], is used to obtain a series of discrete solutions to the initial value problem stated above. A uniform time increment, Δt , is used. Index n denotes the current time step number, at which the solution is known, and $n+1$ is the index number of the following time step, at which a solution is sought. The Newmark procedure uses two somewhat arbitrary parameters, α and β , that determine the exact form of the time-derivative approximations used. The following parameter values are used here: $\alpha = 1/2$, and $\beta = 1/4$. This leads to the following time-derivative approximations:

$$\dot{q}_i^{n+1} = \dot{q}_i^n + \frac{\Delta t}{2} (\ddot{q}_i^n + \ddot{q}_i^{n+1}) \quad (3.1.16)$$

$$q_i^{n+1} = q_i^n + \Delta t \dot{q}_i^n + \frac{\Delta t^2}{4} (\ddot{q}_i^n + \ddot{q}_i^{n+1}) \quad (3.1.17)$$

Equation (3.1.17) is solved for \ddot{q}_i^{n+1} :

$$\ddot{q}_i^{n+1} = a_0 q_i^{n+1} - a_0 q_i^n - a_1 \dot{q}_i^n - \ddot{q}_i^n \quad (3.1.18)$$

where

$$a_0 = \frac{4}{\Delta t^2} \quad a_1 = \frac{4}{\Delta t} \quad (3.1.19)$$

By expressing equation (3.1.14) at time step number $n+1$ and eliminating $\{\dot{q}^{n+1}\}$ and $\{\ddot{q}^{n+1}\}$ using equations (3.1.16) and (3.1.18), the following equations are obtained:

$$(a_o\ddot{C}_{ij} + a_o b_2 \dot{C}_{ij} + C_{ij})q_j^{n+1} + C_{ijk}q_j^{n+1}q_k^{n+1} + C_{ijk}q_j^{n+1}q_k^{n+1}q_l^{n+1} = E_i \quad (3.1.20)$$

$(i = 1, 2, \dots, M)$

where

$$E_i = -C_i + \ddot{C}_{ij}(a_o q_j^n + a_1 \dot{q}_j^n + \ddot{q}_j^n) + \dot{C}_{ij}(a_o b_2 q_j^n + \dot{q}_j^n) \quad (3.1.21)$$

and

$$b_2 = \frac{\Delta t}{2} \quad (3.1.22)$$

Equation (3.1.20) serves as the basis for determining the solution $\{q^{n+1}\}$ in terms of known quantities. Once $\{q^{n+1}\}$ is known, the time-derivatives $\{\dot{q}^{n+1}\}$ and $\{\ddot{q}^{n+1}\}$ can be determined by applying equations (3.1.18) and (3.1.16) in sequence.

The solution $\{q^{n+1}\}$ can be determined using Newton-Raphson iteration. Let $\{q^r\}$ be the r^{th} estimate for $\{q^{n+1}\}$ in the iterative solution procedure. The residual error vector and the tangent stiffness matrix for the r^{th} solution, denoted $\{R^r\}$, and $[K^r]$, respectively, are given by

$$R_i^r = (a_o\ddot{C}_{ij} + a_o b_2 \dot{C}_{ij} + C_{ij})q_j^r + C_{ijk}q_j^r q_k^r + C_{ijk}q_j^r q_k^r q_l^r - E_i \quad (3.1.23)$$

and

$$K_{ij}^r = \left. \frac{\partial R_i^r}{\partial q_j} \right|_{\{q^r\}} \quad (3.1.24)$$

$$= a_o\ddot{C}_{ij} + a_o b_2 \dot{C}_{ij} + C_{ij} + q_k^r(C_{ijk} + C_{ikj}) + q_k^r q_l^r(C_{ijkl} + C_{ikjl} + C_{iljk})$$

The improved solution, $\{q^{r+1}\}$, is then given by

$$\{q^{r+1}\} = \{q^r\} + \{\Delta q\} \quad (3.1.25)$$

where the correction, $\{\Delta q\}$, is given by

$$\{\Delta q\} = -[K^r]^{-1}\{R^r\} \quad (3.1.26)$$

Iteration is continued until the correction $\{\Delta q\}$ becomes negligible compared to the solution $\{q^{r+1}\}$.

The damping coefficient μ and the time increment Δt should be selected based on characteristic aspects of the dynamic response. Criteria for selecting these two parameters are not considered here.

3.2 Thermal Loading

The capability of modelling thermal loading has been incorporated in NLPAN for the case where each plate strip is subjected to a uniform temperature. ("Temperature" as used here refers to a change in temperature relative to a reference value). Each plate strip may have its own temperature value, but the temperatures in all plate strips are proportional to a single thermal-load parameter. Thermal loading may be used in conjunction with any option for control of the generalized in-plane loading (see Table 1). Thermal loading is controlled independently of the generalized in-plane loading.

This section is devoted to describing an additional contribution to the expanded form of the displacements (equation (2.4.1)) necessary for simulating thermal loading. The incorporation of the thermal load contribution into the final problem formulation is described in Section 3.5.

A unit temperature \hat{T} is specified for each plate strip, and this value may be different from plate strip to plate strip. The thermal load parameter γ is used in the nonlinear analysis, and the temperature change experienced by a given plate strip is then $T = \gamma \hat{T}$.

When non-zero thermal loading is present, the expanded form of the displacements on each plate strip has an additional contribution $\gamma\{u_T\}$ as shown here:

$$\{u\} = \lambda\{u_L\} + \gamma\{u_T\} + q_i\{u_i\} + q_j q_j\{u_{ij}\} \quad (3.2.1)$$

where $\{u_T\} = [u_T \ v_T \ 0]^T$ is a displacement solution corresponding to the unit temperature system. Solution $\{u_T\}$ is a linear, unbuckled solution which satisfies the homogeneous in-plane boundary conditions. As with the unit solution $\{u_L\}$ described in Section 2.5, the bending in the component plate strips is constrained to be zero for the solution $\{u_T\}$.

The expanded form of the mid-surface strains has a new contribution $\gamma\{\epsilon_T\}$ shown in the following equation:

$$\{\epsilon\} = \lambda\{\epsilon_L\} + \gamma\{\epsilon_T\} + (q_i - q_i^0)\{\epsilon_i\} + \dots \quad (3.2.2)$$

where

$$\{\epsilon_T\} = \begin{Bmatrix} u_{T,x} \\ v_{T,y} \\ 0 \end{Bmatrix} \quad (3.2.3)$$

Equation (3.2.2) gives the mid-surface strains relative to the imperfect reference configuration. For a given plate strip, the in-plane mechanical strains associated with the unit response, $\{\epsilon_T^m\}$, are given by the difference between the actual strains and the thermal strains for an unconstrained plate strip:

$$\{\epsilon_T^m\} = \{\epsilon_T\} - \hat{T}\{\alpha\} \quad (3.2.4)$$

where $\{\alpha\} = [\alpha_x \ \alpha_y \ 0]^T$ are the coefficients of thermal expansion for the plate strip. Therefore mid-surface mechanical strains $\{\epsilon^m\}$, which compensate for both imperfections and thermal loading, contain the contribution $\gamma\{\epsilon_T^m\}$:

$$\{\epsilon^m\} = \lambda\{\epsilon_L\} + \gamma\{\epsilon_T^m\} + (q_i - q_i^0)\{\epsilon_i\} + \dots \quad (3.2.5)$$

The in-plane stress resultants reflect thermal loading by the presence of a new contribution, included in the following equation:

$$\{N\} = \lambda\{N_L\} + \gamma\{N_T\} + (q_i - q_i^0)\{N_i\} + \dots \quad (3.2.6)$$

where

$$\{N_T\} = [A]\{\epsilon_T^m\} \quad (3.2.7)$$

and $[A]$ is defined in equation (2.1.12). The formulae for determining the complete unit thermal solution are developed in detail in Appendix A, Section A.2.

3.3 Rotationally Elastic End Support

Rotationally elastic support of the longitudinal ends is simulated using linear rotational springs located at discrete points at the ends of the panel. Spring locations are specified in terms of points on the cross-section, denoted as y_k , where k is the index number of the spring, and y is used here as a generalized transverse in-plane coordinate (ie. y signifies both a particular plate strip and a point along its local y -axis). Springs of specified strength are then simulated at these points on the cross-section of both longitudinal ends. A spring with rotational stiffness K_* resists $\partial u / \partial y$ (in-plane) rotation, and a spring with rotational stiffness K_w resists $\partial w / \partial x$ (out-of-plane) rotation.

Assume that springs of the two types mentioned are present, with stiffnesses, placement, and generalized deformation given by K_u^n, y^n, u_y^n ($n = 1, 2, \dots, N$) for the first spring type, and K_w^r, y^r, w_x^r ($r = 1, 2, \dots, R$) for the second spring type. The elastic strain energy U associated with these springs is given by

$$U = \sum_{n=1}^N \frac{K_u^n}{2} (u_y^n - (u_y^n)^0)^2 \Big|_{x=0,L} + \sum_{r=1}^R \frac{K_w^r}{2} (w_x^r - (w_x^r)^0)^2 \Big|_{x=0,L} \quad (3.3.1)$$

where it is assumed that the springs are unloaded at the rest state of the imperfect structure, $\{u\} = \{u^0\}$. Using the expanded form for displacements along with the functional form of the various shape functions (see equations (2.4.1), (2.6.7), and (2.7.4)), equation (3.3.1) is evaluated and expressed as

$$U = \text{Constant} + \left(\frac{1}{2} q_i q_j - q_i q_j^0 \right) (F_{ij}^u + F_{ij}^w) \quad (3.3.2)$$

where summation over the repeated indices is implied, the "Constant" term has no dependence on the modal amplitudes, and

$$F_{ij}^u = [1 + (-1)^{m_i} (-1)^{m_j}] \sum_{n=1}^N K_u^n (\xi_i' \xi_j') \Big|_{y^n} \quad (3.3.3)$$

$$F_{ij}^w = [1 + (-1)^{m_i} (-1)^{m_j}] \left(\frac{\pi}{L} \right)^2 m_i m_j \sum_{r=1}^R K_w^r (\phi_i \phi_j) \Big|_{y^r}$$

where functions $\xi(y)$ and $\phi(y)$ are the y -dependent portions of the eigenfunction components $u(x, y)$ and $w(x, y)$, respectively (see equation (2.6.7)), and f' denotes differentiation of function f with respect to y .

The elastic strain energy of the springs given in equation (3.3.2) is added to the total potential energy of the structure. To obtain the stationary total potential energy condition governing equilibrium, the following derivative is required:

$$\frac{\partial U}{\partial q_i} = (q_j - q_j^0) (F_{ij}^u + F_{ij}^w) \quad (3.3.4)$$

Comparing equation (3.3.4) with equation (2.8.29), it can be seen that to account for the elastic support discussed here, each ij^{th} coefficient \hat{C}_{ij} and \hat{C}_i of equation (2.8.29) is augmented by the quantity $(F_{ij}^u + F_{ij}^w)$.

3.4 Constraint of the End Displacements

The buckling analysis of VIPASA simulates an infinite-length prismatic structure supported at uniform intervals along the length against transverse buckling displacements. It is the conventional assumption that the buckling eigensolutions will model closely the behavior of a finite-length structure if the halfwave lengths of the buckling modes are selected to be integer fractions of the length of the panel. The ends of the finite-length structure are assumed to be simply supported (see Section 2.3.2). In an effort to extend the method of NLPAN to structures with a greater variety of end-support conditions, a method has been developed for imposing constraints on certain generalized displacement components at the longitudinal ends of the structure. By using appropriately selected sets of buckling modes as shape functions and applying the generalized displacement constraints, a greater variety of end-support conditions can be simulated.

Two different types of displacement constraints can be imposed at the ends of a panel in order to simulate three different types of support conditions. With the first type of constraint, the axial displacement u at specified points on the end of a panel is required to be equal to the effective axial dis-

placement of the panel end. This type of constraint is used to simulate either eccentric application of the end load (taken with respect to the neutral bending axis of the panel) or clamping of the panel end against wide-column buckling motion. With the second type of constraint, the slope $\partial w/\partial x$ is constrained to be zero at a set of specified points at the ends of the panel. This type of constraint is used to simulate clamping of individual plate elements against out-of-plane rotation. The derivation of the constraint equations for both types of constraints is presented in this section. The incorporation of the constraints into the general procedure of obtaining equilibrium solutions is described in Section 3.5.

The individual VIPASA buckling modes used as shape functions are not suitable for modelling the response of a structure having the modified forms of end support mentioned above. However, using a set of appropriately selected shape functions in conjunction with a set of generalized displacement constraints, the desired types of response can be simulated. The point constraints are satisfied exactly, so in order to avoid having an over-constrained system, the number of point constraints must be fewer than the number of shape functions affected by the constraints. To simulate a stiffened structure with clamped ends, it is recommended to constrain the gross rotation of the ends using a couple of strategically placed axial constraints. The zero-slope constraint is suitable for simulating a simple rectangular plate with clamped ends. It is unwise to mix the two types of displacement constraints because the number of shape functions needed to provide meaningful results becomes excessively large.

3.4.1 Constraints on axial displacements. Locations at which the axial displacements are constrained are specified in terms of points y_k on the cross-section, where k is the index number of the point on the cross-section, and y is used here as a generalized transverse in-plane coordinate (ie. y signifies both a particular plate strip and a point along its local y -axis). The displacement u is constrained at these cross-sectional points, at both longitudinal ends, to be equal to the effective axial displacement of the respective panel end. In the current implementation, when axial displacement constraints are used it is required that displacement control of the in-plane loading be used (CTRL='D' in Table 1). With this limitation, the effective change in length Δu_{eff} is given by

$$\Delta u_{eff} = \lambda \Delta u_L \quad (3.4.1)$$

where λ is the displacement-control parameter, and Δu_L is the value of Δu corresponding to the linear response to the unit in-plane load system.

An additional contribution must be added to the general expanded displacement form given in equation (2.4.1) or equation (2.8.1) for the following reason. The axial component of the primary shape functions (VIPASA eigenfunctions) denoted $u_i(x, y)$, has the following functional form on each plate strip of the structural model:

$$u_i = \xi_i(y) \cos \frac{m_i \pi x}{L} \quad (i = 1, 2, \dots, M) \quad (3.4.2)$$

where m_i is the longitudinal halfwave number of the mode shape. The effective neutral bending axis of the panel is determined by the zeros of the functions $\xi_i(y)$ (one function on each plate strip), since these zeros identify points on the panel end about which the end rotates during buckling. If the axial displacement of arbitrary points of the panel ends are to be constrained to zero in such a way as to simulate a different, eccentric, line of load application, then a corrective displacement contribution must be included which effectively shifts the zeros of the functions $\xi_i(y)$ from their original locations to new, specified, locations. For cases in which the modified function $\tilde{u}_i = u_i + B_i u_b$ is used (see Section 2.6), the contribution $B_i u_b$ is included in evaluating the axial displacements at the ends.

The corrective contribution to displacements $\{u\}$ is taken to be $q_e \{u_L\}$, where $\{u_L\}$ is the linear unbuckled response of the panel to the unit in-plane load system (see Section 2.5), and where q_e is an initially unknown amplitude parameter. The expanded form of the displacements is now given by

$$\{u\} = \lambda \{u_L\} + q_e \{u_L\} + q_i \{\tilde{u}_i\} + q_j \{u_{ij}\} \quad (3.4.3)$$

where summation over repeated indices is implied, and

$$\{\tilde{u}_i\} = \{u_i\} + B_i\{u_B\} \quad (3.4.4)$$

Note that $\{\tilde{u}_{ij}\}$ which appears in equation (2.8.1) is replaced here by $\{u_{ij}\}$. This is because the restriction to displacement control (CONTRL='D' in Table 1) enforced here results in the equivalence of $\{\tilde{u}_{ij}\}$ and $\{u_{ij}\}$ (see Table 4). In anticipation of later developments, parameter q_e is represented as a series in the modal amplitudes, q_i :

$$q_e = L_i q_i \quad (3.4.5)$$

where summation over i is implied, and L_i ($i = 1, 2, \dots, M$) are constant coefficients. The displacement now are written as

$$\{u\} = \lambda\{u_L\} + q_i\{\hat{u}_i\} + q_j\{u_{ij}\} \quad (3.4.6)$$

where

$$\{\hat{u}_i\} = \{u_i\} + B_i\{u_B\} + L_i\{u_L\} \quad (3.4.7)$$

The condition at each constrained point is stated as follows: the displacement u , minus the initial value associated with imperfections u^o , minus a second value u^f associated with a stress-producing forced rotation of the panel ends, is equal to the effective axial displacement of the panel end:

$$(u^k - (u^o)^k - (u^f)^k) = \lambda u_L \quad \begin{matrix} (k = 1, 2, \dots, K) \\ (x = 0, L) \end{matrix} \quad (3.4.8)$$

where $u^k = u(y^k)$, and K is the number of cross-sectional stations at which displacements are constrained.

It is noted that because of the functional form of u_{ij} ,

$$u_{ij}|_{x=0} = u_{ij}|_{x=L} \equiv 0 \quad (3.4.9)$$

The constraint equations (3.4.8) are evaluated in terms of the form for u of equation (3.4.6) and the simplification of equation (3.4.9) is applied, providing the following condition:

$$(q_i - q_i^o - q_i^f)(u_i^k + B_i u_B + L_i u_L) = 0 \quad \begin{matrix} (k = 1, 2, \dots, K) \\ (x = 0, L) \end{matrix} \quad (3.4.10)$$

where the parameters q_i^f are modal amplitudes used to specify forced rotation of the panel ends. Using the functional form for u_i of equation (3.4.2),

$$\begin{aligned} u_i|_{x=0} &= \xi_i(y) \\ u_i|_{x=L} &= (-1)^{m_i} \xi_i(y) \end{aligned} \quad (3.4.11)$$

If m_i is odd, then the corresponding values of B_i and L_i may be non-zero. However if m_i is even then the corresponding value B_i is zero (see Section 2.6), and it is stated in anticipation that the corresponding value L_i is also zero. Equation (3.4.10) evaluated at $x = 0$ is subtracted from equation (3.4.10) evaluated at $x = L$, and the substitutions of equation (3.4.11) are used, to obtain

$$\sum_{i=o_1, o_2, \dots} (q_i - q_i^o - q_i^f)(-2\xi_i^k + B_i \Delta u_B + L_i \Delta u_L) = 0 \quad (k = 1, 2, \dots, K) \quad (3.4.12)$$

where $\xi_i^k = \xi_i(y^k)$, parameters o_1, o_2, \dots are the index numbers of modes for which m_i is odd, and Δu_L and Δu_B are the contributions to Δu (the change in panel length) due to u_L and u_B , respectively.

The coefficients L_i are determined by arbitrarily requiring that the first equation ($k = 1$) of equations (3.4.12) be satisfied identically for any value of the modal amplitudes q_i . The quantity inside the right set of parenthesis is set to zero for each value i , and parameters L_i are determined to be

$$L_i = \frac{2\xi_i^k}{\Delta u_L} - B_i \frac{\Delta u_B}{\Delta u_L} \quad \begin{matrix} (k=1) \\ (i = o_1, o_2, \dots) \end{matrix} \quad (3.4.13)$$

If K is greater than one, then the remaining $K - 1$ non-trivial constraint equations are obtained by substituting L_i of equation (3.4.13) into equation (3.4.12). The final form obtained is

$$(q_i - q_i^o - q_i^f)E_{ki} = 0 \quad (k = 2, 3, \dots, K) \quad (3.4.14)$$

where

$$E_{ki} = \begin{cases} (-2\xi_i^k + B_i \Delta u_B + L_i \Delta u_L) & (i = o_1, o_2, \dots) \\ 0 & (i = e_1, e_2, \dots) \end{cases} \quad (3.4.15)$$

where e_1, e_2, \dots are the index numbers of modes for which m_i is even.

Next, equation (3.4.10) evaluated at $x=0$ is added to equation (3.4.10) evaluated at $x=L$, and the substitutions of equation (3.4.11) are used. Noting that B_i and L_i are both zero for $i = e_1, e_2, \dots$, the result is

$$\sum_{i=e_1, e_2, \dots} (q_i - q_i^o - q_i^f)(2\xi_i^k) = 0 \quad (k = 1, 2, \dots, K) \quad (3.4.16)$$

These equations are distinct from equations (3.4.14), but can be expressed in the same form:

$$(q_i - q_i^o - q_i^f)E_{ki} = 0 \quad (k = 1, 2, \dots, K) \quad (3.4.17)$$

where

$$E_{ki} = \begin{cases} 2\xi_i^k & (i = e_1, e_2, \dots) \\ 0 & (i = o_1, o_2, \dots) \end{cases} \quad (3.4.18)$$

3.4.2 Constraints on out-of-plane rotation. The locations at which out-of-plane rotation is constrained are specified in terms of points y_k on the cross-section, where k is the index number of the point and y is used here as a generalized transverse in-plane coordinate (ie. y signifies both a particular plate strip and a point along its local y -axis). The rotation $\partial w / \partial x$ (referred to a local plate-strip coordinate system) is constrained at these points on both longitudinal ends of the cross-section. At each end of the panel, K constraint conditions are imposed:

$$w_{,x}^k = (w_{,x}^o)^k + (w_{,x}^f)^k \quad \begin{matrix} (k = 1, 2, \dots, K) \\ (x = 0, L) \end{matrix} \quad (3.4.19)$$

where $w_{,x}^k$ is the slope at the cross-sectional station y^k , $w_{,x}^o$ corresponds to the imperfection shape of the panel, and $w_{,x}^f$ corresponds to a forced rotation of the ends. When equation (3.4.19) is evaluated in terms of the expanded form for w and the functional forms for w_i and w_{ij} , the constraint equations at $x=0$ have the form

$$(q_i - q_i^o - q_i^f)m_i\phi_i^k = 0 \quad (k = 1, 2, \dots, K) \quad (3.4.20)$$

and the constraint equations at $x=L$ have the form

$$(q_i - q_i^o - q_i^f)(-1)^{m_i}m_i\phi_i^k = 0 \quad (k = 1, 2, \dots, K) \quad (3.4.21)$$

where summation over i is implied, m_i is the halfwave number of the i^{th} buckling mode shape, $\phi_i(y)$ is the y -dependent function corresponding to $w_i(x, y)$ (see Section 2.6), $\phi_i^k = \phi_i(y^k)$, and $\{q^f\}$ is a set of model amplitudes used to specify a forced rotation of the panel ends. There are $2K$ constraint equations; however if halfwave numbers m_i are either all even or all odd, then the two sets of constraint equations

(3.4.20) and (3.4.21) are equivalent, and there are only K independent constraint conditions. Each of the K or $2K$ constraint equations can be written in the form

$$(q_i - q_i^o - q_i^f)E_{ki} \quad (3.4.22)$$

where

$$E_{ki} = m_i \phi_i^k \quad (k = 1, 2, \dots, K) \quad (3.4.23)$$

and, if both odd and even values of m_i are present,

$$E_{ki} = (-1)^{m_i} m_i \phi_i^k \quad (k = K + 1, K + 2, \dots, 2K) \quad (3.4.24)$$

3.5 Solution Procedure with Thermal Loading and Displacement Constraints

This section describes modifications to the NLPAN problem formulation and solution procedures necessary to accommodate thermal loading and/or displacement constraints. The nature of the thermal loading, and the associated additions to the assumed form of the displacements, are discussed in Section 3.2. The nature of the displacement constraints, the displacement-constraint equations, and the associated modifications to the assumed form of the displacements, are all discussed in Section 3.4. In this section, the general form of the displacements which accounts for the new features is used to form a new total potential energy expression, and the constraint equations are incorporated by using the Lagrange multiplier method. The adaptation of the advanced solution strategies to algebraic equations containing Lagrange multipliers is also discussed.

3.5.1 Energy functional with Lagrange multipliers. When both thermal loading and axial-displacement constraints are imposed, the displacements have the expanded form

$$\{u\} = \lambda\{u_L\} + \gamma\{u_T\} + q_i\{\tilde{u}_i\} + q_i q_j\{\tilde{u}_{ij}\} \quad , \quad i, j = 1, 2, 3, \dots \quad (3.5.1)$$

where summation over repeated indices is implied, γ is the thermal-load control parameter, $\{u_T\}$ is the unit thermal response discussed in Section 3.2, and

$$\begin{aligned} \{\tilde{u}_i\} &= \{u_i\} + B_i\{u_B\} + L_i\{u_L\} \\ \{\tilde{u}_{ij}\} &= \{u_{ij}\} + A_{ij}(\{u_A\} - \{u_L\}) \end{aligned} \quad (3.5.2)$$

where the form of $\{\tilde{u}_{ij}\}$ is explained in Section 2.7, coefficient B_i ($i = 1, 2, \dots$) is defined in Section 2.6, and the presence of coefficient L_i ($i = 1, 2, \dots$) implies that constraint equations may accompany the problem statement. As stated in Section 3.4, axial displacement constraints are permitted only when displacement control is used (CTRL='D' in Table 1), and this has the implication that

$$L_i \equiv 0 \quad (i = 1, 2, \dots) \quad \text{-or-} \quad A_{ij} \equiv 0 \quad (i, j = 1, 2, \dots) \quad (3.5.3)$$

The expansion of the mid-surface mechanical strains given in equation (2.8.3) is modified here to include one new term and one altered term:

$$\{\epsilon^m\} = \lambda\{\epsilon_L\} + \gamma\{\epsilon_T^m\} + (q_i - q_i^o)\{\tilde{\epsilon}_i\} + (q_i q_j - q_i^o q_j^o)\{\tilde{\epsilon}_{ij}\} + \dots \quad (3.5.4)$$

where γ is the thermal-load control parameter, $\{\epsilon_T^m\}$ is defined in equation (3.2.4), and

$$\{\tilde{\epsilon}_i\} = \{\epsilon_i\} + B_i\{\epsilon_B\} + L_i\{\epsilon_L\} \quad (3.5.5)$$

The expansion of the in-plane stress resultants now has the form

$$\{N\} = \lambda\{N_L\} + \gamma\{N_T\} + (q_i - q_i^o)\{\tilde{N}_i\} + (q_i q_j - q_i^o q_j^o)\{\tilde{N}_{ij}\} + \dots \quad (3.5.6)$$

where $\{N_T\}$ is defined in equation (3.2.7), and

$$\{\bar{N}_i\} = \{N_i\} + B_i\{N_B\} + L_i\{N_L\} \quad (3.5.7)$$

The total potential energy π of equation (2.8.22) is evaluated, using the expressions for $\{\varepsilon^m\}$ and $\{N\}$ of equations (3.5.4) and (3.5.6) in place of the original expressions given in equations (2.8.3) and (2.8.7), respectively. The resulting expression for π is written as

$$\begin{aligned} \pi = & \text{Constant} \\ & + q_i(\lambda \bar{C}_i^L + \gamma \bar{C}_i^T - \beta C_i^Q - q_j^o \bar{C}_i^j - q_j^o q_k^o \bar{C}_{jk}^i - q_j^o q_k^o q_l^o C_{jkl}^i) \\ & + q_i q_j (\lambda \bar{C}_{ij}^L + \gamma \bar{C}_{ij}^T - \beta C_{ij}^Q + \frac{1}{2} \bar{C}_i^j - q_k^o \bar{C}_{ij}^k - q_k^o q_l^o \bar{C}_{ij}^{kl}) \\ & + q_i q_j q_k (\lambda \bar{C}_{ijk}^L + \gamma \bar{C}_{ijk}^T + \bar{C}_{ij}^k - q_l^o \bar{C}_{ijk}^l) \\ & + q_i q_j q_k q_l (\lambda \bar{C}_{ijkl}^L + \gamma \bar{C}_{ijkl}^T + \bar{C}_{ijk}^l + \frac{1}{2} \bar{C}_{ij}^{kl}) + O(q_i^5) \end{aligned} \quad (3.5.8)$$

where the "Constant" terms are those which do not depend on the modal amplitudes. The coefficients appearing in the above equation follow the definitions given in equations (2.8.25) except as noted here. Four coefficients have additional contributions, given by

$$\begin{aligned} \Delta \bar{C}_i^L &= L_i C_L^L \\ \Delta \bar{C}_i^j &= L_i C_j^L + L_j C_i^L + L_i L_j C_L^L + (L_i B_j + B_i L_j) C_B^L \\ \Delta \bar{C}_{ij}^k &= L_k C_{ij}^L \\ \Delta \bar{C}_{ijk}^l &= L_l C_{ijk}^L \end{aligned} \quad (3.5.9)$$

and two coefficients, not present in equation (2.8.24), are given by

$$\begin{aligned} \bar{C}_i^T &= C_i^T + B_i C_B^T + L_i C_L^T \\ \bar{C}_{ij}^T &= C_{ij}^T + A_{ij} (C_A^T - C_L^T) \end{aligned} \quad (3.5.10)$$

Seven primitive coefficients ($C_L^T, C_B^T, C_A^T, C_i^T, C_{ij}^T, C_{ijk}^T, C_{ijkl}^T$) appear in the above equations, and these are defined as illustrated here by two examples:

$$\begin{aligned} C_L^T &= \sum_{p=1}^P \left(\int_A \{N_T\}^T \{\varepsilon_L\} dA \right)_p \\ C_{ij}^T &= \sum_{p=1}^P \left(\int_A (\{N_T\}^T \{\varepsilon_{ij}\}) dA \right)_p \end{aligned} \quad (3.5.11)$$

where the notation used is the same as in Section 2.8.3.

The constraint equations for the different types of generalized displacement constraints all have the same form, visible in equations (3.4.14), (3.4.17), (3.4.22). It is assumed that there are a total of N constraint equations, written collectively as

$$(q_j - q_j^o - q_j^f) E_{nj} = 0 \quad (n = 1, 2, \dots, N) \quad (3.5.12)$$

where summation over j is implied. The constraint equations are incorporated into the problem statement using the Lagrange multiplier method. A new functional Π is formed:

$$\Pi = \pi + \Gamma_n (q_j - q_j^o - q_j^f) E_{nj} \quad (3.5.13)$$

where Γ_n ($n = 1, 2, \dots, N$) are the Lagrange multipliers, and where summation over repeated indices is implied. The equilibrium condition for the constrained system is obtained by setting the first variation of the new functional to zero:

$$\begin{aligned}\delta\Pi &= \frac{\partial\Pi}{\partial q_i} \delta q_i + \frac{\partial\Pi}{\partial \Gamma_n} \delta \Gamma_n \\ &= 0\end{aligned}\quad (3.5.14)$$

Because each value δq_i or $\delta \Gamma_n$ is both independent and arbitrary, equation (3.5.14) gives rise to the following $(M + N)$ independent conditions:

$$\begin{aligned}\frac{\partial\Pi}{\partial q_i} &= (\lambda \hat{C}_i^L + \gamma \hat{C}_i^T + \beta \hat{C}_i^Q - q_j^o \hat{C}_i^j - q_j^o q_k^o \hat{C}_i^{jk} - q_j^o q_k^o q_l^o \hat{C}_i^{jkl}) \\ &\quad + q_j (\lambda \hat{C}_{ij}^L + \gamma \hat{C}_{ij}^T + \beta \hat{C}_{ij}^Q + \hat{C}_{ij} - q_k^o \hat{C}_{ij}^k - q_k^o q_l^o \hat{C}_{ij}^{kl}) + \Gamma_n F_{in} \\ &\quad + q_j q_k (\lambda \hat{C}_{ijk}^L + \gamma \hat{C}_{ijk}^T + \hat{C}_{ijk} - q_l^o \hat{C}_{ijk}^l) \\ &\quad + q_j q_k q_l (\lambda \hat{C}_{ijkl}^L + \gamma \hat{C}_{ijkl}^T + \hat{C}_{ijkl}) \\ &= 0 \quad (i = 1, 2, \dots, M)\end{aligned}\quad (3.5.15)$$

$$\begin{aligned}\frac{\partial\Pi}{\partial \Gamma_n} &= (q_j - q_j^o - q_j^f) E_{nj} \\ &= 0 \quad (n = 1, 2, \dots, N)\end{aligned}\quad (3.5.16)$$

where the coefficients of equation (3.5.15) are all defined in equation (2.8.30) except for the following:

$$\begin{aligned}F_{in} &= E_{ni} \\ \hat{C}_i^T &= \bar{C}_i^T \\ \hat{C}_{ij}^T &= 2\bar{C}_{ij}^T \\ \hat{C}_{ijk}^T &= C_{ijk}^T + 2C_{jik}^T \\ \hat{C}_{ijkl}^T &= 2(\bar{C}_{ijkl}^T + \bar{C}_{jikl}^T)\end{aligned}\quad (3.5.17)$$

Equations (3.5.15) and (3.5.16) govern the equilibrium solutions which are sought. There are now three generalized load-control parameters, λ , γ , and β . The modal amplitudes q_i and Lagrange multipliers Γ_n constitute $(M + N)$ variable parameters to be determined in obtaining each equilibrium solution.

3.5.2 Modifications to the solution strategies. The solution procedures described in Section 2.9 and Appendix D require some additions and modifications to accommodate the additions to, and modifications of, the nonlinear algebraic equations discussed in the preceding section. First, the new parameters appearing in equations (3.5.15-16) must be normalized.

The thermal load parameter γ is normalized by a reference value γ_{ref} so that the normalized load parameter $\bar{\gamma}$ is given by

$$\bar{\gamma} = \gamma / \gamma_{ref} \quad (3.5.18)$$

The value γ_{ref} is selected to be the maximum-amplitude target value for γ used in specifying the load range or ranges over which a nonlinear analysis is to be performed.

The Lagrange multipliers Γ_n are normalized by reference values R_n so that the normalized Lagrange multipliers $\bar{\Gamma}_n$ are given by

$$\bar{\Gamma}_n = \Gamma_n / R_n \quad (n = 1, 2, \dots, N) \quad (3.5.19)$$

The values R_n are selected as follows. For each value of n the value of i is identified which corresponds to the largest-amplitude coefficient F_{in} for all i , where F_{in} appears in equation (3.5.15). For the selected value of i , the following expression is set to zero:

$$C_{ii} + \Gamma_n F_{in} = 0 \quad (3.5.20)$$

where no summation is implied. Equation (3.5.19) is solved for Γ_n and that expression is used in equation (3.5.20) to get

$$C_{ii} + \bar{\Gamma}_n R_n F_{in} = 0 \quad (3.5.21)$$

Parameter R_n is determined by setting $\bar{\Gamma}_n$ to unity in equation (3.5.21), providing

$$R_n = -C_{ii}/F_{in} \quad (3.5.22)$$

The normalized parameters $\bar{\gamma}$ and $\bar{\Gamma}_n$ are incorporated using the same approach as was described in Section 2.9.1 for incorporating the normalized parameters $\bar{\lambda}$ and $\bar{\beta}$. The nonlinear algebraic equations (3.5.15) are expressed in terms of the normalized parameters, and the resulting equations are identical in form to equations (3.5.15), but with normalized parameters $\bar{\gamma}$ and $\bar{\Gamma}_n$ replacing γ and Γ_n , respectively, and with the constant coefficients having been transformed in the obvious manner to account for the definition of $\bar{\gamma}$ and $\bar{\Gamma}_n$. Without assigning new notation, it is assumed from here on that the parameters and coefficients which appear are the normalized ones.

Following the general procedures described in Sections 2.9.2 and 2.9.3, the form of the nonlinear algebraic equations is simplified after specification of the modal imperfection amplitudes $\{q^o\}$ and collapsing of the load parameters λ , γ , and β into a single load parameter Λ . Equations (3.5.15) and (3.5.16) are converted to obtain equations of the following form:

$$(C_i + \Lambda C_i^L) + q_j(C_{ij} + \Lambda C_{ij}^L) + q_j q_k(C_{ijk} + \Lambda C_{ijk}^L) + q_j q_k q_l(C_{ijkl} + \Lambda C_{ijkl}^L) + \Gamma_n F_{in} = 0 \quad (i = 1, 2, \dots, M) \quad (3.5.23)$$

$$E_n + q_j E_{nj} = 0 \quad (n = 1, 2, \dots, N) \quad (3.5.24)$$

where the coefficients of equation (3.5.23) are analogous to those of equation (2.9.12) (with the tilde dropped from the notation), and where

$$E_n = -(q_j^o + q_j^f) E_{nj} \quad (3.5.25)$$

where summation over j is implied, and it is assumed that the modal amplitudes $\{q^o\}$ which determine the forced end rotation have been specified.

Equations (3.5.23) differ in form from equations (2.9.12) by the presence of the terms with Γ_n , and by the accompanying constraint conditions of equations (3.5.24). Equations (3.5.23) and (3.5.24) can be converted into a set of $M+N$ equations with the same form as equations (2.9.12):

$$(C_i + \Lambda C_i^L) + q_j(C_{ij} + \Lambda C_{ij}^L) + q_j q_k(C_{ijk} + \Lambda C_{ijk}^L) + q_j q_k q_l(C_{ijkl} + \Lambda C_{ijkl}^L) = 0 \quad (i = 1, 2, \dots, M+N) \quad (3.5.26)$$

where repeated indices are summed over the range 1 through $M+N$, and

$$q_i = \Gamma_n, \quad i = M+n \quad (n = 1, 2, \dots, N) \quad (3.5.27)$$

The only non-zero coefficients in equations (3.5.26) with subscript values i, j, k , or l , greater than M , are given by

$$C_{ij} = F_{in}, \quad j = M+n \quad \begin{matrix} (i = 1, 2, \dots, M) \\ (n = 1, 2, \dots, N) \end{matrix} \quad (3.5.28a)$$

$$C_i = E_n, \quad i = M+n \quad (n = 1, 2, \dots, N) \quad (3.5.28b)$$

$$C_{ij} = E_{nj}, \quad i = M+n \quad \begin{matrix} (n = 1, 2, \dots, N) \\ (j = 1, 2, \dots, M) \end{matrix} \quad (3.5.28c)$$

Many aspects of the solution strategies discussed in Section 2.9.4 and Appendix D can be applied directly to equations (3.5.26). However while there are $M + N$ variable parameters (excluding the load parameter) in the $M + N$ equations, there are only $M - N$ independent geometric variables (modal amplitudes) because of the N constraint conditions of equations (3.5.24). Thus, the eigenvalue problems which are solved as a part of the solution strategies described in Appendix D have only $M - N$ eigensolutions, and so some modifications must be made to the solution strategies.

Appendix D Section D.3 concerns the control of solution branching using Thurston's method. Equations which appear in that section are modified here to accommodate the use of Lagrange multipliers. The $M + N$ equations represented by equations (3.5.23) and (3.5.24) are written symbolically as

$$f_i(\bar{q}, \bar{\Gamma}, \lambda) = 0 \quad (i = 1, 2, \dots, M + N) \quad (3.5.29)$$

where the over-bars signify vectors. Let $(\bar{q}, \bar{\Gamma}, \lambda)$ be a starting solution (a known exact or approximate solution to equation (3.5.29)) and let $(\bar{q} + \bar{\xi}, \bar{\Gamma} + \bar{\zeta}, \lambda + \delta)$ be a solution which is sought near the starting solution, where the increments to the parameters are small compared to the parameter values. The new solution satisfies

$$f_i(\bar{q} + \bar{\xi}, \bar{\Gamma} + \bar{\zeta}, \lambda + \delta) = 0 \quad (i = 1, 2, \dots, M + N) \quad (3.5.30)$$

The first M of equations (3.5.30) are expressed in the expanded notation of equation (3.5.23), and terms are regrouped based on their order in the incremental parameters:

$$(D_i + \delta D_i^\delta) + \xi_j(D_{ij} + \delta D_{ij}^\delta) + \xi_j \xi_k(D_{ijk} + \delta D_{ijk}^\delta) + \xi_j \xi_k \xi_l(D_{ijkl} + \delta C_{ijkl}^\lambda) + \zeta_n F_{in} = 0 \quad (i = 1, 2, \dots, M) \quad (3.5.31)$$

where

$$D_i = f_i(\bar{q}, \bar{\Gamma}, \lambda) \quad (3.5.32)$$

and the other coefficients are defined in Appendix D. The last N of equations (3.5.30) are expressed in the notation of equation (3.5.24):

$$(E_n + q_j E_{nj}) + \xi_j E_{nj} = 0 \quad (n = 1, 2, \dots, N) \quad (3.5.33)$$

Equations (3.5.24) are linear in the modal amplitudes, and hence these equations are always satisfied exactly, even in an iterative solution procedure. Thus the quantity in the parentheses in equation (3.5.33) is known to be zero, and the equation reduces to

$$\xi_j E_{nj} = 0 \quad (n = 1, 2, \dots, N) \quad (3.5.34)$$

The eigenvalue problem for the constrained system here, corresponding to Appendix D equation (D27), is

$$\left(\left[\begin{array}{c|c} D & F \\ \hline E & 0 \end{array} \right] + \delta_k \left[\begin{array}{c|c} D^\delta & 0 \\ \hline 0 & 0 \end{array} \right] \right) \left\{ \begin{array}{c} \theta^k \\ \tau^k \end{array} \right\} = \left\{ \begin{array}{c} 0 \\ 0 \end{array} \right\} \quad (k = 1, 2, \dots) \quad (3.5.35)$$

where δ_k are eigenvalues, and $[\theta^k | \tau^k]^T$ are eigenvectors with components corresponding to the parameters $[\xi | \zeta]^T$. A series of operations is used in NLPAN to reduce equations (3.5.35) to a system of $M - N$ equations which can be solved to obtain $M - N$ eigenvalues and eigenvectors. The details of this process are tedious, but straightforward. The first step is to reorder the components of $\{\theta^k\}$ so that the first N columns of the reordered matrix $[E]$ and the first N rows of the reordered matrix $[F]$ form non-singular square matrices. The last N rows of equation (3.5.35) are then used to express N components of $\{\theta^k\}$ in terms of the remaining $M - N$ components. Similarly, the N components of $\{\tau^k\}$ can be expressed in terms of the $M - N$ remaining components of $\{\theta^k\}$ and the eigenvalue δ_k . A condensed eigenvalue problem of dimension $M - N$ is thus obtained, and this is solved using conventional methods.

In Appendix D equation (D29), the incremental solution vector $\{\xi\}$ is expressed as a series in the eigenvectors $\{\theta^k\}$. The analogous equation for the modified case here is given by

$$\left\{ \begin{array}{c} \xi \\ \zeta \end{array} \right\} = \sum_{k=1}^{M-N} a_k \left\{ \begin{array}{c} \theta^k \\ \tau^k \end{array} \right\} \quad (3.5.36)$$

The other aspects of the solution strategy described in Appendix D Section D.3 are not affected by the presence of Lagrange multipliers, provided that: i) the $M+N$ equations of the form of equation (3.5.26) are used as the equilibrium equations (the Lagrange multipliers Γ_n are treated the same as modal amplitudes), and ii) it is realized that there are only $M-N$ eigensolutions. For example, Appendix D equation (D25) would be of dimension $M+N$ whereas Appendix D equation (D31) would be of dimension $M-N$.

Appendix D Section D.2 concerns the application of the arc-length-control solution strategy. Once again, the solution strategy can be used for the most part without modification, assuming that equation (3.5.26) serves as the starting set of equations. However special treatment is required in solving the eigenvalue problem of Appendix D equation (D20). The corresponding equation for cases with Lagrange multipliers is

$$\left(\left[\begin{array}{c|c} D & F \\ \hline E & 0 \end{array} \right] - \omega_k \left[\begin{array}{c|c} I & 0 \\ \hline 0 & 0 \end{array} \right] \right) \left\{ \begin{array}{c} \phi^k \\ \Omega^k \end{array} \right\} = \left\{ \begin{array}{c} 0 \\ 0 \end{array} \right\} \quad (k = 1, 2, \dots) \quad (3.5.37)$$

where ω_k are eigenvalues, $[\phi^k | \Omega^k]^T$ are eigenvectors corresponding to the variables $[\xi | \zeta]^T$, and $[I]$ is the identity matrix. Equation (3.5.37) has the same general form as equation (3.5.35), and thus the method used to reduce equation (3.5.35) to a problem of dimension $M-N$ is used again to reduce equation (3.5.37) to a problem of dimension $M-N$.

4. IMPROVEMENTS IN THE COMPUTATION OF THE SECOND-ORDER DISPLACEMENT FIELDS

In this section, consideration is given to alternate methods for computing the second-order displacement fields. This is done in an attempt to rectify some dilemmas and discrepancies which arise when the method described in Section 2.7 is used without modification. First, the troublesome aspects of the second-order fields are identified. Next, the beneficial effects of requiring the second-order fields to be orthogonal to the buckling mode shapes are discussed. Several possibilities for new or modified approaches to computing the second-order displacement fields are outlined. Finally, the approach used in the current implementation of NLPAN is described.

4.1. Problems with the Second-Order Displacement Fields

4.1.1 Boundary conditions at the longitudinal ends. The buckling modes $\{u_i\}$ are the primary shape functions in the NLPAN analysis, and their harmonic dependence on x determines the effective boundary support condition at the longitudinal ends of the structure. The functional form of $\{u_i\}$ of equation (2.6.7) suggests that boundary support is in place which guarantees that

$$v = w \equiv 0 \quad \text{at } x = 0, L \quad (4.1.1)$$

The linear prebuckling solution $\{u_i\}$ does not rigorously satisfy equations (4.1.1), because of in-plane Poisson expansion, and the coupling of in-plane and out-of-plane displacements between adjoining plate strips. In addition, and of primary concern in the current discussion, the two contributions to both v_{ij} and w_{ij} of the second-order fields have a cosine dependence on x (see equation (2.7.4)), and thus it is not guaranteed that v_{ij} and w_{ij} are zero at $x = 0, L$. Indeed, it was observed in Ref [7] that if left unchecked, some contributions to selected functions $\{u_{ij}\}$ grossly violate the boundary conditions at the longitudinal ends.

The functional form of $\{u_{ij}\}$ was selected to accommodate the non-homogeneous terms in the governing differential equations (equations (2.7.1)) so as to permit the equations to be expressed in terms of separated variables. Boundary conditions at $x = 0, L$ were not considered in selecting the functional form of u_{ij} , but justification for the functional form is found by considering the behavior of simple rectangular plates.

In the postbuckling analysis of simple rectangular plates using von Karman plate theory, where $w(x, y)$ is represented, as it is here, as a series of terms of the form $\phi_i(y) \sin(m_i \pi x / L)$, the functional forms for $u_{ij}(x, y)$ and $v_{ij}(x, y)$ of equation (2.7.4) are the appropriate forms to allow the in-plane equilibrium equations to be satisfied exactly for any arbitrary set of terms in the series for w . (The in-plane boundary conditions at $x = 0, L$ corresponding to u_{ij} and v_{ij} are $u_{,x} = 0$ and $N_{,x} = 0$.) The in-plane displacement terms u_{ij} and v_{ij} are essential for obtaining accurate solutions for a plate undergoing significant postbuckling deflections.

For a linked-plate configuration, the coupling of the transverse displacement components v and w between adjoining, non-coplanar plate strips suggests that component w_{ij} should have the same harmonic dependence on x as component v_{ij} . It is concluded that with the use here of global functions, the boundary condition of equation (4.1.1) is too restrictive. It seems more appropriate to require that at the longitudinal ends of each plate strip the out-of-plane displacements must be small, and are permissible only to the extent that in-plane displacements must be accommodated and displacement compatibility at the node-lines must be enforced. The boundary value problem described in Section (2.7) requires intervention if the qualitative boundary condition just described is to be enforced.

4.1.2. Load-dependence of the second-order fields. The differential equations (2.7.1) which govern $\{u_{ij}\}$ were obtained from an expansion of the plate equilibrium equations in terms of the modal amplitudes. The appearance of the load parameter λ in equation (2.7.1) suggests that the functions $\{u_{ij}\}$ are load-dependent; this is an undesirable quality from the standpoint of computational economy. A second complication related to the appearance of λ in the differential equations is the existence of sin-

gular values of λ for which the amplitude of $\{u_{ij}\}$ becomes unbounded. Understanding the reason for these singularities gives insight as to how $\{u_{ij}\}$ might be computed differently, therefore the cause of the singularities is discussed here.

When the buckling equations (equations (2.6.4), (2.6.1b-c)) are expressed in terms of separated variables, the following homogeneous ordinary differential equations governing the function $\{\xi_i\}$ are obtained:

$$\left\{ \begin{array}{l} C_1 \xi_i'' + C_2 \xi_i + C_3 \eta_i' \\ D_1 \xi_i' + D_2 \eta_i'' + D_3 \eta_i \\ E_1 \phi_i'''' + E_2 \phi_i'' + E_3 \phi_i \end{array} \right\} + \lambda_i \left\{ \begin{array}{l} 0 \\ D_3^\lambda \eta_i \\ E_2^\lambda \phi_i'' + E_3^\lambda \phi_i \end{array} \right\} = \left\{ \begin{array}{l} 0 \\ 0 \\ 0 \end{array} \right\} \quad (4.1.2)$$

where primes denote differentiation with respect to y , and the sub- and super-scripted coefficients C , D , and E depend on the halfwave number m_i . Similarly, when equations (2.7.1) are expressed in terms of separated variables, the following nonhomogeneous ordinary differential equations governing the functions $\{\xi_{aij}\}$ are obtained:

$$\left\{ \begin{array}{l} -C_1 \xi_{aij}'' - C_2 \xi_{aij} + C_3 \eta_{aij}' \\ -D_1 \xi_{aij}' + D_2 \eta_{aij}'' + D_3 \eta_{aij} \\ E_1 \phi_{aij}'''' + E_2 \phi_{aij}'' + E_3 \phi_{aij} \end{array} \right\} + \lambda \left\{ \begin{array}{l} 0 \\ D_3^\lambda \eta_{aij} \\ E_2^\lambda \phi_{aij}'' + E_3^\lambda \phi_{aij} \end{array} \right\} = \left\{ \begin{array}{l} F(\{\xi_i\}, \{\xi_j\}) \\ G(\{\xi_i\}, \{\xi_j\}) \\ H(\{\xi_i\}, \{\xi_j\}) \end{array} \right\} \quad (4.1.3)$$

where the sub- and super-scripted coefficients C , D , and E are the same as those in equations (4.1.2), except that they depend the halfwave number \hat{m} of equation (2.7.5) instead of m_i . It can be seen by comparing equations (4.1.2) and (4.1.3) that if λ in equation (4.1.3) is selected to be an eigenvalue for a buckling mode with the halfwave number \hat{m} , then the left-hand side of equation (4.1.3) (when expressed in terms of unknown coefficients for the functions $\{\xi_{aij}\}$) will be singular. (This fact was pointed out to the author by Prof. S. Sridharan of Washington University at St. Louis.) Thus for some ranges of values of λ , the functions $\{u_{ij}\}$ take on large amplitudes and have the approximate shape of buckling modes, except that the phase of v_{ij} and w_{ij} causes the maximum displacement amplitudes to be at $x=0, L$, resulting in a gross violation of boundary condition. In these situations the second-order functions $\{u_{ij}\}$ are reflecting instability-related response which is already represented by first-order functions $\{u_i\}$.

4.2. Implications of Imposing Orthogonality Between $\{u_{ij}\}$ and $\{u_i\}$

In the literature of the classical perturbation approach to the analysis of structural stability, it is stated that second- (and higher-) order displacement fields should be orthogonal to the buckling modes (Ref. [22]), although it is not necessarily clear how this orthogonality is to be enforced. In this section, the implications of requiring orthogonality between the functions $\{u_i\}$ and $\{u_{ij}\}$ are studied. Evidence is offered that the problems discussed in the preceding section are alleviated by enforcement of this condition.

Abbreviated notation is introduced here. Define operators L and N such that $L(N)$ and $N(N, u)$ are given by

$$L(N) = \left\{ \begin{array}{l} L_1(N) \\ L_2(N) \\ L_3(M) \end{array} \right\} = \left\{ \begin{array}{l} N_{x'x} + N_{xy'y} \\ N_{xy'x} + N_{y'y} \\ M_{x'xx} + 2M_{xy'xy} + M_{y'yy} \end{array} \right\} \quad (4.2.1)$$

$$N(N, u) = \left\{ \begin{array}{l} N_1(N_y, u) \\ N_2(N_x, v) \\ N_3(N, w) \end{array} \right\} = \left\{ \begin{array}{l} (N_y u_{,y})_{,y} \\ (N_x v_{,x})_{,x} \\ (N_x w_{,x} + N_{xy} w_{,y})_{,x} + (N_{xy} w_{,x} + N_y w_{,y})_{,y} \end{array} \right\} \quad (4.2.2)$$

Define the inner products $\langle u, L(N) \rangle$ and $\langle u, N(N, u) \rangle$ by

$$\begin{aligned}
\langle u, L(N) \rangle &= \sum_{p=1}^P \left\{ \int_A [u L_1(N) + v L_2(N) + w L_3(M)] dA \right\}_p \\
\langle u, N(N, u) \rangle &= \sum_{p=1}^P \left\{ \int_A [u N_1(N_y, u) + v N_2(N_x, v) + w N_3(N, w)] dA \right\}_p
\end{aligned} \tag{4.2.3}$$

Using the abbreviated notation, the plate equilibrium equations are given by

$$L(N) + N(N, u) = 0 \tag{4.2.4}$$

the buckling equations are given by

$$L(N_i) + \lambda_i N(N_L, u_i) = 0 \tag{4.2.5}$$

and the equations governing $\{u_{ij}\}$ (equations 2.7.1) are written as

$$L(N_{ij}) + \frac{1}{2} N(N_i, u_j) + \frac{1}{2} N(N_j, u_i) + \lambda N(N_L, u_{ij}) = 0 \tag{4.2.6}$$

where it is noted that in equations (2.6.4) and (2.7.1), it is assumed that $N_1(N_x, u) \approx 0$.

The orthonormality relationship satisfied by the buckling modes is derived in Appendix B and given in equation (B10). It is written here as

$$\langle u_j, N(N_L, u_i) \rangle = -\delta_{ij} a_i \tag{4.2.7}$$

where δ_{ij} is the Kroniker delta functions, and a_i is an arbitrary normalizing constant. The condition expressing orthogonality between the second-order displacement fields and the buckling modes is given in Appendix B equations (B12) and (B14) in two alternate forms:

$$\langle u_k, N(N_L, u_{ij}) \rangle = 0 \tag{4.2.8a}$$

$$\langle u_{ij}, N(N_L, u_k) \rangle = 0 \tag{4.2.8b}$$

Enforcement of the above orthogonality conditions would cause the second-order fields to have components w_{ij} (in the local reference systems) which are closely in accordance with the goal of having minimal transverse displacements at the panel ends. This is because the large transverse displacements which characterize the buckling modes would be suppressed in the second-order fields by the orthogonality condition. The second-order fields would thus be truly second-order in character, absent of the displacement contributions already available in the family of buckling modes.

It is also contended here that enforcement of the orthogonality condition would cause the second-order fields to be independent of the load parameter. The term $\lambda_i N(N_L, u_i)$ of equation (4.2.5) is the term which drives the buckling instabilities associated with the mode shape $\{u_i\}$. Function $\{u_{ij}\}$ is now orthogonal to all the buckling modes and thus should not represent an instability-driven displacement field; therefore it would seem reasonable that the term $\lambda N(N_L, u_{ij})$ of equation (4.2.6) should have little effect on the solution for $\{u_{ij}\}$.

A more theoretical basis for this argument is established by considering terms in the stationary total potential energy expression. The total potential energy of the structure is expressed in equation (2.8.24) as a power series in terms of the modal amplitudes, which can be expressed symbolically as

$$\pi = \pi_0 + \pi_1 + \pi_2 + \pi_3 + \pi_4 + \dots \tag{4.2.9}$$

The equilibrium condition of equation (2.8.28) can similarly be written as

$$\begin{aligned}
\delta\pi &= \delta\pi_1 + \delta\pi_2 + \delta\pi_3 + \delta\pi_4 + \dots \\
&= 0
\end{aligned} \tag{4.2.10}$$

It is noted that while the boundary-value problems governing the functions $\{u_k\}$, $\{u_i\}$, and $\{u_j\}$ were determined by expanding the plate equilibrium equations and the associated boundary conditions, identical boundary-value problem statements for the first two functions can be obtained by evaluating $\delta\pi_1 = 0$ and $\delta\pi_2 = 0$, respectively. The relationship between $\delta\pi_3$ and the boundary-value problem used in Section 2.7 to obtain $\{u_{ij}\}$ is more complex.

Appendix C contains an evaluation of $\delta\pi_3$ in which the following form is obtained (equation (C7)):

$$\delta\pi_3 = \delta q_i q_j q_k \left\{ -\langle u_i, [L(N_{jk}) + \frac{1}{2} N(N_k, u_j) + \frac{1}{2} N(N_j, u_k) + \lambda N(N_L, u_{jk})] \rangle - 2(\lambda - \lambda_k) \langle u_{ij}, N(N_L, u_k) \rangle \right\} \quad (4.2.11)$$

In this equation, the weighted term inside the first inner product is the term set to zero in the differential equations (4.2.6), and the second inner product is the quantity which is set to zero in the orthogonality condition of equation (4.2.8b). If equations (4.2.8a-b) are enforced, equation (11) becomes

$$\delta\pi_3 = \delta q_i q_j q_k \left\{ -\langle u_i, [L(N_{jk}) + \frac{1}{2} N(N_k, u_j) + \frac{1}{2} N(N_j, u_k)] \rangle \right\} \quad (4.2.12)$$

The load-dependent term $\lambda N(N_L, u_k)$ has been eliminated in the expression for $\delta\pi_3$. This is offered as further evidence that the second-order displacement fields are load-independent when orthogonality is enforced between the functions $\{u_{ij}\}$ and $\{u_k\}$.

4.3 Computation of $\{u_{ij}\}$ with Orthogonality Imposed

With the load-dependent term omitted, the differential equations (4.2.6) are written as

$$L(N_{ij}) + \frac{1}{2} N(N_j, u_i) + \frac{1}{2} N(N_i, u_j) = 0 \quad (4.3.1)$$

A consequence of enforcing the orthogonality condition of equation (4.2.8) is that equation (4.3.1) can not, in general, be solved exactly over the domain of the structure. It seems appropriate to devise a method which minimizes the error of equation (4.3.1). Three possible approaches to computing $\{u_{ij}\}$ are discussed in the following, then the approach currently used in NLPAN is described.

4.3.1 Least-squares approach. One solution approach is to use the Lagrange multiplier method to satisfy the orthogonality-constraint equations while minimizing the error of the field equations in the least-squares sense. Equation (4.3.1) represents three equations. Define three residual error functions associated with the ordinary differential equations governing $\{\xi_{aij}\}$ (equations (4.1.3)), where the load-dependent term is now omitted:

$$\begin{aligned} R^u(y) &= -C_1 \xi'' - C_2 \xi + C_3 \eta' - F(y) \\ R^v(y) &= -D_1 \xi' + D_2 \eta'' + D_3 \eta - G(y) \\ R^w(y) &= E_1 \phi'''' + E_2 \phi'' + E_3 \phi - H(y) \end{aligned} \quad (4.3.2)$$

where subscripts are dropped here, and throughout the remainder of this section, from ξ_{aij} , η_{aij} , and ϕ_{aij} .

The constraint equation (4.2.8b), is evaluated to get the equation

$$\sum_{\alpha=1}^2 \left\{ \sum_{p=1}^P \left(\int_0^b \left[-N_{x_L} \left(\frac{m_k \pi}{L} \right)^2 \eta_k \right] \eta + \left[-N_{x_L} \left(\frac{m_k \pi}{L} \right)^2 \phi_k + N_{y_L} \phi_k'' \right] \phi \right) dy \right)_p \times \int_0^L \cos \left(\frac{\hat{m} \pi x}{L} \right) \sin \left(\frac{m_k \pi x}{L} \right) dx \right\} = 0 \quad (4.3.3)$$

If (\hat{m}, m_k) are (even, even) or (odd, odd) then the x -integral of equation (4.3.3) is zero. Otherwise, the y -dependent portion of the equation is satisfied independently for each value of α ; this is written as

$$\sum_{p=1}^P \left(\int_0^b [H_k(y) \eta + \Phi_k(y) \phi] dy \right)_p = 0 \quad (4.3.4)$$

where

$$H_k(y) = \left[-N_{x_L} \left(\frac{m_k \pi}{L} \right)^2 \eta_k \right], \quad \Phi_k(y) = \left[-N_{x_L} \left(\frac{m_k \pi}{L} \right)^2 \phi_k + N_{y_L} \phi_k'' \right] \quad (4.3.5)$$

The second-order displacement fields are now determined by minimizing the functional W , given by

$$W = \sum_{p=1}^P \left(\int_0^b [(R^u)^2 + (R^v)^2 + (R^w)^2] dy \right)_p + \Gamma_k \sum_{p=1}^P \left(\int_0^b [H_k(y) \eta + \Phi_k(y) \phi] dy \right)_p \quad (4.3.6)$$

where Γ_k ($k = 1, 2, \dots$) are Lagrange multipliers, and where boundary conditions at the node-lines must also be met. The functional W is minimized by setting to zero the first variation of W with respect to the functions ξ , η , and ϕ , and with respect to the Lagrange multipliers Γ_k .

Preliminary work has been done on developing a procedure for solving equation (4.3.6) using a finite-difference representation of the functions ξ , η , and ϕ , such as is used in the existing solution method, described in [7]. In the solution procedure of [7], the generalized force-resultants and generalized displacements at the node-lines are isolated algebraically, so that the (homogeneous) node-line boundary conditions can be applied directly to the system of equations governing the finite-difference solution. It appears that this is also possible in a finite-difference solution of equation (4.3.6), except that the moment resultants at the node-lines do not appear in the resulting system of equations. It thus appears that for each node-line which is unrestrained with respect to rotation, the zero-moment boundary condition must be enforced using a constraint equation which is incorporated into the functional W using an additional Lagrange multiplier.

4.3.2 Subtraction of buckling mode shape contribution. In this approach, $\{u_{ij}\}$ is initially computed using the method described in Section 2.7, and is then modified by subtracting contributions in the shapes of buckling modes. The contributions are identified using the orthonormality condition for the buckling modes, equation (4.2.7). This equation is evaluated in terms of separated variables, and is then written in the following way, where new operator and inner-product definitions are introduced:

$$\begin{aligned} \langle \{\xi_j\}, \hat{L}(\{\xi_i\}) \rangle &= \sum_{p=1}^P \left[- \left(\frac{m_i \pi}{L} \right)^2 N_{x_L} \int_0^b (\eta_j \eta_i + \phi_j \phi_i) dy + N_{y_L} \int_0^b \phi_j \phi_i'' dy \right]_p \\ &= -\delta_{ij} b_i \end{aligned} \quad (4.3.7)$$

where b_i is a constant coefficient. Similarly, orthogonality between $\{u_{ij}\}$ and $\{u_k\}$, equation (4.2.8a), can be expressed in terms of the contributions for each value of α as

$$\begin{aligned} \langle \{\xi_k\}, \hat{L}(\{\bar{\xi}_{\alpha ij}\}) \rangle &= \sum_{p=1}^P \left[- \left(\frac{\hat{m} \pi}{L} \right)^2 N_{x_L} \int_0^b (\eta_k \bar{\eta}_{\alpha ij} + \phi_k \bar{\phi}_{\alpha ij}) dy + N_{y_L} \int_0^b \phi_k \bar{\phi}_{\alpha ij}'' dy \right]_p \\ &= 0 \end{aligned} \quad (4.3.8)$$

where $\{\bar{\xi}_{\alpha ij}\}$ is the modified function which satisfies the orthogonality constraints.

The unmodified function $\{\xi_{\alpha ij}\}$ is expressed as the sum of the modified function and a series of buckling-mode contributions $\{\xi_k\}$:

$$\{\xi_{\alpha ij}\} = \{\bar{\xi}_{\alpha ij}\} + \sum_k c_k \{\xi_k\} \quad (4.3.9)$$

where coefficients c_k are initially unknown, and

$$\{\bar{\xi}_k\} = \begin{Bmatrix} -\xi_k(y) \\ \eta_k(y) \\ \phi_k(y) \end{Bmatrix} \quad (4.3.10)$$

The buckling modes $\{\xi_k\}$ ($k = 1, 2, \dots$) used in equation (4.3.9) should, ideally, be limited to those with associated longitudinal halfwave numbers m_k which equal the halfwave number $|\hat{m}|$ corresponding to the function $\{\xi_{\alpha ij}\}$. There are two reasons for this. First, displacement fields with different halfwave numbers are orthogonal by virtue of their longitudinal waveforms. Second, the relationship between transverse functions shown in equation (4.3.9) implies a relationship between full-field functions, and this relationship makes sense only for the case where equation (4.3.9) is applied on the basis of common longitudinal halfwave numbers.

From equations (4.3.7-9) it can be established that

$$\langle \{\xi_k\}, \hat{L}(\{\xi_{\alpha ij}\}) \rangle = -c_k b_k \quad (4.3.11)$$

Coefficients c_k ($k = 1, 2, \dots$) are computed from the above equation, and then the function $\{\bar{\xi}_{\alpha ij}\}$ can be computed by applying equation (4.3.9).

4.3.3 Direct suppression of displacements. In this approach, the method of Section 2.7 is used to compute $\{u_{ij}\}$, but for selected functions $\{\xi_{ij}\}$ displacement constraints are imposed directly on the model during the finite-difference analysis. The placement of constraints is done on an intuitive basis; the general approach is to place constraints along node lines in a way which suppresses large transverse displacements, while still allowing in-plane expansion/contraction of plate strips. For example consider the blade-stiffened panel of Figure 3. It would be appropriate to enforce $w=0$ (global) at node-line numbers 1, 3, and 4, and impose $v=0$ (global) at node-line number 2.

Based on results presented in [7], the suppression of displacements using this method is justified for fields $\{\xi_{\alpha ij}\}$ with an associated halfwave number \hat{m} of zero. It has also been found that suppression of displacements for $\hat{m}=2$ gives improved agreement of analytical results for postbuckling in column-like modes with predictions based on column theory. For large values of \hat{m} , matching the boundary conditions at $x=0, L$ is less important than predicting the proper behavior away from the ends, so direct suppression of displacements seems inappropriate in this case. Based on results presented in [7], the violation of boundary conditions at $x=0, L$ is less of a problem with the fields having large values \hat{m} .

4.3.4 Current approach used in NLPAN. In the current implementation, NLPAN uses a combination of the methods described in Sections 4.3.2 and 4.3.3. For long wavelength contributions to $\{u_{ij}\}$, $|\hat{m}| \leq 4$, direct suppression of transverse displacements, as described in Section 4.3.3, is used. An automated procedure positions the displacement constraints at selected node lines, assuming that the configuration is a conventional stiffened panel configuration such as a blade-, T-, hat-, z-, etc. stiffened panel. For unconventional configurations such as complex column sections, the automated procedure may place constraints inappropriately, so the specification of constraints needs to be done on a case-by-case basis.

For values $\hat{m} = m_l \pm m_g$ where m_l is large and m_g is small, or vice versa, the method of Section 4.3.2 (subject to certain modifications) is applied. These fields, referred to in the literature as "mixed second-order displacement fields," are known to have a tendency to duplicate the shapes of buckling modes. Let m_g be the (small) halfwave number for the global-buckling mode, and let m_l be the (large) halfwave number for the local-buckling mode. For large m_l and small m_g ,

$$|\hat{m}| = |m_l \pm m_g| \approx m_l \quad (4.3.12)$$

In Section 4.3.2, it was stated that, ideally, $m_r = \hat{m}$ for contributions $\{\xi_r\}$ to be subtracted from the field $\{\xi_{\alpha ij}\}$. In the NLPAN code, one or more modes $\{\xi_r\}$ are already in use which satisfy $m_r = m_i$. These modes are used with the premise that they satisfy the approximate relationship $m_r \approx |\hat{m}|$; however this may or may not be the case in general, because modes are classified using the conditions $m_i \leq 3$ and $m_i \geq 4$. For the treatment of many stiffened panel problems, displacements u_r and v_r are zero for the fields of interest, so that matching of m_r and \hat{m} is not important. It is not known whether a mis-match in these values is detrimental to the accuracy of results for more unusual configurations. A more theoretically pure approach would be to carry along buckling modes which are not necessarily used as shape functions in the NLPAN analysis, but which match the halfwave numbers $|\hat{m}|$ encountered in computing the fields $\{u_{ij}\}$, and which, thus, can be used to identify contributions to be subtracted from the second-order displacement fields. This latter approach has not been implemented.

5. MISCELLANEOUS CONSIDERATIONS

This section includes brief discussions of some miscellaneous considerations regarding the use of the NLPAN analysis method and computer code. First, considerations in the design of geometric representations of stiffened panels are discussed. Next, the convergence of analytical results with respect to the finite-difference discretization and mode-set selection is discussed, and mode selection strategies are suggested for some common cases. Finally, the factors affecting computation time and computer memory requirements are discussed.

5.1 Geometric Representation of Stiffened Panels

For stiffened panels with multiple evenly spaced stiffeners, experience suggests that a unit-cell representation in NLPAN is generally preferable to a full, multiple-stiffener representation. (An example of a unit-cell representation is shown in Figure 5(c).) One reason is that with a unit cell, only a very few local-buckling modes (one to three) need to be incorporated in the analysis to allow the panel to take on various types of local deformation (for example, stiffener-web buckling, skin buckling, and flange buckling), whereas for a full-panel model, a much larger number of modes is required to accomplish the same thing. This is because the various stiffeners and skin bays in a multiple-stiffener model tend to participate to different degrees, and in different manners, in any given buckling mode. Another reason for using a unit-cell representation is that execution time and computer memory requirements increase with the complexity of the cross section. As a consequence, the number of buckling modes which can be incorporated as shape functions in an analysis decreases with the complexity of the cross section. For purposes of comparing the results of a unit-cell analysis with the results of a full-model analysis or test, it is suggested that the reference load values used in normalizing the various result sets be selected on the basis of a common axial strain value (assuming that the loading is uniaxial).

5.2 Convergence Considerations

5.2.1 Discretization of the cross section. The cross section of a configuration is discretized in order to perform both the finite-difference analysis described in Appendix C of [7], and the numerical integration of the coefficient expressions such as those found in equations (2.8.26-27). Specifically, the y -dependent variables on each plate strip are evaluated only at a set of discrete, uniformly spaced points along the local y -axis. Increasing the fineness of the discretization improves the accuracy of results, but also increases computer memory requirements and increases program execution time.

How rapidly the results converge with increasing fineness of the discretization depends on both the node-line boundary conditions, and the in-plane load conditions. For example, consider a square, simply supported plate subjected to a uniaxial compressive load N_x . For the in-plane boundary condition given by BCVEC(2,IB)=2 in Table 3, the load N_x is uniformly zero along the y -normal edges, whereas for BCVEC(2,IB)=3, the y -normal edge remains straight, and the average value \bar{N}_y is zero. Despite the seemingly small difference in these two sets of boundary conditions, in order to obtain similar accuracy in the predictions of postbuckling response for the two cases, the latter boundary condition requires the use of only about one third the number of discretization intervals as the former [7]. For the former case, a minimum of 30 intervals is recommended, whereas for the latter case, ten intervals provides comparable accuracy. If the load axes are reversed for this problem so that uniaxial N_y loading is applied, the number of discretization intervals required for a given level of accuracy is significantly greater than for either of the two cases just described.

The minimum number of intervals allowed on any single plate strip is four. When using a unit-stiffener-cell representation of a uniaxially loaded stiffened panel, where symmetry conditions are imposed on the skin at the edges of the cell, the use of a minimum of twelve discretization intervals for the skin to either side of the stiffener is recommended for local/global mode interaction problems. A convergence study is recommended as the best way to assure that a model is adequately discretized.

5.2.2 Mode set. The selection of VIPASA buckling modes used as shape functions in an NLPAN analysis affects the accuracy of the analytical results in two ways. First, the true qualitative response of the physical structure can be predicted analytically only if a suitable mode set is incorporated. Second, assuming that the appropriate family of buckling modes has been identified, increasing the number of modes used in the nonlinear analysis enables the computation of accurate results deeper into the nonlinear regime.

In some situations, the set of suitable buckling modes can be selected using intuition. For example, the mode set for an axially compressed square, simply-supported plate with an edge-length a is given by $\sin(m\pi x/a) \times \sin(n\pi y/a)$ ($m, n = 1, 3, 5, \dots$) where modes are added starting with the lowest values for m and n . For general NLPAN configurations, it is much less obvious what comprises an appropriate mode set, and unfortunately, the use of an inadequate set can cause errors ranging from erroneous stresses and strains, to the complete failure to predict some modes of response.

For flat, stiffened or unstiffened panels subjected to in-plane loading, some guidelines for selecting modes are provided here. The guidelines are based on experience in modelling panels in which the buckling modes are classifiable as "global" or "local". A global mode is characterized by a long wavelength and minimal distortion of the cross-section. A local mode is characterized by short wavelength buckling of plate strips in the structure, with significant distortion of the cross-section. Separate guidelines are offered for symmetric structural sections and unsymmetric structural sections, because the former can generally be modelled with fewer modes. ("Symmetric" refers to the initial geometry, not to the response.)

The mode selection guidelines are presented in Table 5. In the table, the label (m,i) is used to designate the i^{th} buckling mode in the infinite sequence of modes having the longitudinal halfwave number m , where the modes are ordered based on their eigenvalues. Label m_c is used to designate the longitudinal halfwave-number for the critical local-buckling mode. A modal-interaction analysis is appropriate if the critical loads for global buckling and local buckling both have the same order of magnitude. It should be noted that when a clamped-end simulation is used, the global buckling load is approximately four times the buckling load computed by VIPASA for mode (1,1).

The modes suggested for Local Postbuckling are intended to preserve the basic shape of the buckling mode while allowing refinement of the shape with increasing loading. The level-1 modes suggested for Local/Global Mode Interaction are intended to model the basic mechanism leading to imperfection sensitivity and structural collapse. The level-2 modes for Local/Global Mode Interaction are intended to simulate "amplitude modulation," which is the modulation (along the length of the structure) of the amplitude of the local-mode deflections due to the variation of bending curvature (along the length) due to the global-mode displacements. The strategy for selecting mode sets for local/global mode interaction is discussed in greater detail in [23].

The following additional comments apply to Table 5:

1. It is assumed that a global mode of a symmetric structure is symmetric.
2. If m_c is even and Local/Global Mode Interaction is to be simulated, it is advised to set m_c to the next lower (odd) integer. This is because the large bending curvatures at the mid-length of the structure tend to cause local-mode displacements to be maximized at the mid-length.
3. For Local/Global Mode Interaction problems with symmetric structures, two different mode sets (labeled A and B) are provided with the intention that each mode set be used independently in separate analyses. One set models symmetric local-mode displacements, and the other models unsymmetric local-mode displacements. These recommendations are based on results published in [23], in which the direction of the global-mode response determined whether the local-mode response was symmetric or unsymmetric.

Thermal loading, as modelled with NLPAN, tends to induce in-plane normal loads. The mode sets suggested in Table 5 are suitable for use in modelling thermal loading if the unit in-plane loads used in generating the mode shapes are similar to the in-plane reaction loads generated during thermal loading. Regarding pressure loading, whether or not suitable buckling mode shapes exist (for use as global shape functions) depends on the specific configuration considered, and this, in turn, affects the ability of NLPAN to model the response to pressure loads. For example, the pressure response of simply supported rectangular plates can be accurately modelled, whereas NLPAN does not perform well in modelling the highly three-dimensional response of a pressure-loaded stiffened panel (see Section 6.3). NLPAN has been used to investigate the snap phenomenon in postbuckled plates [24], in which a secondary instability (in the postbuckled regime) initiates a sudden change in the waveform. While the solution strategies incorporated in NLPAN are well suited to the analysis of this type of response, the accurate quantitative (and qualitative) prediction of secondary instabilities requires the incorporation of a large number of appropriately selected modes. The proper selection of these modes is a difficult process (see, for example, [19]) and therefore no general strategies for making such selections are offered here.

5.3 Computer Execution Time and Memory Requirements

The execution time for an NLPAN run is approximately proportional to the complexity of the cross section (in terms of the number of discretization points) and approximately doubles with each buckling mode added as a shape function. Typical execution times for mainframe computers and mini-computers are a few seconds for a single-mode analysis, and a few minutes for an analysis with ten or so modes.

Computer memory requirements also vary with the complexity of the cross section and the number of buckling modes used. The NLPAN code is designed to run entirely within computer memory, so the size of the NLPAN analysis is limited with respect to the two characteristics mentioned. NLPAN employs a single data vector to store, in sequence, all large data arrays, and the array dimensions are set based on the actual requirements needed for each specific problem. Because of this feature, NLPAN can use all of the computer memory which it reserves. The limit to the size of a problem which can be analyzed is adjusted by changing a single dimension parameter in the FORTRAN source code and re-compiling the code.

6. RESULTS

In this section, some key features of the NLPAN code are evaluated through applications to test problems. First, the local-postbuckling response of a stiffened composite panel with a complex cross-section is investigated. Second, the nonlinear response of an imperfection-sensitive thin-blade-stiffened panel under uniaxial loading is explored. Third, a stiffened composite panel subjected to transverse pressure loading is considered. Fourth, the thermally induced buckling and postbuckling response of an unstiffened square composite panel is modelled. Finally, conclusions from a separately reported study [23] of panels and columns with constrained end-rotation are summarized.

Some of the new features discussed in this document have been applied to test problems which are reported elsewhere. Results which illustrate various aspects of the nonlinear solution strategies (described in Appendix D) are included [16]. Results from an application of NLPAN to the problem of the snap of a rectangular plate from one buckled waveform to another are presented in [24].

6.1 I-Stiffened Graphite/Epoxy Panel Under Axial Compression

NLPAN was used to model an I-stiffened graphite/epoxy panel loaded in uniaxial compression. The configuration is one which was tested experimentally; specifically the configuration is that of test panel U6 of [25]. Some features of the panel and its buckling response are summarized in Figure 5. The overall dimensions are shown in Figure 5(a). The panel featured a flat skin to which four stiffeners were bonded. The panel ends were mounted in potting material, and were then machined flat and parallel to form contact surfaces for flat-end loading. The cross-section of a representative stiffener is shown in Figure 5(b). A complete description of the panel is given in [25].

The stiffener flanges of the test panel were tapered, as depicted in Fig. 5(b). In the NLPAN analysis, the tapered flanges were approximated (on each side of the stiffener web) as three-step flanges by using three plate strips of different thicknesses. A unit-stiffener-cell representation of the panel was used, with symmetry conditions imposed on the skin at the edges of the unit cell. The profile of the primary buckling mode (as computed by VIPASA) is plotted in Figure 5(c). (The three-step flange model can be seen in the figure.) The buckling mode has five longitudinal halfwaves, as indicated in Figure 5(a).

The theoretical buckling load for the full panel is reported in [25] to be 156 KN, determined using PASCO [13]. Reference [25] states that the mean lamina thickness was 0.014 cm. The use of this mean thickness in the current investigation resulted in PASCO predictions of a buckling load of 210 KN. (To obtain this value, the critical value of axial strain computed by PASCO for the unit-cell model was imposed on the full-panel model assuming linear response.) The discrepancy between the two computed buckling loads was judged to be too large to be due to a difference in the axial buckling strain for the unit-cell model and the full-panel model. A second analysis was performed assuming a mean lamina thickness of 0.0127 cm (0.0050 in.), and this resulted in a predicted buckling load of 157 KN, almost exactly the value reported in [25]. Because of this agreement, the lamina thickness 0.0127 cm was used for the NLPAN nonlinear analysis. (Critical values of end displacement corresponding to assumed lamina thicknesses of 0.014 cm and 0.0127 cm were computed to be 0.094 cm and 0.077 cm, respectively, compared to the experimentally measured value 0.08 cm, reported to one significant digit [25]. This result further supports the use of the smaller lamina thickness value.)

As reported in [25], the critical load for global buckling (a single longitudinal halfwave) was well above the critical load for the local-buckling mode depicted in Fig 5(c), so it was assumed that the postbuckling response would be limited to a local-buckling type of deflection pattern. Thus, only four modes were incorporated as shape functions, namely (using the notation of Table 5) modes (5,1), (5,3), (15,1), and (15,3). The last three modes serve to refine the general shape of the first mode as the load increases beyond the buckling load. The unsupported length of 72.5 cm was used in the NLPAN calculations. A shape imperfection was simulated in the analysis, having the shape of the primary buckling mode and an amplitude of one percent of the skin thickness. All loading, displacement, and strain results

presented here are normalized by the theoretical values at the critical buckling load, as computed by PASCO.

Experimental and analytical results are presented in Figures 6 and 7. Results of end load versus end shortening are plotted in Figure 6(a), where both measures are normalized by the critical values for theoretical buckling. Panel failure occurred at a postbuckling load factor of 2.96 [25]. The theoretical end-shortening values plotted are the values computed by NLPAN plus a correction for the axial compressibility of the potted ends, assuming that the axial strain in the ends is proportional to the axial load as determined by the axial stiffness before panel buckling. The NLPAN results show slightly less axial stiffness beyond the buckling point than was measured experimentally; this may be due to the difference between the clamped condition of the skin at the ends of the test panel and the simply supported condition of the skin at the ends in the analytical model. The distribution of the longitudinal membrane strains in the skin across the center skin bay at the mid-length of the panel is plotted for three load levels in Figure 6(b). It can be seen that the NLPAN results are in good agreement with the experimentally obtained values for all three load levels, the only appreciable disagreement being near the center of the bay for the higher load levels.

Results for the variation of longitudinal surface strains with end load are plotted in Fig. 7 (with all values normalized). The panel locations where strains are measured are indicated in Fig. 7(a). The surface strains on the skin at the center of the panel (locations A and B) are plotted in Figure 7(b). There is minor disagreement between the analysis and the experiment, but overall agreement is good. The opposing surface strains on and under a stiffener flange (locations C and D) are plotted in Figure 7(c). The experimental and analytical strain values differ by a uniform percentage over the entire load range. This discrepancy, which is present even in the early prebuckling regime, remains unexplained. If one or the other results set is scaled so that the prebuckling slopes match, then the two sets of results are in very close agreement. Whatever the cause of the inconsistency noted here, the agreement between the two results sets is still fairly good in this region of complex cross-sectional detail.

6.2 Imperfection Sensitivity in a Thin-Blade-Stiffened Isotropic Panel

NLPAN was used to model a thin-blade-stiffened isotropic panel loaded in uniaxial compression. The response of the configuration is sensitive to imperfections because of the interaction of the local and global buckling deformations. The configuration is one which was tested experimentally by Thompson and associates [26]. The cross-sectional proportions of a unit-stiffener-cell of the panel are shown in Figure 8(a). This unit-cell representation was used in the analysis; the test panel had nine skin bays and ten stiffeners. The panel was fabricated from epoxy resin.

This configuration was modelled with NLPAN previously, as reported in [7]. In the previous investigation, NLPAN was found to successfully predict imperfection sensitivity, but gave unconservative predictions for the limit loads of imperfect panels compared to experimental measurements. The purpose of revisiting the problem here is to investigate the influence of two new factors in the analysis on the accuracy of the predictions. The first factor is the use of the procedures described in Section 4.3.4 for enforcing, approximately, orthogonality between the second-order displacement fields and the buckling mode shapes. The second factor is the use of a mode selection strategy which enables the modelling of the amplitude modulation phenomenon. In this mode-selection strategy, once the local-buckling mode(s) to be used in the analysis is (are) identified, having a longitudinal halfwave number m_{loc} , then additional local-buckling modes are incorporated which have transverse profiles similar to that (those) of the primary local-buckling mode(s), but having longitudinal halfwave numbers $(m_{loc} - 2)$ and $(m_{loc} + 2)$. This strategy is reflected in the mode-selection guidelines of Table 5, and is discussed further in [23]. It was hoped that the presence of these two new factors would improve the agreement of the analytical results with the experimental data.

Global (Euler-buckling mode) response was modelled using mode (1,1). The critical local-buckling mode is mode (7,1). The ratio of the critical load for local buckling P_L to the critical load for Euler buckling P_E was $P_L/P_E = 1.05$. The local-buckling mode (7,3) was also deemed important so that two

possible modes of collapse initiation could be activated (skin buckling or stiffener buckling). Using the guidelines from Table 5, the following modes were selected for modelling local-buckling deformations: (5,1), (5,3), (7,1), (7,3), (9,1), and (9,3).

Local-mode imperfections of two different amplitudes were used. These were in the shape of mode (7,1), with amplitudes of 2% and 10% of the skin thickness. A range of amplitudes of Euler-mode imperfections were used. Positive Euler-mode deflections increase the compression of the skin, and negative Euler-mode imperfections increase the compression of the stiffener blade. The results for limit load versus Euler-mode imperfection amplitude are plotted in Figure 8(b), where the limit loads are normalized by the theoretical critical load for Euler-mode buckling. The solid lines show the baseline analytical results. A second set of analytical results was generated without performing the orthogonalization of the mixed-second-order displacement fields (see Section 4.3.4). These are plotted in Figure 8(b) with dashed lines.

For the baseline analytical results, the limit loads for negative values of Euler-mode imperfections are slightly lower than those reported in [7] (not shown here), but are still unconservative. For positive values of Euler-mode imperfections, the baseline limit loads are actually higher (more unconservative) than the analytical results reported in [7]. With the orthogonality condition not imposed, the predicted limit loads for positive Euler-mode imperfections drop sharply; they match the experimental data more closely for lower-amplitude Euler-mode imperfections, but diverge from the experimentally observed trends for larger amplitude imperfections. For negative Euler-mode imperfections, dropping the orthogonality condition resulted in a slight increase in the predicted limit loads.

It was hoped that the analytical features added in the current investigation relative to the analyses reported in [7] would provide improved agreement with the experimental measurements. The mode-selection strategy used can be judged as an improvement, based simply on the argument that it enables the analysis to simulate the amplitude modulation which is known to occur in reality. However the imposition of the orthogonality condition has a mixed influence on the agreement between the analytical and the experimental results. Therefore, despite any theoretical justification for imposing orthogonality, it's not clear whether or not the accuracy of the method is improved by the practice. There do remain questions about some aspects of the experimental results [7]. These questions include the validity of assuming linear elastic material properties, and the exact shape of the local-mode imperfections, where the latter question concerns the fact that the imperfection amplitudes were measured only on the skin. Sridharan and Peng published results [4] showing good agreement between analytical results and experiment for this problem, but to obtain the results for negative Euler-mode imperfections, they used local-mode imperfections which highly amplify the stiffener waviness (compared to the nominal imperfection amplitudes) for the case of negative Euler-mode imperfections. This suggests that in the test panels, the stiffener waviness may have been greater than the skin waviness. In order to assess the accuracy of the NLPAN predictions with more certainty, it is suggested that finite-element analyses be performed which duplicate the NLPAN configuration and boundary conditions. This would allow an assessment of the NLPAN analysis without the uncertainty which accompanies experimental results.

The use of an alternate method for generating VIPASA buckling mode shapes might improve the analytical predictions of NLPAN. It is noted in the discussion in [7] that a linear combination of the two buckling modes (7,1) and (7,3) can be used to approximately simulate isolated skin buckling or isolated stiffener buckling. However, the word "approximate" is important here. Mode (7,3) features large stiffener rolling displacements, but also includes short wavelength curvature of the skin in the transverse direction which would be expected to have a high level of associated strain energy. This may lead to suppression of the (7,3) mode, thus inhibiting the ability of the two local modes to represent two isolated forms of local deformation. If the two local-buckling mode shapes each represented an isolated mode of displacement (skin buckling or stiffener buckling) without the superfluous waviness present in the (7,3) mode, then the local-buckling displacements might be more easily excited, resulting in increased modal interaction and imperfection sensitivity. Such alternate local-buckling modes could be generated by exploiting the ability of PASCO to modify the transverse distribution of pre-buckling stresses so as to simulate transverse pressure, load eccentricity, or bowing imperfections. The local-buckling modes

generated in this way will tend to exhibit the types of isolated response deemed desirable here. This procedure has not yet been incorporated in NLPAN.

6.3 Stiffened Composite Panel Under Pressure Loading

NLPAN was used to model a stiffened AS4/3502 graphite/epoxy composite panel restrained at the edges and subjected to transverse pressure loading. The panel was rectangular with a single T-stiffener bonded to the center of the panel parallel to one axis. The configuration is one which was tested experimentally, specifically Panel A of Ref. [27]. The nominal configuration of the panel test section is shown in Figure 9(a), and the stiffener cross-section and the laminate stacking sequences are shown in Figure 9(b). (The origin of the coordinate system appearing in the figure corresponds to that used in [27], which differs from that used in the NLPAN model.) The lamina elastic properties used in the analysis are also listed in Figure 9(b). The side (y -normal) edges of the panel were clamped and fixed with respect to in-plane displacements. The physical panel extended beyond the test section at each longitudinal end. The panel ends were not clamped at the ends of the test section; instead, the panel was supported against out-of-plane deflections, and the clamped condition was simulated by loading the panel with pressure on both sides of the end-supports. The physical ends of the panel were restrained against in-plane displacements. Because the length of the test section was greater than the length of the outer pressure-loaded bays, the effective boundary condition at the ends of the panel may have differed somewhat from an ideal clamped condition.

The direction of the pressure loading is indicated in Figure 9(a). The observed panel response was fairly symmetrical with respect to the stiffener, so for the NLPAN analysis, only symmetric mode shapes were incorporated. The unit system of generalized in-plane loads used for generating the VIPASA buckling mode shapes consisted of a unit axial load imposed at the x -normal ends with v held to zero at the y -normal edges. The critical axial load for these boundary conditions was 1983 lbs. for the first unsymmetric mode, mode (1,1). The critical loads for symmetric modes (1,2) and (3,2) were 3265 lbs. and 2496 lbs., respectively. Ten modes were incorporated in the analysis, namely the first five symmetric modes with one longitudinal halfwave, and the first five symmetric modes with three longitudinal halfwaves.

NLPAN was run first with a clamped-end condition simulated by imposing axial displacement constraints at the top and bottom of the stiffener blade at each end of the panel. Because the displacements computed using this representation were somewhat strange (discussed below), additional NLPAN runs were made, first modelling simply supported ends, then applying rotationally elastic support to the ends of the stiffener. The results are summarized in plots of displacement profiles presented in Figure 10. In the figure, the rotational spring constant is denoted K_{θ} , and the normalized spring constant, defined in the figure, is denoted \bar{K} . The transverse displacements w (positive for skin-side-out deflections) are normalized by the skin thickness $h = .04$ in.. The distribution of displacements across the width of the panel at the mid-length are plotted in Figure 10(a). The distribution of displacements along the length of the panel are plotted in Figure 10(b) for the panel centerline (under the stiffener), and in Figure 10(c) for the skin at $y/B=0.25$. (The data plotted in Figure 6 of [27] was rescaled for plotting here in Figure 10(b-c), to provide consistency with Figure 5 of [27]. The latter figure has the correct scale; this was learned through an inquiry to author M.W. Hyer.) For the clamped-end simulation, the analysis predicts the transverse displacement of the stiffener to be essentially zero (actually, slightly negative) along the length of the panel, which is inconsistent with the measured response. By varying the degree of end constraint, the computed displacements can be brought into the ballpark of the measured displacements, but clearly the analysis has some shortcomings.

The chief shortcoming identified by the author is the poor suitability of the buckling mode shapes of the panel for representing the pressure response. The buckling mode shapes are skin-dominated, and for all 5 of the modes having 3 longitudinal halfwaves, the stiffener blade remains essentially undisplaced compared to the skin. This causes the clamped-end boundary condition (imposed on the stiffener blade) to suppress the single-halfwave displacement contributions at the stiffener. These results expose an inherent shortcoming in the approach of NLPAN for modelling pressure-type response. The

deformations in the panel considered here are highly three-dimensional, and the VIPASA buckling modes for the panel are found to be poorly suited for representing these deformations. The pressure simulation has been found to work well for simple rectangular plates, and can be expected to work well for driving bowing-type deformation of a wide panel, because, in these cases, the buckling mode shapes are similar to pressure-induced displacements.

In Figure 10(c), it can be seen that the displacement w predicted by NLPAN for the skin at the ends of the panel is non-zero, despite the nominal boundary condition $w=0$ at the ends. These non-zero displacements are due to the second-order displacement fields. Despite the use of direct suppression of displacements as described in Sections 4.3.3-4.3.4, there is a significant violation of the boundary condition. This occurred because the displacements at the ends are suppressed only at the node lines, and there is a wide expanse of skin (on each side of the stiffener) between the node line at the edge of the stiffener flange and the node line at the edge of the panel. A second NLPAN model was generated which had an additional node line in the skin on each side of the stiffener. With the displacements suppressed at these two additional points, the violation of the boundary condition was greatly reduced, and the overall displacement levels were somewhat reduced for the cases where the stiffener was not clamped. However there was no significant overall improvement in the analytical predictions.

6.4 Thermally Loaded Unstiffened Composite Panel

NLPAN was used to model the buckling and postbuckling behavior of a square, unstiffened graphite/epoxy panel subjected to thermal loading. The configuration is one for which analytical results were generated by Meyers and Hyer [28]. The plate is an eight-ply laminate with the edges simply supported, but with edge-normal displacements constrained to zero. The laminate stacking sequence is [+45/-45/0/0]_s. The configuration details and material properties used in the analysis are presented in Figure 11(a). The plate is subjected to a uniform (change in) temperature. Meyers predicts a critical buckling temperature of 69.4 deg. F, whereas NLPAN predicts a buckling temperature of 71.4 deg. F. The slight difference may be due to the fact that Meyers accounts for the laminate stiffness constants D_{16} and D_{26} , whereas these values are assumed to be zero in NLPAN.

NLPAN postbuckling analyses were performed using four different mode sets. All buckling modes used are sinusoidal in both the x - and y -directions. Let (m,n) denote the buckling mode with m and n halfwaves in the x - and y -directions, respectively. Four different mode sets were used with NLPAN, as listed here:

- i. 1 Mode: (1,1)
- ii. 3 Modes: (1,1), (1,3), (3,1)
- iii. 6 Modes: (1,1), (1,3), (1,5), (3,1), (3,3), (5,1)
- iv. 10 Modes: (1,1), (1,3), (1,5), (1,7), (3,1), (3,3), (3,5), (5,1), (5,3), (7,1)

The normalized center deflection of the plate is plotted versus the normalized temperature in Figure 11(b). All four mode sets used with NLPAN produce similar results up to a normalized temperature of about 1.8. Beyond that temperature, the NLPAN results for 3, 6, and 10 modes diverge from the results for 1 mode, with the results for 6 and 10 modes being practically identical. The multiple-mode NLPAN analyses predict that the center deflection increases with temperature up to a normalized temperature of about 4.5, beyond which the center deflection decreases.

The results from [28] agree with the NLPAN results up to a normalized temperature of about 1.8, beyond which the center deflection predicted in [28] falls progressively below that predicted by NLPAN. The method of analysis used in [28] is more general than the method of NLPAN (for simple rectangular plates) in terms of modelling flexibility, but both methods share the characteristic of modelling transverse out-of-plane displacements using double sine functions. This author believes that the current results are more accurate than the results of [28] (for this specific configuration) for the following reason. The assumed form for displacements used in NLPAN guarantees that for simple rectangular plates, the in-plane equilibrium equations are satisfied exactly for any arbitrary set of buckling modes used. This is because

the in-plane displacements are second-order in terms of the modal amplitudes, so the selection of buckling modes determines the terms used in the in-plane displacements. With the method of [28], the shape functions used for in-plane displacements are selected independently of the shape functions (buckling modes) used for out-of-plane displacements, so that the in-plane equilibrium equations are not satisfied exactly unless the proper set of terms for the in-plane displacements have been included. The characteristic halfwave numbers for the important in-plane displacement terms are derived from the sums and differences of the halfwave numbers for the buckling modes (see equations (2.7.4) and (2.7.5)), so that the important in-plane displacement terms do not form a contiguous group when they are ordered based on their characteristic halfwave numbers. Because of this, a convergence study performed by progressively increasing the number of in-plane displacement terms may exhibit a false convergence before important terms have been included. Without knowing exactly which shape functions were used to generate the results reported in [28], no final verdict can be reached, but the convergence of the NLPAN results with increasing numbers of mode shapes gives some confidence in the latter results.

6.5 Panels and Columns with Constrained End-Rotation

The modified-end-support modelling features described in Sections 3.3 - 3.5 were given an initial assessment through applications to several test problems which are described and reported in [23]. The conclusions noted in [23] are summarized here.

The buckling of a slender clamped-end column was simulated. As additional displacement terms are incorporated into the solution procedure, the predicted buckling load converges to the theoretical value predicted by column theory. The NLPAN predictions of buckling load converge from above, and therefore, using a small number of displacement terms as is typically the practice, the results are unconservative. However, for two different tests of an imperfect axially compressed T-stiffened composite panel with clamped ends, NLPAN predicts, with relatively good accuracy, both the mechanisms of structural collapse, and the limit loads suggested by the test data. A greater variety of clamped-end configurations need to be modelled using NLPAN in order to more fully assess the performance of the analytical approach.

The mode-selection strategies discussed in [23] (and Section 5.2.2) were used in the analysis of axially compressed stiffened panels which were expected, based on their proportions, to exhibit local-global mode interaction. Amplitude modulation of the local-buckling modes during mode interaction was successfully modelled. Expected amplitude-modulation trends were observed for both a clamped-end panel and a panel with simply supported ends.

7. CONCLUDING REMARKS AND RECOMMENDATIONS

7.1 Concluding Remarks

A number of improvements and additions to the method of NLPAN were developed as a part of the current effort. The primary additions to the analytical capabilities are listed here:

1. Transverse pressure loading can be modelled.
2. Thermal loading (constant through-the thickness) can be modelled.
3. Clamped ends, rotationally elastic end support, and eccentric end loading can be modelled.
4. Advanced solution strategies have been implemented which allow equilibrium solution paths to be followed past limit points and past solution branch points of multiplicity one or two.
5. The strategy for modelling biaxial in-plane load application has been improved, including the correction of errors present in the original method.

The method of NLPAN is asymptotic in nature so that solutions must be regarded as having potentially significant errors. That is not to say that accurate solutions can not be obtained in the significantly nonlinear regime of response; the method incorporates second order contributions to displacements and fourth order contributions to total potential energy which are sometimes ignored by investigators when applying asymptotic approaches of the type used here. For simple rectangular plates, the NLPAN analysis degenerates to an exact series solution of the von Karman nonlinear plate equations (assuming that sufficiently fine discretization of the domain is used for the numerical portions of the analysis). For general configurations, errors in computed solutions may be present due to the following factors: i) approximations made in deriving the strain-displacement relations, ii) the neglecting of displacement contributions beyond order two and energy contributions beyond order four, iii) the use of an inadequate number, or a poor selection, of VIPASA buckling mode shapes for use in the nonlinear analysis, iv) uncertainties in the method used to compute the second-order displacement fields, and v) the numerical error associated with the finite difference solution of the second-order displacement fields and the numerical integration of various functions over the transverse domain of the structure.

For structures in which the buckling and postbuckling response is limited to local-buckling displacement shapes (little or no global-mode displacements), NLPAN gives good predictions up to loads of several times the buckling load. Because of its modelling flexibility, NLPAN is well suited for analyzing relatively complicated cross sections for this type of response. Local/global mode interaction and the associated imperfection sensitivity are successfully predicted by NLPAN, although some questions remain about the quantitative accuracy of the predictions. Modifications were made to the theoretical approach, and improved mode-selection strategies were established, in attempts to improve the accuracy of predictions for this type of response, but the results of these effort are inconclusive.

When NLPAN is used to model the response of a structure (panel) to transverse pressure, it has been found that the accuracy of the predictions is limited because of the inability of the buckling mode shapes to represent some types of pressure response. For simply supported rectangular plates, the buckling modes are well suited for modelling pressure response. The buckling modes are similarly well suited for modelling the pressure response of panels which buckle in a wide-column mode. However, for a relatively short-length, tall-stiffener panel with clamped ends and clamped edges, the buckling mode shapes were found to be poorly suited for modelling the highly three-dimensional response produced by pressure loading.

NLPAN predictions of the post-thermal-buckling response of an unstiffened rectangular composite panel with constrained edges agree with other published analytical results in the early postbuckling regime. Arguments are made which support the accuracy of the NLPAN results over the other published results in the deeper postbuckling regime. Because the constant through-the-thickness thermal loading used in NLPAN acts like a form of in-plane loading (which secondarily induces bending and buckling

displacements), NLPAN should perform equally well in analyzing the response to either thermal loading or in-plane loading.

The clamped-end modelling feature was found to give relatively accurate predictions of the response of a stiffened composite panel which was tested in uniaxial compression. A greater variety of test cases must be explored in order to more fully assess the accuracy of this modelling option.

The advanced nonlinear solution strategies are found to generally work well, although the performance is somewhat dependent on several control parameter values and on the amplitude of imperfection shapes used. Sometimes numerical or approximation errors have the same effect as geometric imperfections, and can thus cause unexpected results. Extremely small modal imperfection amplitudes should be avoided, because this results in solution paths with zones of extremely high curvature which the solution procedure has trouble characterizing. In general, the use of significant modal-imperfection amplitudes for the dominant buckling modes results in robust performance of the solution procedures.

7.2 Recommendations for Future Work

Suggestions are offered here for future work toward improving the NLPAN analysis program. Improvements are sought primarily for the accuracy of the predictions for local/global mode interaction.

1. Investigate the use of VIPASA local-buckling mode shapes which have been generated using positive and negative eccentricities in the PASCO analysis.
2. Compute second-order displacement fields by rigorously imposing orthogonality with respect to the buckling modes, and compare the fields with those computed using the methods discussed in this document and with results from finite element analysis.
3. Investigate modifications to the strain-displacement relationships which may be warranted based on rotation and mid-surface-curvature amplitudes typically encountered.
4. Improve the integration of the PASCO and NLPAN computer programs so as to eliminate the need for the redundant specification of some input parameters.

APPENDIX A: FORMULAE FOR THE LINEAR, UNBUCKLED SOLUTIONS

Formulae for computing the linear, unbuckled solutions corresponding to both the unit in-plane loads and the unit thermal loads are discussed in this appendix. The two sections correspond to the two distinct load systems.

A.1 Response to the Unit In-Plane Loading

The specific formulae for determining the solution $\{u_k\}$ associated with the unit in-plane load system (see Section 2.5) are presented here. The formulae are compatible with the equations used in PASCO [13] but are redeveloped here for completeness in the documentation, using notation consistent with the present development. Biaxial loading is permitted only if there is a continuous planar skin connecting the boundary node lines; otherwise only uniaxial loading N_{xG} is permitted. Nonetheless, the solution is developed here assuming that a planar skin exists, and that biaxial loading is imposed, because this provides a solution that is applicable to all models, so long as the unit in-plane load system adheres to the limitations specified in Section 2.3.

A vector $\{k\}$ of length P is used to specify which plates are part of the panel skin, where P is the number of plate strips in the model. The elements k_p of vector $\{k\}$ are defined such that

$$k_p = \begin{cases} 1 & \text{if plate strip } p \text{ is part of the panel skin} \\ 0 & \text{otherwise} \end{cases} \quad (p = 1, 2, \dots, P) \quad (\text{A.1.1})$$

The unit global load N_{xGL} is the mean unit axial load in the longitudinal direction per unit width of the panel, and can be expressed as

$$N_{xGL} = \frac{1}{B} \sum_{p=1}^P (N_{xL} b)_p \quad (\text{A.1.2})$$

where B is the reference width of the panel, N_{xL} is the value of N_x (on plate strip p) corresponding to the unit solution, and b is the width of the plate strip. The unit global load N_{yGL} is the unit edge-normal load per unit length of the panel, and it acts on the panel skin at the boundary node lines. This load is carried by all plate strips in the panel skin, so that the unit y -normal stress resultant in plate strip p is given by

$$(N_{yL})_p = k_p N_{yGL} \quad (p = 1, 2, \dots, P) \quad (\text{A.1.3})$$

The unit normal stress resultants within each plate strip are related to the unit normal mid-surface strains of the plate strip through the plate constitutive equations (equations (2.1.11)):

$$(N_{xL})_p = (A_{11}\epsilon_{xL} + A_{12}\epsilon_{yL})_p \quad (p = 1, 2, \dots, P) \quad (\text{A.1.4})$$

$$(N_{yL})_p = (A_{12}\epsilon_{xL} + A_{22}\epsilon_{yL})_p \quad (p = 1, 2, \dots, P) \quad (\text{A.1.5})$$

where the unit longitudinal strain, ϵ_{xL} , is uniform throughout the panel.

Using equation (3) and the equation (5), the unit transverse (in-plane) strain in each plate strip can be expressed in terms of the unit longitudinal strain and the unit load N_{yGL} :

$$(\epsilon_{yL})_p = \frac{N_{yGL} k_p - \epsilon_{xL} (A_{12})_p}{(A_{22})_p} \quad (p = 1, 2, \dots, P) \quad (\text{A.1.6})$$

The unit longitudinal strain associated with the specified global load components can be determined by using equation (4) and equation (6) in equation (2) to obtain the following expression:

$$\epsilon_{xL} = \frac{N_{xGL} B - N_{yGL} s_2}{s_1} \quad (\text{A.1.7})$$

where s_1 and s_2 are given by

$$s_1 = \sum_{p=1}^P (bC)_p \quad s_2 = \sum_{p=1}^P k_p (bR)_p \quad (\text{A.1.8})$$

where

$$C_p = (A_{11} - A_{12}^2/A_{22})_p \quad R_p = (A_{12}/A_{22})_p \quad (\text{A.1.9})$$

With the unit axial strain now known, equation (6) is used to determine the unit y-normal strain within each plate strip. Equations (4) and (5) are then applied to determine the unit normal in-plane stress resultants within each plate strip.

The change in width Δv_L (the change in dimension between the two boundary node lines) is simply the sum of the changes in width of the plate strips comprising the panel skin, and this can be expressed mathematically as

$$\Delta v_L = \sum_{p=1}^P k_p (b\epsilon_{yL})_p \quad (\text{A.1.10})$$

Define the mean y-normal strain of the panel skin to be

$$\bar{\epsilon}_{yGL} = \frac{\Delta v_L}{B} \quad (\text{A.1.11})$$

Using equations (6) and (10) to re-express equation (11), the mean y-normal strain in the skin can be expressed in terms of known values:

$$\bar{\epsilon}_{yGL} = \frac{1}{B} (N_{yGL}s_3 - \epsilon_{xL}s_2) \quad (\text{A.1.12})$$

where constant s_3 is given by

$$s_3 = \sum_{p=1}^P k_p (b/A_{22})_p \quad (\text{A.1.13})$$

A few additional relationships are required for use when the boundary conditions are specified in particular ways. By substituting equation (7) into equation (12), the normal unit load on the side boundaries can be expressed as

$$N_{yGL} = \left(\bar{\epsilon}_{yGL} + N_{xGL} \frac{s_2}{s_1} \right) \left(\frac{Bs_1}{s_1s_3 + (s_2)^2} \right) \quad (\text{A.1.14})$$

From equation (7) it can be determined that

$$N_{yGL} = N_{xGL}B - \epsilon_{xL} \frac{s_1}{s_2} \quad (\text{A.1.15})$$

Equating the above two expressions for N_{yGL} , the following expression for N_{xGL} can be obtained:

$$N_{xGL} = \epsilon_{xL} \left(\frac{s_1s_3 + (s_2)^2}{Bs_3} \right) + \bar{\epsilon}_{yGL} \frac{s_2}{s_3} \quad (\text{A.1.16})$$

For configurations having no continuous planar skin ($\{k\} = \{0\}$), equation (16) degenerates to

$$N_{xGL} = \epsilon_{xL} \frac{s_1}{B} \quad (\text{A.1.17})$$

There are four different cases identified for sets of parameters which may be used to specify boundary conditions for the unbuckled panel. These cases are discussed individually below.

Case 1) N_{xGL} and N_{yGL} specified. For this case, equations (3) through (13) provide the solution. The sequence of application of the equations is (8), (7), (6), (4), (3), (13), and (12).

Case 2) N_{xGL} specified and $\bar{\epsilon}_{yGL} = 0$ ($\Delta v_L = 0$). For this case, equation (14) is used to determine the effective unit load N_{yGL} . Next, the sequence given for Case (1a) above will provide the complete solution.

Case 3) ϵ_{xL} and $\bar{\epsilon}_{yGL}$ specified. First, equation (16) is used to determine the effective unit load N_{xGL} , then equation (14) is used to compute the effective unit load N_{yGL} . Next, the sequence given for Case 1) above provides the complete solution.

Case 4) ϵ_{xL} and N_{yGL} specified. This case is required for determining the unit solution $\{u_A\}$ used in modifying the second-order displacement fields (see Section 2.7). For this case, the sequence of application of equations is (8), (13), (12), (6), (16), (4), and (3).

A.2 Response to the Unit Thermal Loading

The equations used to obtain the solution $\{u_T\}$ to the unit thermal loading (see Section 3.2) are discussed here. Let Δv_T be the change in width between the two boundary node lines, for the case where a flat, continuous skin is present (a case where bi-axial loading is admissible). Parameter $\bar{\epsilon}_{yGT}$ is the mean y-normal strain in the skin, so that

$$\bar{\epsilon}_{yGT} = \Delta v_T / B \quad (A.2.1)$$

where B is the reference width. N_{xGT} is mean load per unit panel width acting normal to the panel ends, and N_{yGT} is the mean edge-normal load per unit length along the boundary node lines acting in the global y-direction.

The following equations relate the various parameters applying to an individual plate strip (from equations (3.2.4) and (3.2.7)):

$$\epsilon_{xT}^m = \epsilon_{xT} - \hat{T} \alpha_x \quad (A.2.2)$$

$$\epsilon_{yT}^m = \epsilon_{yT} - \hat{T} \alpha_y \quad (A.2.3)$$

$$N_{xT} = A_{11} \epsilon_{xT}^m + A_{12} \epsilon_{yT}^m \quad (A.2.4)$$

$$N_{yT} = A_{12} \epsilon_{xT}^m + A_{22} \epsilon_{yT}^m \quad (A.2.5)$$

where \hat{T} is the unit thermal loading on the strip, other symbols are defined in Section 3.2, and the following equations relate the parameters of the various plate strips to the global parameters (see equations (A.1.2-3), (A.1.10), (A.2.1)):

$$(N_{yT})_p = k_p N_{yGT} \quad (A.2.6)$$

$$N_{xGT} = \frac{1}{B} \sum_{p=1}^P (b N_{xT})_p \quad (A.2.7)$$

$$\bar{\epsilon}_{yGT} = \frac{1}{B} \sum_{p=1}^P k_p (b \epsilon_{yT})_p \quad (A.2.8)$$

where p is the plate-strip index number, P is the total number of plate strips, b is the width of an individual plate strip, and k_p is defined in equation (A.1.1).

To aid in the expression of the equations used to obtain the unit thermal solution, parameters C_p , R_p , s_1 , s_2 , and s_3 defined in Section A.1 are used, along with the following additional parameters:

$$F_p = [(A_{12}/A_{22})\alpha_x + \alpha_y]_p \quad s_4 = \sum_{p=1}^P (\hat{T}bC\alpha_x)_p \quad s_5 = \sum_{p=1}^P k_p(b\hat{T}F)_p \quad (\text{A.2.9})$$

The sequence of operations used to obtain the complete unit thermal response depends on which options are selected for control of the generalized in-plane loading (see Table 1). Four different cases are discussed.

Displacement control, Option 1. The homogeneous boundary conditions are given by

$$\begin{aligned} \epsilon_{x_T} &= 0 \\ \bar{\epsilon}_{y_{G_T}} &= 0 \end{aligned} \quad (\text{A.2.10})$$

The following equations are applied:

$$N_{y_{G_T}} = -s_5/s_3 \quad (\text{A.2.11})$$

$$(\epsilon_{y_T})_p = k_p N_{y_{G_T}}/(A_{22})_p + (\hat{T}F)_p \quad (p = 1, 2, \dots, P) \quad (\text{A.2.12})$$

and the remainder of the solution is obtained by application of equations (2), (3), (4), (5), and (7).

Displacement control, Option 2. The homogeneous boundary conditions are given by

$$\begin{aligned} \epsilon_{x_T} &= 0 \\ N_{y_{G_T}} &= 0 \end{aligned} \quad (\text{A.2.13})$$

The following equations are applied:

$$(\epsilon_{y_T})_p = (\hat{T}F)_p \quad (p = 1, 2, \dots, P) \quad (\text{A.2.14})$$

and the remainder of the solution is obtained by application of equations (2), (3), (4), (5), (7), and (8).

Load control, Option 1. The homogeneous boundary conditions are given by

$$\begin{aligned} N_{x_{G_T}} &= 0 \\ \bar{\epsilon}_{y_{G_T}} &= 0 \end{aligned} \quad (\text{A.2.15})$$

The following equations are applied:

$$\epsilon_{x_T} = \frac{s_2 s_5 + s_3 s_4}{s_2^2 + s_1 s_3} \quad (\text{A.2.16})$$

$$N_{y_{G_T}} = (s_4 - s_1 \epsilon_{x_T})/s_2 \quad (\text{A.2.17})$$

$$(\epsilon_{y_T})_p = k_p N_{y_{G_T}}/(A_{22})_p + (\hat{T}F)_p - R_p \epsilon_{x_T} \quad (p = 1, 2, \dots, P) \quad (\text{A.2.18})$$

and the remainder of the solution is obtained by application of equations (2), (3), (4), and (5).

Load control, Option 2. The homogeneous boundary conditions are given by

$$\begin{aligned} N_{x_{G_T}} &= 0 \\ N_{y_{G_T}} &= 0 \end{aligned} \quad (\text{A.2.19})$$

The following equations are applied:

$$\varepsilon_{x_T} = s_4/s_1 \quad (A.2.20)$$

$$(\varepsilon_{y_T})_p = (\hat{TF})_p - R_p \varepsilon_{x_T} \quad (p = 1, 2, \dots, P) \quad (A.2.21)$$

and the remainder of the solution is obtained by application of equations (2), (3), (4), (5), and (8).

APPENDIX B: ORTHOGONALITY OF THE DISPLACEMENT SHAPE FUNCTIONS

In this appendix, the equations governing orthogonality between various shape functions sets are presented. First, the orthogonality condition satisfied by the buckling eigenfunctions (referred to in the following as buckling "modes") is developed. Second, the condition needed to enforce orthogonality between the buckling eigenfunctions and the second-order displacement fields is established.

B.1 Orthogonality of the Buckling Modes

The left-hand sides of the buckling equations (equations (2.6.5), (2.6.1b), and (2.6.1c)) are weighted by buckling mode components u_j , v_j , and w_j , respectively, and integrated over the domain of the structure. Because each weighted expression is uniformly zero, the integral the of weighted expressions must also be zero. The following equation is thus obtained:

$$\sum_{p=1}^P \left(\int_A \left\{ u_j (N_{x_i,x} + N_{xy,y}) + v_j (N_{xy,x} + N_{y_i,y} + \lambda_i N_{x_L} v_{i,xx}) + \right. \right. \quad \begin{matrix} i = 1, 2, \dots \\ j = 1, 2, \dots \end{matrix} \quad (B1) \\ \left. \left. + w_j [M_{x_i,xx} + 2M_{xy,xy} + M_{y_i,yy} + \lambda_i (N_{x_L} w_{i,xx} + N_{y_L} w_{i,yy})] \right\} dA \right)_p = 0$$

Equation (B1) is manipulated by applying Green's Theorem, and invoking the definitions of $\{\epsilon_i\}$, and $\{\kappa_i\}$, of equation (2.6.3), and $\{N_i\}$, and $\{M_i\}$ of equation (2.6.2). The following equation can be obtained:

$$\sum_{p=1}^P \left(- \int_A \left\{ \{N_i\}^T \{\epsilon_j\} + \{M_i\}^T \{\kappa_j\} + \lambda_i [N_{x_L} (v_{i,x} v_{j,x} + w_{i,x} w_{j,x}) + N_{y_L} w_{i,y} w_{j,y}] \right\} dA \right. \quad (B2) \\ \left. + \int_0^b n_x [N_{x_i} u_j + (N_{xy_i} + \lambda_i N_{x_L} v_{i,x}) v_j + (M_{x_i,x} + 2M_{xy_i,y} + \lambda_i N_{x_L} w_{i,x}) w_j - M_{x_i} w_{j,x}] \Big|_{x=0,L} dy \right. \\ \left. + \int_0^L n_y [N_{xy_i} u_j + N_{y_i} v_j + (2M_{xy_i,x} + M_{y_i,y} + \lambda_i N_{y_L} w_{i,y}) w_j - M_{y_i} w_{j,y}] \Big|_{y=0,b} dx \right)_p = 0$$

The functional form of the buckling modes guarantees that the quantities N_{x_i} , v_j , w_j , and M_{x_i} are all identically zero at $x=0$ and $x=L$, so the second integral of equation (B2) is zero. The third integral in equation (B2) can be recognized to be the integral along the length of the structure of the components of $\{f_{ii}\}$ (see equation (2.6.6)) weighted by the components of $\{u_{ii}\}$. Using the local/global transformation relationships of equations (2.2.1-2) and the definitions of $\{F^a\}$, the third integral of equation (B2) can be expressed as

$$\sum_{n=1}^N \int_0^L \{F_i^n\}^T \{U_j^n\} dx \quad (B3)$$

where N is the number of node-lines in the structure. At the non-boundary node-lines, the components of $\{F_i^n\}$ are all zero (equation (2.3.1)). At the boundary node-lines, each component of $\{F_i^n\}$ is either zero or its associated component of $\{U_i^n\}$ is zero, since the buckling eigenfunctions satisfy the homogeneous form of whatever conditions have been specified along the boundary node-lines. Thus, expression (B3) is identically zero.

Equation (B2) has now been reduced to the equation

$$\sum_{p=1}^P \left(- \int_A \left\{ \{N_i\}^T \{\epsilon_j\} + \{M_i\}^T \{\kappa_j\} + \lambda_i [N_{x_L} (v_{i,x} v_{j,x} + w_{i,x} w_{j,x}) + N_{y_L} w_{i,y} w_{j,y}] \right\} dA \right)_p = 0 \quad (B4)$$

Equation (B4) is reexpressed with modes i and j switched, and this equation is subtracted from equation (B4). Terms are eliminated from the resulting equation by recognizing that:

$$\begin{aligned}\{N_i\}^T \{\epsilon_j\} &= \{N_j\}^T \{\epsilon_i\} \\ \{M_i\}^T \{\kappa_j\} &= \{M_j\}^T \{\kappa_i\}\end{aligned}\quad (B5)$$

The following expression of the orthogonality of the buckling modes is thus obtained:

$$(\lambda_i - \lambda_j) \sum_{p=1}^P \left(\int_A [N_{x_L}(v_{i,x}v_{j,x} + w_{i,x}w_{j,x}) + N_{y_L}w_{i,y}w_{j,y}] dA \right)_p = 0 \quad \begin{matrix} i = 1, 2, \dots \\ j = 1, 2, \dots \end{matrix} \quad (B6)$$

A set of eigenfunctions can be obtained which satisfies the orthonormality condition

$$\sum_{p=1}^P \left(\int_A [N_{x_L}(v_{i,x}v_{j,x} + w_{i,x}w_{j,x}) + N_{y_L}w_{i,y}w_{j,y}] dA \right)_p = \delta_{ij} a_i \quad (B7)$$

where δ_{ij} is the Kroniker delta function, and a_i is a constant which depends on how the eigenfunctions are normalized. Condition (B7) follows automatically from equation (B6) for eigensolution pairs which have different eigenvalues ($\lambda_i \neq \lambda_j$). If $\lambda_i = \lambda_j$ but longitudinal halfwave numbers m_i and m_j are different, then equations (B7) is satisfied by virtue of the x -dependence of the integrand. If $\lambda_i = \lambda_j$ and $m_i = m_j$ (for $i \neq j$), an orthogonal set of buckling modes can be generated using the Gram-Schmidt orthogonalization process.

An alternate expression of the orthogonality condition (B7) is developed here. By applying Green's Theorem to equation (B7) and eliminating boundary terms which are known to be zero, the following equations is obtained:

$$\sum_{p=1}^P \left(- \int_A [v_j(N_{x_L}v_{i,xx}) + w_j(N_{x_L}w_{i,xx} + N_{y_L}w_{i,yy})] dA \right)_p + \int_0^L n_y N_{y_{GL}} \Psi_i^n W_j^n \Big|_{n_1, n_2} dx = \delta_{ij} a_i \quad (B8)$$

where $N_{y_{GL}}$ is the unit global y -normal in-plane load, $n_y = \pm 1$ indicates the direction of the global edge-normal unit vector, and n_1 and n_2 are the index numbers for the two boundary node-lines. The second integral of equation (B8) is zero if the following condition is met:

$$\begin{aligned}N_{y_{GL}} &= 0 \\ \text{-or-} \\ [\Psi^n = 0 \quad \text{-or-} \quad W^n = 0] \quad (n = n_1, n_2)\end{aligned} \quad (B9)$$

The above condition is violated only if a panel has side-edges which are both i) unrestrained both with respect to out-of-plane deflection and out-of-plane rotation, and ii) subjected to y -normal in-plane loading; commonly encountered configurations generally do satisfy equation (B9). If it is assumed that the conditions of equation (B9) are satisfied, the orthogonality condition of equation (B7) has the following equivalent form:

$$\sum_{p=1}^P \left(\int_A [v_j(N_{x_L}v_{i,xx}) + w_j(N_{x_L}w_{i,xx} + N_{y_L}w_{i,yy})] dA \right)_p = -\delta_{ij} a_i \quad (B10)$$

B.2 Orthogonality Between the Buckling Modes and the Second-Order Fields

Assume that it is desired to enforce orthogonality between each second-order displacement field $\{u_{ij}\}$ and each buckling mode $\{u_k\}$. In the orthogonality condition for the buckling modes, equation (B7), replace $\{u_k\}$ with $\{u_{ij}\}$:

$$\sum_{p=1}^P \left(\int_A [N_{x_L} (v_{ij,x} v_{k,x} + w_{ij,x} w_{k,x}) + N_{y_L} w_{ij,y} w_{k,y}] dA \right)_p = 0 \quad \begin{matrix} (i, j = 1, 2, \dots) \\ (k = 1, 2, \dots) \end{matrix} \quad (B11)$$

By applying Green's Theorem to equation (B11), cancelling boundary terms that are identically zero, and assuming that equation (B9) is satisfied, equation (B11) can be converted into two alternate forms:

$$\sum_{p=1}^P \left(\int_A [v_k (N_{x_L} v_{ij,xx}) + w_k (N_{x_L} w_{ij,xx} + N_{y_L} w_{ij,yy})] dA \right)_p = 0 \quad (B12)$$

$$\begin{aligned} & - \sum_{p=1}^P \left(\int_A [v_{ij} (N_{x_L} v_{k,xx}) + w_{ij} (N_{x_L} w_{k,xx} + N_{y_L} w_{k,yy})] dA \right)_p \\ & + \sum_{p=1}^P \left(\int_0^b n_x N_{x_L} (v_{ij} v_{k,x} + w_{ij} w_{k,x}) \Big|_{x=0,L} dy \right)_p = 0 \end{aligned} \quad (B13)$$

Functions v_{ij} and w_{ij} do not necessarily go to zero $x=0, L$; however, according to the nominal boundary conditions, the transverse displacements v and w should be approximately zero at $x=0, L$. Assume that the solution procedure used to compute $\{u_{ij}\}$ is successful in assuring that this boundary condition is approximately satisfied, so that the boundary term in equation (B13) can be neglected. Equation (B13) then becomes

$$\sum_{p=1}^P \left(\int_A [v_{ij} (N_{x_L} v_{k,xx}) + w_{ij} (N_{x_L} w_{k,xx} + N_{y_L} w_{k,yy})] dA \right)_p = 0 \quad (B14)$$

Thus, equations (B11), (B12), and (B14) are equivalent expressions for orthogonality of the functions $\{u_{ij}\}$ with respect to functions $\{u_i\}$.

APPENDIX C: AN EXPANSION OF $\delta\pi_3$

In terms of the notation used in equations (2.8.29-30), $\delta\pi_3$ can be written as

$$\delta\pi_3 = \delta q_i q_j q_k (\hat{C}_{ijk} + \lambda \hat{C}_{ijk}^L) \quad (C1)$$

for the case of a perfect structure. In order to keep the following derivation manageable, attention is limited to the case where displacement control is used for the in-plane loading (CTRL='D' in Table 1), and where coefficients B_i ($i = 1, 2, \dots$) appearing in equation (2.6.12) are zero. With these restrictions, equation (C1) can be expressed in terms of "primitive" coefficients as

$$\delta\pi^3 = \delta q_i q_j q_k [(2C_{ij}^k + C_{jk}^i) + \lambda(C_{ijk}^L + 2C_{jik}^L)] \quad (C2)$$

The primitive coefficients have the following definitions:

$$C_{ij}^k = \sum_{p=1}^P \left(\int_A (\{N_k\}^T \{\epsilon_{ij}\} + \{M_k\}^T \{\kappa_{ij}\}) dA \right)_p \quad C_{ijk}^L = \sum_{p=1}^P \left(\int_A \{N_L\}^T \{\epsilon_{ijk}\} dA \right)_p \quad (C3)$$

where $\{N_L\}$ is defined in equation (2.5.3), $\{N_i\}$ and $\{M_i\}$ are defined in equations (2.6.2), $\{\epsilon_{ij}\}$ and $\{\kappa_{ij}\}$ are defined in equations (2.7.3), and $\{\epsilon_{ijk}\}$ is defined in equation (2.8.6).

Through applications of Green's theorem and cancellation of boundary terms at the x -normal ends which are known to be zero (because of the function forms of $\{u_i\}$ and $\{u_{ij}\}$), the following two equivalent expressions are developed for C_{ij}^k :

$$\begin{aligned} C_{ij}^k &= -[\langle u_{ij}, L(N_k) \rangle + \frac{1}{2} \langle u_i, N(N_k, u_j) \rangle] \\ &\quad + \sum_{p=1}^P \left(\int_0^b n_x [N_{xy} v_{ij} + (M_{x,x} + 2M_{xy,y}) w_{ij}] \Big|_{x=0,L} dy \right. \\ &\quad \left. + \int_0^L n_y \{ [N_{xy} u_{ij} + N_{yx} v_{ij} + (2M_{xy,x} + M_{yx,y}) w_{ij} - M_{yx} w_{ij,y}] \right. \\ &\quad \left. + \frac{1}{2} [N_{yx} u_{j,y} u_i + (N_{xy} w_{j,y} + N_{yx} w_{j,y}) w_i] \} \Big|_{y=0,b} dx \right)_p \\ &= -\langle u_k, L(N_{ij}) \rangle \\ &\quad + \sum_{p=1}^P \left(\int_0^b n_x (-M_{xy} w_{k,x}) \Big|_{x=0,L} dy \right. \\ &\quad \left. + \int_0^L n_y [N_{xy} u_k + N_{yx} v_k + (2M_{xy,x} + M_{yx,y}) w_k - M_{yx} w_{k,y}] \Big|_{y=0,b} dx \right)_p \end{aligned} \quad (C4)$$

where the inner products and operators which appear are defined in equations (4.2.1-3). Similarly, the following two equivalent expressions are developed for C_{ijk}^L :

$$\begin{aligned} C_{ijk}^L &= -\langle u_{jk}, N(N_L, u_i) \rangle \\ &\quad + \sum_{p=1}^P \left(\int_0^b n_x N_{xL} (v_{i,x} v_{jk} + w_{i,x} w_{jk}) \Big|_{x=0,L} dy + \int_0^L n_y N_{yL} w_{i,y} w_{jk} \Big|_{y=0,b} dx \right)_p \\ &= -\langle u_i, N(N_L, u_{jk}) \rangle + \sum_{p=1}^P \left(\int_0^L n_y N_{yL} w_{jk,y} w_i \Big|_{y=0,b} dx \right)_p \end{aligned} \quad (C5)$$

Equation (C2) is evaluated using equations (C4) and (C5). For C_{ij}^k , the first form in equation (C4) is used, and for C_{jk}^i , the second form is used. For C_{ij}^k , the second form in equation (C5) is used, and for C_{jk}^i , the first form is used. Terms on the y -normal boundaries of plate strips are transformed to refer to the node-lines and global coordinate directions, and the contributions to the generalized node-line force resultants are summed, where appropriate. The following equation is obtained:

$$\begin{aligned} \delta\pi_3 = \delta q_i q_j q_k \{ & -\langle u_i, L(N_{jk}) + N(N_k, u_j) + \lambda N(N_L, u_{jk}) \rangle - 2\langle u_{ij}, L(N_k) + \lambda N(N_L, u_k) \rangle \\ & + \sum_{p=1}^P \left(\int_0^b n_x (-M_{xjk} w_{i,x}) \big|_{x=0,L} dy \right)_p + \sum_{n=1}^N \int_0^L \{U_i^n\}^T \{F_{jk}^n\} dx \\ & \sum_{p=1}^P \left(\int_0^b n_x 2[v_{ij}(N_{xyk} + \lambda N_{x_L} v_{k,x}) + w_{ij}(M_{xk,x} + 2M_{xyk,y} + \lambda N_{x_L} w_{k,x})] \big|_{x=0,L} dy \right)_p \\ & + \sum_{n=1}^N \int_0^L 2\{U_{ij}^n\}^T \{F_{xk}^n\} dx + 2(\lambda - \lambda_k) \int_0^L n_y N_{yG_L} W_{ij}^n \Psi_k^n \big|_{n_1, n_2} dx \} \end{aligned} \quad (C6)$$

Several simplifications are made to the above equation. First, the integrals containing $\{U_i^n\}$, $\{U_{ij}^n\}$, $\{F_{jk}^n\}$, and $\{F_k^n\}$ are deleted, because the homogeneous node-line boundary conditions specify that one or the other term of each product is zero. Second, while the functional form for $\{u_{ij}\}$ does not guarantee it to be so, it is assumed that at $x=0, L$ the quantities M_{xjk} , v_{ij} , and w_{ij} are approximately zero (consistent with the buckling mode characteristics $M_x = v_i = w_i = 0$ at $x=0, L$). This eliminates the integrals at the x -normal ends of the structure. Third, the structural configuration is assumed to satisfy Appendix B equation (B9), thus eliminating the integral at the boundary node lines n_1 and n_2 . (This assumption states that the configuration does not have a free y -normal edge with y -normal in-plane loading.) Finally, the buckling equations as written in equation (4.2.5) are used to further simplify the second inner product in equation (C6). The following equation is obtained:

$$\begin{aligned} \delta\pi_3 = \delta q_i q_j q_k \{ & -\langle u_i, [L(N_{jk}) + \frac{1}{2} N(N_k, u_j) + \frac{1}{2} N(N_j, u_k) + \lambda N(N_L, u_{jk})] \rangle \\ & - 2(\lambda - \lambda_k) \langle u_{ij}, N(N_L, u_k) \rangle \} \end{aligned} \quad (C7)$$

where the expression $[q_j q_k N(N_k, u_j)]$ of equation (C6) was manipulated to obtain symmetry in indices j and k .

APPENDIX D. DESCRIPTION OF THE NONLINEAR SOLUTION STRATEGIES

D.1. Form of Equations Governing Equilibrium

It is assumed that the total potential energy of a structure can be expressed in the following algebraic form:

$$\begin{aligned}\pi &= \pi(\bar{q}, \alpha, \beta) \\ &= \pi_o + q_i(A_i + \alpha A_i^\alpha + \beta A_i^\beta) + q_j q_j(A_{ij} + \alpha A_{ij}^\alpha + \beta A_{ij}^\beta) \\ &\quad + q_j q_k q_k(A_{ijk} + \alpha A_{ijk}^\alpha + \beta A_{ijk}^\beta) + q_j q_k q_l(A_{ijkl} + \alpha A_{ijkl}^\alpha + \beta A_{ijkl}^\beta)\end{aligned}\quad (D1)$$

where summation over i, j, k , and l is implied, \bar{q} is a vector of generalized coordinates, α and β are generalized load parameters, the sub- and super-scripted coefficients A are constant, and the term π_o has no dependence on the generalized coordinates. It is assumed that the generalized coordinates and load parameters in equation (D1) have been normalized so that they take on values of order of magnitude unity in the course of an analysis. The method described here is not limited to total potential energy expressions with two load parameters and fourth order terms; these specific characteristics are adopted for demonstration purposes.

The equations governing equilibrium are obtained by imposing a stationary total potential energy condition, expressed as

$$f_i(\bar{q}, \alpha, \beta) = 0 \quad (i = 1, 2, \dots) \quad (D2)$$

where

$$\begin{aligned}f_i &= \frac{\partial \pi}{\partial q_i} \\ &= (B_i + \alpha B_i^\alpha + \beta B_i^\beta) + q_j(B_{ij} + \alpha B_{ij}^\alpha + \beta B_{ij}^\beta) \\ &\quad + q_j q_k(B_{ijk} + \alpha B_{ijk}^\alpha + \beta B_{ijk}^\beta) + q_j q_k q_l(B_{ijkl} + \alpha B_{ijkl}^\alpha + \beta B_{ijkl}^\beta)\end{aligned}\quad (D3)$$

The newly introduced coefficients appearing in the above equation are given by, for example,

$$\begin{aligned}B_i &= A_i & B_{ijk} &= A_{ijk} + A_{jik} + A_{jki} \\ B_{ij} &= A_{ij} + A_{ji} & B_{ijkl} &= A_{ijkl} + A_{jilk} + A_{jkli} + A_{ljki}\end{aligned}\quad (D4)$$

The two load parameters α and β can be controlled asynchronously using a single load parameter λ . A series of K load ranges is specified in terms of target values for α and β : $(0, 0)$, (α_1, β_1) , (α_2, β_2) , ..., (α_K, β_K) . Over the k^{th} load range, α and β vary linearly with λ as λ increases from 0 to 1:

$$\begin{pmatrix} \alpha \\ \beta \end{pmatrix} = \begin{pmatrix} \alpha_{k-1} \\ \beta_{k-1} \end{pmatrix} + \lambda \begin{pmatrix} \alpha_k - \alpha_{k-1} \\ \beta_k - \beta_{k-1} \end{pmatrix} \quad 0 \leq \lambda \leq 1 \quad (D5)$$

For the k^{th} load interval, the equilibrium equations then take the form

$$\begin{aligned}f_i(\bar{q}, \lambda) &= (C_i + \lambda C_i^\lambda) + q_j(C_{ij} + \lambda C_{ij}^\lambda) + q_j q_k(C_{ijk} + \lambda C_{ijk}^\lambda) + q_j q_k q_l(C_{ijkl} + \lambda C_{ijkl}^\lambda) \\ &= 0 \quad (i = 1, 2, \dots, M)\end{aligned}\quad (D6)$$

where for example,

$$\begin{aligned}C_i &= B_i + \alpha_{k-1} B_i^\alpha + \beta_{k-1} B_i^\beta \\ C_i^\lambda &= (\alpha_k - \alpha_{k-1}) B_i^\alpha + (\beta_k - \beta_{k-1}) B_i^\beta\end{aligned}\quad (D7)$$

and where it is assumed henceforth that a finite basis of M generalized coordinates is in use.

D.2. Arc-Length Control Method

The implementation of the Riks-Wempner arc-length control method described here was guided in large part by the presentation given in [D1]. Concepts presented in [D1] are also used here in a procedure for locating and classifying critical stability points.

D.2.1. Arc-length parameter "s". Let (\bar{q}, λ) be a known solution to equation (D6), and let $(\bar{q} + \bar{\xi}, \lambda + \delta)$ be a new solution which is sought in the vicinity of the known solution. The new solution satisfies the equation

$$f_i(\bar{q} + \bar{\xi}, \lambda + \delta) = 0 \quad (i = 1, 2, \dots, M) \quad (D8)$$

The independent parameter s is introduced, so that $\bar{q} = \bar{q}(s)$ and $\lambda = \lambda(s)$. Parameter s is the arc-length measure in $(M + 1)$ -dimensional space for an equilibrium solution path, and is governed by the equation

$$\dot{q}_j \dot{q}_j + \dot{\lambda}^2 = 1 \quad (D9)$$

where summation over j is implied, and where $\dot{q}_j = \partial \bar{q}_j / \partial s$ and $\dot{\lambda} = \partial \lambda / \partial s$. A Taylor series expansion about the starting solution is used to obtain an expression for the incremental solution $(\bar{\xi}, \delta)$ in terms of the an arc-length increment Δs :

$$\bar{\xi} = \dot{\bar{q}} \Delta s + O(\Delta s^2), \quad \delta = \dot{\lambda} \Delta s + O(\Delta s^2) \quad (D10)$$

D.2.2. Determination of the derivatives $(\dot{\bar{q}}, \dot{\lambda})$. By expressing each equation of equation (D8) as a Taylor series expansion about the solution (\bar{q}, λ) , applying the substitution of equations (D10), and taking the limit as Δs approaches zero, it can be shown that [D1]

$$D_{ij} \dot{q}_j + D_i^\delta \dot{\lambda} = 0, \quad (i = 1, 2, \dots, M) \quad (D11)$$

In equation (D11), D_{ij} is the tangent stiffness matrix, given by

$$D_{ij} = \left. \frac{\partial f_i}{\partial q_j} \right|_{(\bar{q}, \lambda)} = \bar{C}_{ij} + q_k (\bar{C}_{ijk} + \bar{C}_{ikj}) + q_k q_l (\bar{C}_{ijkl} + \bar{C}_{ikjl} + \bar{C}_{iljk}) \quad (D12)$$

where, for example,

$$\bar{C}_{ijk} = C_{ijk} + \lambda C_{ijk}^\lambda \quad (D13)$$

and vector D_i^δ is defined by

$$D_i^\delta = \left. \frac{\partial f_i}{\partial \lambda} \right|_{(\bar{q}, \lambda)} = C_i^\lambda + q_j C_{ij}^\lambda + q_j q_k C_{ijk}^\lambda + q_j q_k q_l C_{ijkl}^\lambda \quad (D14)$$

The derivatives $(\dot{\bar{q}}, \dot{\lambda})$ are determined by arbitrarily specifying one of the $M + 1$ unknown values, solving for the remaining values using equation (D11), then scaling the solution so that equation (D9) is satisfied. The values $(\dot{\bar{q}}, \dot{\lambda})$ thus obtained are ambiguous to the extent of a factor ± 1 . For a starting solution ($\lambda = 0$), $\dot{\lambda}$ is positive. In a solution stepping procedure, it is assumed that the direction of the vector $(\dot{\bar{q}}, \dot{\lambda})$ does not change radically between successive solutions, so that at the n^{th} equilibrium solution (\bar{q}^n, λ^n) , the sense of the vector $(\dot{\bar{q}}^n, \dot{\lambda}^n)$ is determined by the following requirement:

$$\dot{q}_j^{n-1} \dot{q}_j^n + \dot{\lambda}^{n-1} \dot{\lambda}^n > 0 \quad (D15)$$

The use of this simple technique negates the criticism of the arc-length control method, issued in [D2], that the sign of $\dot{\lambda}$ is ambiguous.

D.2.3. Solution stepping using arc-length control. Using equations (D9,10) it can be determined that for a sufficiently small increment Δs the following approximate relationship holds:

$$\Delta s \approx \dot{q}_j \xi_j + \dot{\lambda} \delta \quad (D16)$$

where summation over j is implied. Arc-length control is imposed by specifying the increment Δs from the n^{th} solution to the $(n+1)^{\text{th}}$ solution, and assuming that the approximate relationship of equation (D16) is an exact one. The solution is then governed by both equation (D8) and equation (D16). Newton-Raphson iteration is used to determine the new solution in the following way. Where (\bar{q}^r, λ^r) denotes the r^{th} estimate of the new solution, the iterative solution procedure can be written as

$$(\bar{q}^{r+1}, \lambda^{r+1}) = (\bar{q}^r, \lambda^r) + (\Delta \bar{q}^{r+1}, \Delta \lambda^{r+1}) \quad (D17)$$

where the correction $(\Delta \bar{q}^{r+1}, \Delta \lambda^{r+1})$ is obtained by solving the linear system of equations

$$D_{ij}^r \Delta q_j^{r+1} + (D_i^\delta)^r \Delta \lambda^{r+1} = -R_i^r \quad (i = 1, 2, \dots, M) \quad (D18a)$$

$$\dot{q}_j \Delta q_j^{r+1} + \dot{\lambda} \Delta \lambda^{r+1} = \Delta s - [\dot{q}_j (q_j^r - q_j^n) + \dot{\lambda} (\lambda^r - \lambda^n)] \quad (D18b)$$

where matrix D_{ij}^r and vector $(D_i^\delta)^r$ are evaluated at (\bar{q}^r, λ^r) , and R_i^r is the residual error vector for the r^{th} estimate:

$$R_i^r = f_i(\bar{q}^r, \lambda^r) \quad (D19)$$

D.2.4. Stability criterion; properties and classification of critical points. The following eigenvalue problem is evaluated for use in assessing the stability of an equilibrium solution:

$$([D] - \omega_k [I])(\phi^k) = \{0\} \quad (k = 1, 2, \dots, M) \quad (D20)$$

where $[D]$ is the tangent stiffness matrix and $[I]$ is the identity matrix. Eigenvalues ω_k are assumed to be ordered according to increasing value. When all eigenvalues are positive, the tangent stiffness matrix is positive definite, the total potential energy is a local minimum, and the equilibrium state is stable. At a critical stability point (a limit point or bifurcation point) the first eigenvalue ω_1 is zero. Consider ω_1 to be a function of the path parameter s , and let s^* be the value of s at a critical point. The critical stability point then has the property

$$\omega_1(s^*) = 0 \quad (D21)$$

A limit point has the property

$$\dot{\lambda}(s^*) = 0 \quad (D22)$$

whereas a bifurcation point has the property [D1]:

$$B_1(s^*) = 0 \quad (D23)$$

where $B_k(s)$ is defined as

$$B_k(s) = (\phi_j^k D_j^\delta) \Big|_s \quad (k = 1, 2, \dots, M) \quad (D24)$$

It is noted that at a limit point, the path tangent $\dot{\bar{q}}$ is a scalar multiple of the eigenvector $\bar{\phi}^1$. This can be seen by considering equations (D11,20-22).

D.2.5. Detection and classification of forward critical points. The criteria given in equations (D21-23) for identifying and classifying a critical point apply only at the critical point itself. A method is described here for detecting and classifying a "forward" critical point, meaning one which is being approached in the process of solution stepping. The values of ω_1 , $\dot{\lambda}$, and B_1 are computed for each discrete equilibrium solution. In the vicinity of the most recently obtained solution, the three functions

$\omega_1(s)$, $\lambda(s)$, and $B_1(s)$ are approximated as quadratic functions of s by fitting curves to the parameter values from the three most recently obtained solutions. The equations $\omega_1(s^*)=0$, $\lambda(s_l^*)=0$, and $B_1(s_b^*)=0$ are then solved to obtain extrapolated values for s^* , s_l^* , and s_b^* , which are the values of s at the next forward critical point, limit point, and bifurcation point, respectively. Each of the parameters s^* , s_l^* , and s_b^* is set equal to the smallest positive real solution of its associated quadratic equation, if such a solution exists; otherwise the parameter is set to a large, positive real number.

Define Δs^* , Δs_l^* , and Δs_b^* , to be the incremental values from the current value s to the values s^* , s_l^* , and s_b^* , respectively. If, Δs_l^* approaches Δs^* as a critical point is approached (ie. as Δs^* approaches zero) then the critical point is classified as a limit point, and if Δs_b^* approaches Δs^* , the critical point is classified as a bifurcation point. (A critical point may be both a limit point and a bifurcation point.) In order to evaluate these trends, it is necessary to compute several equilibrium solutions which approach the critical point without overshooting it. To do this, Riks [D1] suggests selecting Δs to be $\Delta s = c\Delta s^*$ (where c is a factor less than one and greater than zero) until the extrapolated value Δs^* is smaller than a specified cutoff value. Because the critical point can be approached only to within some finite increment Δs^* , there is some uncertainty involved in evaluating the trends of the extrapolated values. The approach used here is to inspect the ratios $(\Delta s_l^*/\Delta s^*)$ and $(\Delta s_b^*/\Delta s^*)$ evaluated at the smallest value of Δs^* used. If a ratio has an order of magnitude of unity (a value less than, say, 3) then it is assumed that the associated values are converging. The use of quadratic interpolation functions has been found by the author to provide a considerably more robust method of locating critical points than when the linear interpolation functions suggested in [D1] are used.

Plate problems have been encountered in which the parameter B_1 is uniformly zero along a postbuckling equilibrium path. In this case the extrapolation procedure described for determining Δs_b^* is not appropriate, and any critical point encountered is a bifurcation point.

While equation (D21) defines a critical stability state ($\omega_1 = 0$), other singular points may be encountered where the first eigenvalue ω_1 is negative, but another eigenvalue ω_k is zero for some value k greater than one. The criteria of equations (D22) and (D23) can still be used to classify the singular point as a limit point and/or bifurcation point, except that B_k is used in equation (D23) rather than B_1 .

D.2.6. Computing the solution at a critical point. If it is determined that a critical point is not a bifurcation point, then the critical equilibrium solution (a limit point) is determined by selecting Δs of equation (D18b) equal to the extrapolated value of Δs^* , once the latter measure is sufficiently small, and using the iterative solution procedure already described [D1]. If it is determined that a critical point is a bifurcation point, arc-length control is not well suited for centering on the critical point because of the solution branching. It is the author's experience that it is possible to approach a critical point quite closely using arc-length control, to the point that the value of Δs^* is very small compared to unity. It thus seems sufficiently accurate to perform a simple extrapolation to determine the bifurcation point by using a first-order approximation of equations (D10) with $\Delta s = \Delta s^*$.

D.3. Control of Solution Branching with Thurston's Method

This section describes an implementation of Thurston's method [D3], used for analyzing solution branching in the vicinity of a bifurcation point which has been identified and located using the procedures described in Section D.2. In [D3], Thurston's method is applied to the differential equations governing equilibrium before any necessary discretization of the structural response has been performed. Here, the discretization has already been performed in obtaining equations (D6) which govern equilibrium, and Thurston's method is applied directly to these equations.

D.3.1. Transformation of the equilibrium equations. Let (\bar{q}, λ) be a known exact or approximate solution to equations (D6), and let $(\bar{q} + \xi, \lambda + \delta)$ be a new solution which is sought in the vicinity of the known solution. The latter solution is governed by equation (D8). By expressing equation (D8) in the expanded form of equation (D6) and grouping terms based on their power in ξ_i and δ , the following equation is obtained:

$$(D_i + \delta D_i^\delta) + \xi_j(D_{ij} + \delta D_{ij}^\delta) + \xi_j \xi_k(D_{ijk} + \delta D_{ijk}^\delta) + \xi_j \xi_k \xi_l(D_{ijkl} + \delta C_{ijkl}^\lambda) = 0 \quad (D25)$$

($i = 1, 2, \dots, M$)

where D_i^δ and D_{ij} are given in equations (D14) and (12), respectively and

$$\begin{aligned} D_i &= f_i(\bar{q}, \lambda) \\ D_{ij}^\delta &= C_{ij}^\lambda + q_k(C_{ijk}^\lambda + C_{ikj}^\lambda) + q_k q_l(C_{ijkl}^\lambda + C_{ikjl}^\lambda + C_{iljk}^\lambda) \\ D_{ijk}^\delta &= C_{ijk}^\lambda + q_l(C_{ijkl}^\lambda + C_{ijlk}^\lambda + C_{iljk}^\lambda) \\ D_{ijk} &= C_{ijk} + q_l(C_{ijkl} + C_{ijlk} + C_{iljk}) + \lambda D_{ijk}^\delta \\ D_{ijkl} &= C_{ijkl} + \lambda C_{ijkl}^\lambda \end{aligned} \quad (D26)$$

The following eigenvalue problem is derived from the linear terms of equations (D25):

$$([D] + \delta_k [D^\delta])\{\theta^k\} = \{0\}, \quad k = 1, 2, \dots, M \quad (D27)$$

where $[D]$ and $[D^\delta]$ are the matrices of coefficients D_{ij} and D_{ij}^δ , respectively. Equation (D27) differs from the eigenvalue problem of equation (D20) by the presence of the matrix $[-D^\delta]$ in place of $[I]$. The eigenvalues δ_k are numbered in order of ascending value. When all eigenvalues are distinct, the eigenvectors form an orthogonal set, and the eigenvectors are scaled to meet the following orthonormality condition:

$$\theta_i^m D_{ij}^\delta \theta_j^k = -\delta_{km} \quad (D28)$$

where δ_{ij} is the Kroniker delta function. For multiple eigenvalues which coincide, the associated eigenvectors must be orthogonalized before normalization, using, for example, the Gram-Schmidt orthogonalization procedure [D4].

The incremental solution $\bar{\xi}$ is expressed as a series in the eigenvectors, $\bar{\theta}^k$:

$$\bar{\xi} = \bar{\theta}^k a_k \quad (D29)$$

where summation over k is implied, and the coefficients a_k ($k = 1, 2, \dots, M$) are initially unknown. The following relationship is established through the use of equations (D27-29):

$$\theta_i^m (D_{ij} + \delta D_{ij}^\delta) \xi_j = -(\delta - \delta_m) a_m \quad (m = 1, 2, \dots, M) \quad (D30)$$

where summation of repeated indices is implied except for index m . Equation (D25) is now restated, eliminating parameters ξ_j using the substitution of equation (D29). For each value of m ($m = 1, 2, \dots, M$), the i^{th} equation is weighted by θ_i^m and the resulting expressions are summed over i . Equation (D30) is used to simplify the equations thus obtained, providing the following transformed equations:

$$a_m (\delta - \delta_m) = (E_m + \delta E_m^\delta) + a_n a_r (E_{mnr} + \delta E_{mnr}^\delta) + a_n a_r a_s (E_{mnrs} + \delta E_{mnrs}^\delta) \quad (D31)$$

($m = 1, 2, \dots, M$)

where summation over n, r , and s is implied, and the new coefficients are given by

$$\begin{aligned} (E_m, E_m^\delta) &= \theta_i^m (D_i, D_i^\delta) & (E_{mnr}, E_{mnr}^\delta) &= \theta_i^m \theta_j^n \theta_k^r (D_{ijk}, D_{ijk}^\delta) \\ (E_{mnrs}, E_{mnrs}^\delta) &= \theta_i^m \theta_j^n \theta_k^r \theta_l^s (D_{ijkl}, C_{ijkl}^\lambda) \end{aligned} \quad (D32)$$

where summation over i, j, k , and l is implied.

D.3.2. Analysis of solution branching. The form of equations (D31) is a generalization of the form of equations obtained by Thurston in [D5] for the analysis of compressively loaded plates, so comments made in [D5] will be used to guide the use of equations (D31). Near a limit point or an isolated bifurcation point, one of the eigenvalues, say δ_i , will be close to zero and much less in amplitude than

the remaining eigenvalues. In the vicinity of the known solution, both δ and the quantity $(\delta - \delta_i)$ are small. With this in mind, and in view of the form of equations (D31), Thurston hypothesizes that a_i will be much larger in amplitude than the remaining $M - 1$ coefficients a_m . An approximate solution is thus governed by equation number i of equations (D31) with only the variable parameters a_i and δ retained. By specifying a value for a_i , the corresponding value of the load increment δ can be computed directly. Solutions for both positive and negative values of a_i are generated in order to identify both solution branch directions.

When two eigenvalues δ_i and δ_j are both very close to zero (such as near a point of approximately simultaneous buckling in two different mode shapes) the reasoning used above is extended to suggest that an approximate solution is governed by two equations, numbers i and j of equations (D31), with only the variable parameters a_i , a_j , and δ retained. The solution procedure used here is to specify a small numerical value for either a_i or a_j , solve the two equations for δ , and then equate the two expressions for δ . A fifth degree polynomial equation in the remaining unknown parameter (a_i or a_j) is obtained. A polynomial root solver is used to determine all real solutions to the polynomial equation, then the corresponding values of δ are computed. Solutions are generated for both positive and negative values of the specified parameter (a_i or a_j) in order to identify all solution branch directions. The analysis of simultaneous bifurcation in three or more modes has not been attempted as a part of this work.

The set of approximate solutions obtained using a one- or two-mode branching analysis are assessed for physical significance in order to guide the selection of a particular solution branch to follow. The approximate solution on the selected branch is then refined using the following procedure. The approximate post-bifurcation solution is known in terms of a value δ (henceforth denoted δ^b) and one or two non-zero parameters a_m . Using equation (D29), the corresponding approximate solution ξ^b is generated. The arc-length increment corresponding to (ξ^b, δ^b) is given by

$$\Delta s^b = \sqrt{\xi_i^b \xi_i^b + (\delta^b)^2} \quad (D33)$$

and the approximate path derivatives along the new branch are given by

$$\dot{\bar{q}} \approx \xi^b / \Delta s^b, \quad \dot{\lambda} \approx \delta^b / \Delta s^b \quad (D34)$$

The arc-length control method is used to refine the solution by taking the extrapolated critical-point solution (\bar{q}^*, λ^*) as the starting solution, (\bar{q}, λ) of equation (D34) as the path tangent, Δs^b as the arc-length increment, and $(\bar{q}^* + \xi^b, \lambda^* + \delta^b)$ as the initial guess for the new solution.

References

- D1. Riks, E., An Incremental Approach to the Solution of Snapping and Buckling Problems, *Int. J. Solids and Structures*, Vol. 15, 529-551 (1979).
- D2. Yang, Yeong-Bin, and Shieh, Ming-Shan, Solution Method for Nonlinear Problems with Multiple Critical Points, *AIAA Journal*, Vol. 28, 2110-2116 (1990).
- D3. Thurston, G.A., Continuation of Newton's Method Through Bifurcation Points, *Journal of Applied Mechanics*, Vol. 36, 425-430 (1969).
- D4. Mierovitch, L., *Computational Methods in Structural Dynamics*, Sijthoff & Noordhoff, Rockville, Maryland, USA (1980).
- D5. Thurston, G.A., Modal Interaction in Postbuckled Plates - Theory, NASA TP-2943 (1989).

APPENDIX E. USER INSTRUCTIONS FOR THE NLPAN COMPUTER PROGRAM

Contents

	<u>Page</u>
Introduction	71
General Aspects of the Running NLPAN	71
General Aspects of Specifying Geometry	72
NLPAN Operating Modes	74
Linear Solution Pre-Processor	75
Review and Selection of VIPASA Buckling Solutions	75
Restart Procedure	75
Special Output	76
Convergence Considerations	76
Possible Problems	76
Line-By-Line Input Instructions	78
General Instructions	78
Input File 'nlpan.in1'	79
Input File 'nlpan.in2'	90
Example Input Files	95
Unit-Cell Representation of a T-Stiffened Panel	95
Unit-Cell Representation of a Hat-Stiffened Panel	98
References	102

USER INSTRUCTIONS FOR THE NLPAN COMPUTER PROGRAM

Introduction

This document provides user instructions for the NLPAN code as it is currently configured under the Unix operating system. Detailed line-by-line instructions for preparing input are preceded by discussions of general aspects of running NLPAN, general aspects of specifying geometry, various operating modes of NLPAN, convergence considerations, and possible problems which may be encountered. Finally, some example input files are listed. The user must be familiar with PASCO input procedures, because a PASCO input file must be formed for the structure to be analyzed. PASCO input requirements are described in [E1], and are not included in this document.

General Aspects of Running NLPAN

All FORTRAN source code for NLPAN resides in a single sub-directory, along with a 'makefile' used to compile and link the program. These files can be copied to a user's own account if it is desired or necessary to alter the program in order to increase array sizes, generate specialized output, etc..

The source code for PASCO has been incorporated into the NLPAN code, and a conventional PASCO input file is used to specify much of the configuration geometry for an NLPAN analysis. However the PASCO source code has been altered and reduced in its capabilities based on the needs of NLPAN, and thus PASCO can not be used as a stand-alone program from within NLPAN.

NLPAN runs entirely within computer memory, with the exception that a couple of data storage functions use disk files. This limits the numerical size of problems which can be considered. All dimensions for data arrays are set in a PARAMETER statement in the file 'param.f'. A single mass storage array is apportioned as needed to store many large arrays without wasted space. The dimension of the mass storage array is set by parameter MMASS. When dimensions have been exceeded, error messages are printed. The dimensions can be adjusted in the PARAMETER statement of file 'param.f', and then the program is recompiled using the 'make' command with the provided 'makefile'. The standard output file 'nlpan.out' includes a listing of dimension NMASS, which is the length of the mass storage vector required for a particular problem.

Depending on the problem size, NLPAN execution typically takes from a few seconds to a few minutes to run. The execution time is approximately proportional to the complexity of the cross section modelled (in terms of the number of plate strips and the number of discretization intervals on each plate strip) and approximately doubles with each additional VIPASA buckling mode included as a shape function.

NLPAN is executed interactively from within a data sub-directory containing the input files for a particular configuration to be modeled. The run command is '(path)nlpan' where '(path)' is the path specifying the location of the executable file. The Unix command 'alias' can be used to define a simple input string, such as 'nlpan', which initiates program execution without the need to type the complete path each time the program is run. The data sub-directory must contain three input files:

'pasco.in'	PASCO input file
'nlpan.in1'	Basic NLPAN input including modelling options and geometric data.
'nlpan.in2'	Imperfection amplitudes and control parameters for the final nonlinear analysis.

All working files and output files are written to the data sub-directory using generic names, so it is natural

to use a separate sub-directory for each configuration analyzed. The standard output files are:

'pasco.out'	Output from PASCO
'nlpan.out'	Standard output from NLPAN, including basic load-step output
'nlpan.our'	Output of analysis-control parameters used in solution stepping

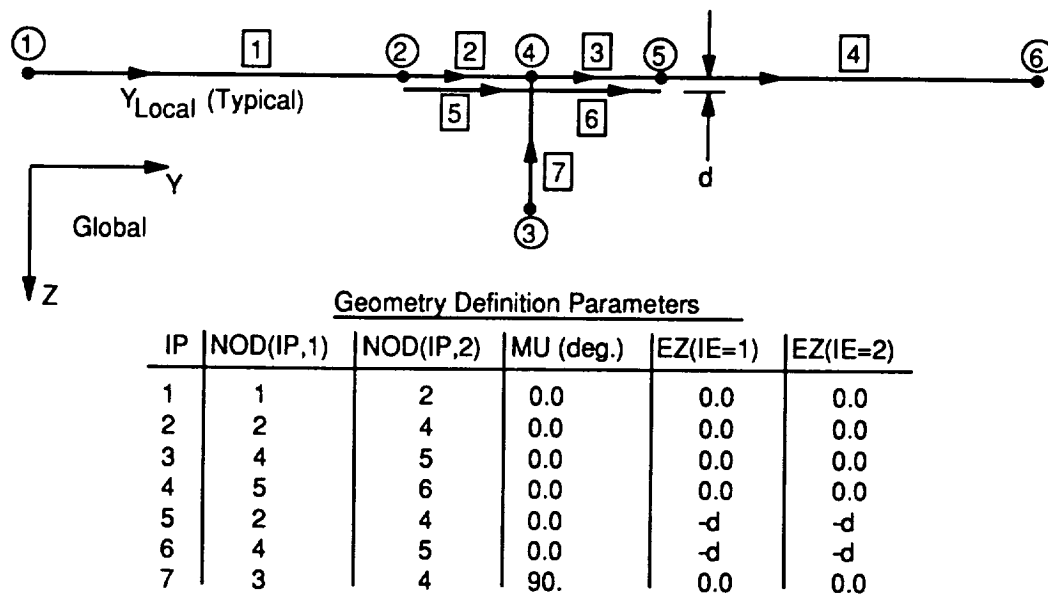
Output files are overwritten with each successive run, so files must be renamed to be saved. Additional output files are generated as selected by the user using parameters described in the section "Line-by-Line Input Instructions." Several files are created for passing data between different program units, including 'stiff.in', 'modes.in', 'reverse.in'. If intermediate calculations are saved for restarting, the files 'nlpan.binstor' and 'nlpan.binind' are created.

General Aspects of Specifying Geometry

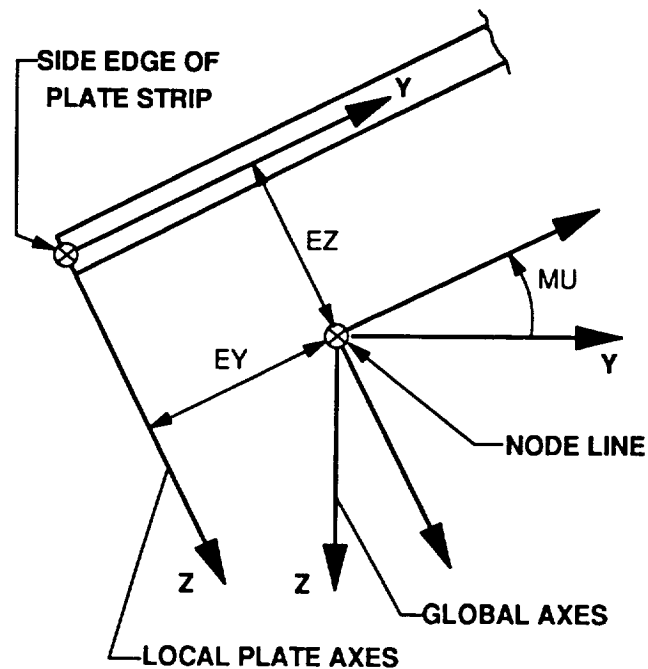
The first step is to form the PASCO input file, which is given the name 'pasco.in'. The following limitations are placed on the PASCO model:

- 1) The configuration must be defined using both HCARD and ICARD input, with ICREP=1 and NOBAY=1. This suppresses substructuring in the VIPASA buckling analysis so that the buckling modes returned from VIPASA include information at all of the node lines.
- 2) Only in-plane normal loads NX(1) and NY(1) may be specified. The PASCO features of shear loading, pressure loading, load eccentricity, bowing imperfection, and vibration frequency should not be used.
- 3) PASCO input data related to design optimization procedures are not used.
- 4) The following PASCO input parameters should NOT be present: MINLAM, NEIG, and NLAM.
- 5) Set CONV1=50000., FREQ=0., MAXJJJ=0, LINK=1

In defining the PASCO geometric model, a cross sectional configuration is defined in terms of a set of numbered plate strips and a set of numbered node lines. An example of a model with 7 plate strips and 6 node lines is shown in Figure E1(a). Each plate strip has a local Y coordinate axis (indicated by arrows in Figure E1(a)) originating at one of the edges of the strip. Each plate strip may be rotated by an angle MU relative to the global coordinate directions, and a plate edge may be offset from its associate node line, as specified by the values EY and EZ defined in Figure E1(b). The connectivity of the model and the rotation angles MU and offset measures EY and EZ are not passed automatically from PASCO to NLPAN, and thus the information must be repeated (in different form) in input file 'nlpan.in1'. The connectivity is specified by using the NOD array in 'nlpan.in1', which lists, for each plate strip, the i.d. numbers of the node lines at Y=0 and Y=B, respectively, where B is the width of the plate strip. The array NOD, the angles MU, and eccentricity measures EZ for the configuration of Figure E1(a) are listed in the figure (EY is zero for all plate strips). The details of specifying these parameters are described in the section "Line-by-Line Input Instructions." The NLPAN input files for the configuration of Figure E1(a) are included in the section "Example Input Files." The following data are passed automatically from PASCO to NLPAN: plate-strip widths, global unit loads, laminate configurations, reference length and width, and material properties including thermal expansion coefficients.



(a) An example PASCO/NLPAN cross-sectional representation showing plate strip numbers (boxed), node-line numbers (circled), global and local coordinate directions, and geometry definition parameters.



(b) Orientation of the edge of a plate strip relative to a node line.

Figure E1. Specification of cross-sectional geometry.

One important modelling detail requires special discussion. In both PASCO and NLPAN, a set of plate-strip properties is stored only for unique combinations of the following three parameters:

- i) wall (laminate) properties
- ii) plate-strip width
- iii) unit in-plane loads

In NLPAN, the user must use the ILBWAL(IP) input to assign to each plate strip the index number of this property set, and thus the user must anticipate the indexing used by PASCO. This is not difficult. Starting with plate strip # 1 and proceeding through the entire set of plate strips, assign index numbers ILBWAL starting with 1. If the trio of properties of a plate strip match the values encountered on a previous plate strip, use the previously assigned value of ILBWAL, otherwise assign the next new value of ILBWAL. The vector ILBWAL(IP) for the configuration of Figure E1(a) is (1,2,2,1,3,3,4), where the laminate of the stiffener flanges is different from the laminate of the skin. On occasion, PASCO does not recognize matching plate strips. A FORTRAN error results if there is a discrepancy between the PASCO indexing and the ILBWAL input. The file 'modes.in' should be inspected. At the top is variable NLBWAL which is the maximum value of ILBWAL used by PASCO. Lines near the top list parameters ILBW, IW, B, NXL, NYL. IW is the wall (laminate) index number, ILBW is the index referred to by ILBWAL(IP), B is the strip width, and NXL and NYL are the unit loads. These values reflect the indexing used by PASCO.

In the PASCO input file, the four boundary condition components at the node-lines are specified in the order dW/dY , W, V, and U. The boundary conditions must be specified again in input file 'nlpan.in1' using the BCVEC parameter. The components of BCVEC are reversed compared to PASCO: (U : Fx), (V : Fy), (W : Fz), and (dW/dY : M).

NLPAN has features for modelling boundary conditions other than simple support at the longitudinal ends. Axial displacement constraints can be imposed using NCU/PCU/YCU input, and slope constraints dW/dX can be imposed using NCW/PCW/YCW input. The generalized displacement constraints are satisfied exactly at discreet points; care must be taken not to over-constrain a problem. Rotationally elastic support can be modelled using either NSPU/IPSPU/YSPU/KSPU or NSPW/IPSPW/YSPW/KSPW input. The options provided for modelling end-support are not intended to enable exact modelling of boundary conditions at the longitudinal ends, but are rather intended to simulate the effects of the end support conditions on the global behavior of the structure. Axial displacement constraints are used in the example input files listed at the end of this document.

NLPAN Operating Modes

NLPAN has several special operating modes, and to understand them, it helps to understand the general stages of the NLPAN analysis:

1. Computation of the linear, unbuckled response to the unit in-plane loads.
2. Computation of VIPASA buckling eigensolutions, and selection of the buckling mode set for use in the nonlinear analysis.
3. Computation of the shape functions for the second-order displacement fields.
4. Calculation of the coefficients for the nonlinear algebraic equations governing equilibrium.
5. Solution of the nonlinear algebraic equations governing equilibrium.

Linear solution pre-processor. NLPAN provides the ability to specify both global in-plane load components in terms of either load measures or displacement measures. If it is desired to use the two edge-normal load components (named NX(1) and NY(1) in 'pasco.in') then PASCO will compute the linear pre-buckling solution, which is passed on to NLPAN. If it is desired to specify the unit end-shortening and/or the unit width-shortening, NLPAN is used as a pre-processor to determine the equivalent loads NX(1) and NY(1) required for PASCO input. This is done by setting ILNPRT=2 (pre-processor mode) in file 'nlpan.in1' and providing the appropriate values for ILSET, NXGL, NYGL, EPXL, and EPYLG in 'nlpan.in1'. NLPAN then computes the corresponding values NX(1) and NY(1), prints these values to file 'nlpan.out', and halts program execution. The provided values can then be put into 'pasco.in' (using a text editor) for use by PASCO, in order to get the proper pre-buckling state for the buckling calculations. ILNPRT should then be set to zero for the subsequent NLPAN run.

For multiply-connected cross-sections, the PASCO linear solution is computed without strict enforcement of displacement compatibility between multiple plate strips. By setting COMPAT='Y' in 'nlpan.in', the linear solution can be determined which satisfies displacement compatibility for configurations with co-planar plate strips, such as skins with attached flanges. First set ILNPRT=2 (pre-processor mode) in 'nlpan.in'. This will cause the PASCO input parameters NX(1), NY(1), and FNY(I) to be printed to file 'nlpan.out', and NLPAN program execution will terminate. (If NY(1) is zero in 'pasco.in', then NLPAN will also specify a small non-zero value NY(1) for use in PASCO.) The values NX(1), NY(1), and FNY(I) are then added to 'pasco.in' using a text editor, and ILNPRT should be set to zero in 'nlpan.in' for subsequent runs. The linear solution obtained using this method may not be a true equilibrium solution because of the presence of unbalanced moments along the node lines.

Review and selection of VIPASA buckling solutions. The set of VIPASA buckling modes used by NLPAN is specified using the parameters NMUSE, MHIN(I), NSOL(I), ISOL(I,J), FORCE, and SYMSTR. Features for reviewing a range of VIPASA eigensolutions are available in order to help select which modes to use. Initially, PASCO is called and instructed to generate the primary buckling solution for each longitudinal halfwave number from 1 to MSRCH. The eigenvalues are printed to 'nlpan.out' along with an indication of whether or not the mode shape is symmetric (based on input parameters SYMSTR and NODSYM(1-2) in 'nlpan.in'.) To inspect these results before further execution, set IHALT=1 in 'nlpan.in'. In order to investigate the characteristics of secondary buckling eigensolutions for selected halfwave numbers, set IHALT=2 in 'nlpan.in'. NMUSE and MHIN(I) are used to specify which halfwave numbers are explored, and for each halfwave number MHIN(I), the number of solutions generated is equal to twice the maximum index number specified in ISOL(I,NSOL(I)). Both eigenvalues and symmetry indicators are printed to 'nlpan.out' for all modes generated, and program execution is halted.

Users may want to set up strategies for automatically selecting mode sets based on particular criteria. The appropriate place for this is subroutine PRIMAR in file 'primar.f'. A strategy implemented by Christine Perry for a certain class of problems can be found there and perhaps modified to suit the user.

Restart procedure. The bulk of the computational effort of NLPAN (in the absence of extensive post-processing) goes into the stages which culminate in the computation of the coefficients of the nonlinear algebraic equations (stages (1) through (4) listed above). The user may choose to have the program store the results of all calculations made up to this point. This allows an unlimited number of subsequent runs to be made (using the stored information) in which the user may vary the shape imperfection, the load step sizes, the asynchronous load strategy, and other parameters affecting the nonlinear solution strategies. The operating mode is selected by answering the following prompt which appears on the screen at the start of the program execution:

ENTER: 1 - NEW START WITH NO SAVE, 2 - NEW START WITH SAVE, 3 - RESTART

The RESTART mode does not restart a sequence of load/response calculations, but rather begins the computation of one or more new load-response sequences. In RESTART mode, the program reads the saved results, followed by input file 'nlpan.in2'. Output to file 'nlpan.out' begins directly with a report of the final nonlinear analysis.

If it is desired to suppress the screen prompts, then replace the statement I99=6 with I99=99 in subroutine NLPAN in source code file 'nlpan.f' and recompile the program. The restart feature will not be used. Screen-directed output will be written to file 'term.out'.

Special output. During each NLPAN run, output file 'nlpan.out' is written which contains a summary of input information, properties of the VIPASA buckling modes, and other basic information about the model and the analysis to be performed. Basic output for the equilibrium solution at each load step includes normalized global load measures, modal amplitudes, and a reference deflection value. Output file 'nlpan.outr' contains a report, at each load step, of the values of various parameters used in the nonlinear solution strategies. (Definitions of the parameters listed in 'nlpan.outr' can be found in comment lines in the beginning of source-code file 'nlanl.f'.) Additional output is available for various stages of the analysis using print flags ILNPRT, ICOORD, IEFPR, IQUPRT, INGPRT, and ICOPRT in file 'nlpan.in1', and post-processing flags IPDISP, IPSTRN, IPSS, IPQY, IPSRES, and IPPROF in 'nlpan.in2'. The details of using these flags are described in the section "Line-By-Line Input Instructions."

NLPAN is also capable of creating configuration, buckling mode, and displacement output files which can be viewed graphically using the commercially available PATRAN computer software by PDA Engineering of Costa Mesa, California. To create these output files, ICOORP must be set to 2 in file 'nlpan.in1'. To create the files containing buckling mode-shapes, set IEFPR=3 in file 'nlpan.in1'. To create displacement output files, set IPPROF=1 in file 'nlpan.in2'. Additional details regarding the PATRAN-readable files are included in the descriptions of parameters ICOORP, IEFPR, NXINT, NEY, and IPPROF, found in the section "Line-By-Line Input Instructions." An example of a PATRAN-generated image of displacement results from an NLPAN analysis is presented in Figure E2 for the case of a unit-stiffener-cell representation of a T-stiffened panel.

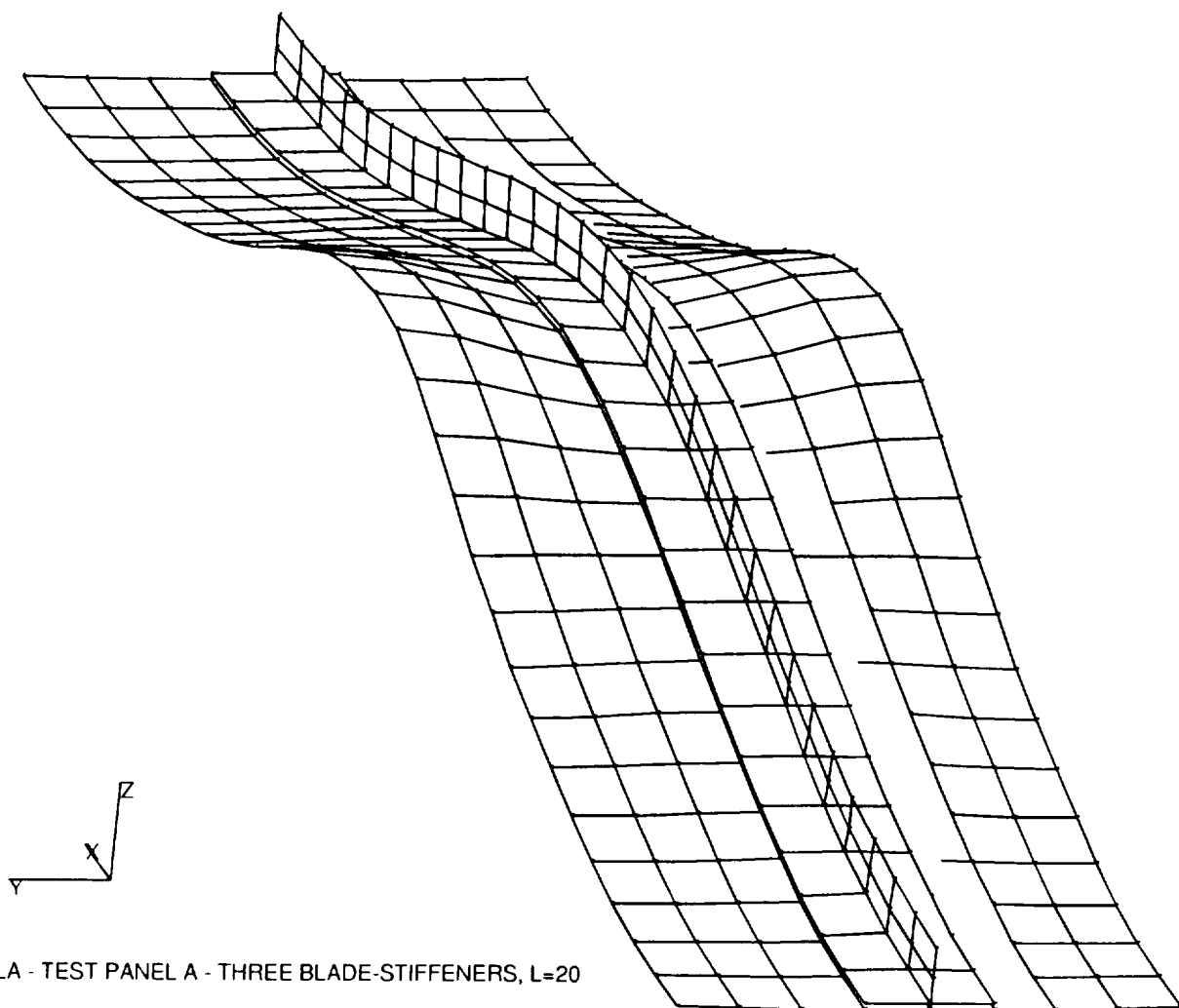
Convergence Considerations

The cross section of a configuration is discretized in order to perform numerical calculations for some steps of the NLPAN analysis. This discretization is determined by the parameter NINTN or parameters NINT(I) in 'nlpan.in1'. Increasing the fineness of the discretization improves the accuracy of results, but increases computer memory requirements and increases program execution time. The convergence of results with respect to the fineness of the discretization should be considered when using the program. Convergence is slowest when the transverse in-plane load component NY is non-zero.

The accuracy of the NLPAN analysis is highly dependent on the suitability of the VIPASA buckling mode set used to represent displacements in the nonlinear analysis. NLPAN program features are provided to help the user screen the buckling modes for suitability, but the question of which modes to include is a difficult one. Mode-selection strategies for some cases are discussed in Section 5.5.2.

Possible Problems

VIPASA/PASCO returns buckling mode shapes in terms of the associated generalized displacements of the node lines of the configuration. The mode shapes are normalized by setting the largest node-line rotation to 0.1. For some buckling modes (column type modes) all node-line rotations are very small, or, in theory, zero. This means that the associated displacements would be infinite in comparison. Experience



PANELA - TEST PANEL A - THREE BLADE-STIFFENERS, L=20
DISPLACEMENTS AT LOAD STEP 24

Figure E2 . Example of the visualization of NLPAN displacement results using PATRAN,
for a unit-stiffener-cell representation of a T-stiffened panel.

has shown that in practice, there is generally enough numerical error so that displacements are finite, though they may have amplitudes with an order of magnitude 1×10^{10} . Mode shapes which have been plotted for such cases look physically reasonable.

The solution strategies used to solve the nonlinear algebraic equations require the specification of several parameters to determine step sizes and cutoff values used in strategy decisions. In regions of severe solution-path curvature or compound solution branching, the solution strategies sometimes misdiagnose the situation, and issue a confusing series of messages. These problems can generally be eliminated by adjusting the values of DSNOM, DSFACT, DSMIN, DELQ, or EVCUT in 'nlpan.in2'. As far as what values to use, some trial and error may be required to obtain meaningful behavior.

Avoid using extremely small non-zero values (< 0.001) of modal imperfection amplitudes Q0(I) (specified in 'nlpan.in2'). Such values tend to create problems of the sort described in the previous paragraph.

Line-By-Line Input Instructions

In this section, detailed line-by-line instructions are given for the two input files 'nlpan.in1' and 'nlpan.in2'. The detailed instructions for input file 'pasco.in' are covered in [E1]. See the section "General Aspects of Specifying Geometry" in this appendix for special requirements which 'pasco.in' must satisfy.

General instructions. The following general comments apply to the line-by-line input instructions, or to the input files.

- 1) The contents of the input files must match, line per line, the data sequences described in this section.
- 2) All input is read by FORTRAN as unformatted input. All input variables must be present, with at least one space separating data entries. Integer, floating-point, character, and logical input values must be written using conventional FORTRAN formats. Characters following the last required input value on a line are ignored.
- 3) After all the required input values on a line have been read, the rest of the line is ignored, so that remaining space can be used for writing comments.
- 4) Any special output requested using input parameters is written to the standard output file 'nlpan.out', except where noted otherwise in the instructions.
- 5) All CHARACTER input values must be enclosed by apostrophes except for the first record (TITLE). Example: SYMSTR may be 'Y' or 'N' .
- 6) The variable type for each input item is indicated under the variable name, using the following abbreviations:
 - I - Integer
 - R - Real
 - C*n - Character variable of length n

File 'nlpan.in1' input lines. (This file is used to specify geometry, and modelling and output options.)

TITLE
C*76

TITLE A descriptive title used for labeling of the output files.

ICOORP	ILNPRT	IEFPRT	IQUPRT
I	I	I	I

ICOORP	Controls printing of the global y-z coordinates of the model at the discretization points 0 No print 1 Print the Y-Z coordinates of the cross section to file 'coords.out' 2 Create file 'nlpan.neu' which contains a PATRAN-readable "neutral file" describing the geometric configuration. This file contains finite-element node and element definition records, allowing the configuration to be viewed graphically using the PATRAN computer software. Discretization of the configuration is determined by input parameters NXINT and NEY(IP) (IP=1,2,...,NPLATE). The file-creation options for writing PATRAN-compatible neutral results files for buckling mode shapes and displacements are enabled (see IEFprt in file 'nlpan.in1' and IPPROF in file 'nlpan.in2').
ILNPRT	Controls the operation of the linear solution module. See the discussion in the section "NLPAN Modes of Operation." 0 Use the global unit loads NX(1) and NY(1) specified in 'pasco.in', and force ILSET to 1 2 Pre-processor mode. Based on the ILSET input value, select the two generalized in-plane load components from the values NXGL, NYGL, EPXL and EPYLG (described below); write corresponding PASCO input values NX(1) and NY(1) (and, if COMPAT='Y', any non-zero PASCO input factors FNY(I)) to the file 'nlpan.out', for later insertion into 'pasco.in' using a text editor. Program execution is halted.
IEFPRT	Controls the printing of buckling mode shapes, measured with respect to local plate-strip coordinate directions except where noted otherwise. 0 No print. 1 Print displacements. 2 Print displacements and all computed derivatives. 3 If ICOORP≠2, then print displacements to file 'modes.out' and halt execution. If ICOORP=2, then print mode shapes to PATRAN-readable files 'nlpanMMM.eig' (MMM=1,2,...) where MMM is the index number of the buckling mode. These are "neutral results files" (in PATRAN nomenclature) containing buckling-mode displacements, and are to be used in conjunction with the configuration neutral file 'nlpan.neu' for graphical viewing of the buckling mode shapes. The displacements are measured with respect to global coordinate directions. Program execution is halted.

IQUPRT Controls printing of second-order displacement fields at discretization points, measured with respect to local plate-strip coordinate directions.

- 0 No print.
- 1 Print displacements.
- 2 Print displacements and all computed derivatives.
- 3 Print displacements to file 'uij.out' and halt execution.

INGPRT	ICOPRT	IPRINT	IPBUG	NXINT
I	I	I	I	I

INGPRT Controls the printing of the coefficients for the expression of global loads NXG and NYG (computed in subroutine ACALC).

- 0 No print
- 1 Print values

ICOPRT Controls the printing of the coefficients of the nonlinear algebraic equations (computed in subroutine CCALC).

- 0 No print
- 1 Print coefficients
- 2 Print coefficients and primitive coefficients

IPRINT Development use only. Set to 0

IPBUG Development use only. Set to 0

NXINT Required only if ICOORP=2 (creating PATRAN-readable output files). NXINT is the number of finite elements along a length-wise cut of any plate strip in the structure, used in producing PATRAN-readable files 'nlpan.neu', 'nlpanMMM.eig', and 'nlpanNNN.dis'. This is used for graphical visualization purposes only, and does not affect the analytical results.

USER	IHALT	MSRCH
C*5	I	I

USER Flag used by program developers. Set to 'STOLL'.

IHALT Used to control the generation and display of the VIPASA buckling eigensolutions, and the subsequent use of the buckling mode shapes in the nonlinear analysis. See the discussion in the section "NLPAN Modes of Operation."

- 0 Proceed with the NLPAN analysis using buckling modes as determined by the input values NMUSE, FORCE, MHIN(I), NSOL(I), ISOL(I,J)
- 1 Compute the VIPASA buckling eigenvalues for longitudinal-halfwave numbers 1 through MSRCH; print the eigenvalues along with an indication of the symmetry of the buckling mode. Halt execution.
- 2 For values of the halfwave number specified by MHIN(I) (I=1,2,...,NMUSE) compute and print several VIPASA eigenvalues, including an indication of the symmetry of each buckling mode. The number of modes computed for MHIN(I) is 2*ISOL(I,(NSOL(I))). Halt execution.

MSRCH This parameter determines the range of longitudinal halfwave numbers investigated when IHALT=1 (see above). MSRCH must be in the range 0 to 20
0 Investigate halfwave numbers 1 through 20
>0 Investigate halfwave numbers 1 through MSRCH

SYMSTR	NODSYM(1)	NODSYM(2)
C*1	I	I

SYMSTR 'Y'/'N' Indicates whether or not the structural cross section is symmetric.

NODSYM(J) Index numbers of two node lines for which global displacements W can be compared to detect symmetry of a buckling mode. Used only if SYMSTR='Y'

NMUSE	FORCE
I	C*1

These parameters, along with parameters NSOL, MHIN, and ISOL in following records, determine which buckling modes (computed by VIPASA) are used in the nonlinear analysis.

NMUSE Number of unique values of the longitudinal halfwave-number for which VIPASA mode shapes will be generated for use.

FORCE Affects the selection of VIPASA buckling modes for the longitudinal halfwave-numbers specified with MHIN(I). In the following description, designate buckling solutions by the indices (M,J). Solution (M,J) is the J'th solution in the infinite sequence of solutions (for halfwave number M) which are ordered in terms of eigenvalue.

'Y' For longitudinal halfwave number MHIN(I), force the use of modes (MHIN(I),ISOL(I,J)), J=1,2,...,NSOL(I).

'N' Input values ISOL are ignored. Use mode (MHIN(I),1). If SYMSTR='Y' and NSOL(I)>1 then add the next NSOL(I)-1 modes (MHIN(I),N) which match mode (MHIN(I),1) with respect to symmetry or lack thereof. If SYMSTR='N' use modes (MHIN(I),J), J=1,2,...,NSOL(I).

NSOL(1)	NSOL(2) ...	NSOL(NMUSE)
I	I	I

NSOL(I) Number of VIPASA mode shapes to be incorporated which have the longitudinal halfwave-number MHIN(I)

MHIN(1)	MHIN(2) ...	MHIN(NMUSE)
I	I	I

MHIN(I) Longitudinal halfwave-number of a VIPASA mode shape to be used in the NLPAN analysis

ISOL(1,1)	ISOL(1,2) ...	ISOL(1,NSOL(1))
ISOL(2,1)	ISOL(2,2) ...	ISOL(2,NSOL(2))
...
ISOL(NMUSE,1)	ISOL(NMUSE,2) ...	ISOL(NMUSE,NSOL(NMUSE))
I	I	I

ISOL(I,J) Indicates which VIPASA buckling modes to use from the sequence of modes having longitudinal halfwave-number MHIN(I), where modes are ordered according to eigenvalue. All input values must be present, but they are only used if FORCE='Y'.

NPLATE	NNODE
I	I

NPLATE Number of plate strips in the model

NNODE Number of node lines in the model

NPOFFS
I

NPOFFS Number of plate strips which have non-zero offsets between one (or both) side edge(s) and the corresponding node line(s).

Conditional - include only if NPOFFS >= 1 :

IP IECVY(IP,1) IECVZ(IP,1) IECVY(IP,2) IECVZ(IP,2) (I=1)

IP IECVY(IP,1) IECVZ(IP,1) IECVY(IP,2) IECVZ(IP,2) (I=2)

...
IP IECVY(IP,1)	IECVZ(IP,1)	IECVY(IP,2)	IECVZ(IP,2)	(I=NPOFFS)	
I I	I	I	I		

IP Index number of a plate strip with non-zero node-line offsets.

IECVY(IP,IE),IECVZ(IP,IE): Integer values used to determine the offset component values. This is done the same way as in PASCO. The absolute value gives the index number I of a thickness value H(I) specified in 'pasco.in', and the sign specifies the direction of the offset component. IE is the edge number, IE=1 for Y=0, IE=2 for Y=B(IP).

MUA(IP)	SKVEC(IP)	PRVEC(IP)	TUA(IP)	(IP=1)
MUA(IP)	SKVEC(IP)	PRVEC(IP)	TUA(IP)	(IP=2)
...
MUA(IP)	SKVEC(IP)	PRVEC(IP)	TUA(IP)	(IP=NPLATE)
R	I	I	R	

MUA(IP) Rotational orientation angle, in degrees, of plate strip # IP in Y-Z plane. Same convention as PASCO. See Figure E1(b).

SKVEC(IP) Indicator for presence of an initially flat skin which is continuous between the boundary node-lines.

1 Plate strip # IP is part of the skin. For the case of overlapping plate strips, such as a skin/stiffener-flange region, only one of the overlapping strips should be assigned SKVEC(IP)=1

0 Plate strip # IP lies off of the skin.

PRVEC(IP) Used for indicating pressure load application and direction. Note: For the case of overlapping plate strips, such as a skin/stiffener-flange region, only one of the overlapping strips should be assigned a non-zero value PRVEC(IP)

0 No pressure load applied to plate strip

1 Pressure load acts on plate strip in local +Z direction.

-1 Pressure load acts on plate strip in local -Z direction.

TUA(IP) Unit value of temperature (the difference from a reference temperature) to be applied uniformly to plate strip # IP. See the description of parameter HEATA in input file 'nlpan.in2'.

NOD(IP,1)	NOD(IP,2)	(IP=1)
NOD(IP,1)	NOD(IP,2)	(IP=2)
...
NOD(IP,1)	NOD(IP,2)	(IP=NPLATE)
I	I	

NOD(IP,IE) Node-line index number of edge # IE of plate strip # IP. Defines the connectivity of the model by specifying the two node lines to which each plate strip attaches. Node-line numbers and plate strip numbers must match those used to specify the geometry in 'pasco.in'. Plate-strip numbers are sequential, and correspond to initial PASCO plate strip numbers (i.e. before the application of HCARD conversions). IE is the edge number, IE=1 for Y=0, IE=2 for Y=B(IP).

BNODE(1)	BNODE(2)
I	I

BNODE(IB) Index numbers of two "boundary" node lines at which boundary conditions are applied. IB=1 nominally corresponds to the global Y=0 boundary, IB=2 nominally corresponds to the Y=B(Global) boundary. The boundary node lines need not span the width of the configuration, but if they do not, then global load NY may not be computed correctly.

BCVEC(1,IB)	BCVEC(2,IB)	BCVEC(3,IB)	BCVEC(4,IB)	(IB=1)
BCVEC(1,IB)	BCVEC(2,IB)	BCVEC(3,IB)	BCVEC(4,IB)	(IB=2)
I	I	I	I	

BCVEC(IC,IB) Boundary-condition indicator for component # IC of boundary node-line # IB. The following table lists options and components:

IC	Comp.	BCVEC(IC,IB)
1	U, Fx	1 or 2
2	V, Fy	1 or 2 or 3
3	W, Fz	1 or 2
4	dW/dy, M	1 or 2

Note that the four components are specified in the opposite order compared to PASCO.

BCVEC = 1 Control the generalized displacement. Set to zero (except for IC=2, where V may be non-zero).

BCVEC = 2 Control the generalized force. Set to zero (except for IC=2 for which Fy (=NY) may be non-zero).

BCVEC = 3 IC=2 only. Keep the edge straight w.r.t. global V, but control the mean global NY load.

NCU	NCW
I	I

NCU Number of axial displacement constraints, each end. Axial displacement U is constrained to follow the effective end-shortening. This is imposed only on modes with odd longitudinal halfwave numbers. These constraints may only be used with CONTRL='D'.

NCW Number of slope (dW/dX) constraints, each end. The slope is measured with respect to the local coordinate directions of specified plate strips.

Conditional - include only if NCU ≥ 1 :

IPCU(1)	YCU(1)
IPCU(2)	YCU(2)
...	...
IPCU(NCU)	YCU(NCU)
I	R

IPCU(I) Plate strip on which the axial displacement constraint is imposed.

YCU(I) Nominal location Y on plate strip # IPCU(I) where the constraint is applied. The actual point of application will be at the closest available discretization point. See the description of parameters NINTN and NINT(IP).

Conditional - include only if $NCW \geq 1$:

IPCW(1)	YCW(1)
IPCW(2)	YCW(2)
...	...
IPCW(NCW)	YCW(NCW)
I	R

IPCW(I) Plate strip on which the slope displacement constraint is imposed

YCW(I) Nominal location Y on plate strip # IPCW(I) where constraint is applied. The actual point of application will be at the closest available discretization point. See the description of parameters NINTN and NINT(IP).

NSPU	NSPW
I	I

NSPU Number of rotational springs (at each end) restraining dU/dY (Y - Local plate-strip axis).

NSPW Number of rotational springs (at each end) restraining dW/dX . (W - Local plate-strip deflection).

Conditional - include only if $NSPU \geq 1$:

IPSPU(1)	YSPU(1)	KSPU(1)
IPSPU(2)	YSPU(2)	KSPU(2)
...
IPSPU(NSPU)	YSPU(NSPU)	KSPU(NSPU)
I	R	R

IPSPU(I) Plate strip on which rotational spring acts (each end)

YSPU(I) Nominal location Y on plate strip # IPSPU(I) where the spring acts. The actual location will be at the closest available discretization point. See the discussion of discretization using parameters NINTN and NINT(IP).

KSPU(I) Rotational-spring constant (Moment/Radian)

Conditional - include only if $NSPW \geq 1$:

IPSPW(1)	YSPW(1)	KSPW(1)
IPSPW(2)	YSPW(2)	KSPW(2)
...
IPSPW(NSPW)	YSPW(NSPW)	KSPW(NSPW)
I	R	R

IPSPW(I) Plate strip on which rotational spring acts (each end)

YSPW(I) Nominal location Y on plate strip # IPSPW(I) where the spring acts. The actual location will be at the closest available discretization point. See the discussion of discretization using parameters NINTN and NINT(IP).

KSPW(I) Rotational-spring constant (Moment/Radian)

Comment line - not used for data.

**** DISCRETIZATION AND REFERENCE VALUES ****

NINTN

I

NINTN Guides the discretization of each plate strip in the local Y-direction. Used for the finite-difference computation of the second-order displacement fields and for numerical integration.

0 Specify the discretization of each plate strip individually using NINT(IP)

N N is an even integer ≥ 4 . The widest plate strip in the structure will have N+1 discretization points evenly spaced over N intervals. The remaining plate strips are discretized such that interval widths on all plate strip are approximately equal, except that no plate strip will have less than 4 intervals.

Conditional - include only if NINTN = 0 :

NINT(1) NINT(2) ... NINT(NPLATE)

I

I

I

NINT(IP) Even integer ≥ 4 giving the number of discretization intervals in the Y-direction on plate strip # IP. Note: Plate strips with matching indices ILBWAL(IP) must have matching numbers NINT(IP).

Conditional - include only if ICOORP=2 (creating PATRAN-readable output files):

NEY(1) NEY(2) ... NEY(NPLATE)

I

I

I

NEY(IP) Even integer ≥ 2 giving the number of discretization intervals in the Y-direction on plate strip # IP to be used for graphical visualization with PATRAN. Generally, NINT(IP) is so large that if all available intervals are used in producing graphical images in PATRAN, the images are too cluttered. NEY(IP) must be selected so that NINT(IP) is an integer multiple of NEY(IP), i.e. $NINT(IP) = N * NEY(IP)$, where N is a positive integer.

IPHREF	IPWDET	IPDFL	IYDFL
I	I	I	I

- IPHREF Controls the reference thickness used in normalizing modal amplitudes and displacements. The reference thickness HREF used by NLPAN is listed in file 'nlpan.out'.
- 0 HREF is the thickness for plate strip # 1
- IP HREF is the thickness for plate strip # IP
- IPWDET Determines the plate strip where the characteristic amplitude of a buckling mode (used for normalizing the modal amplitudes) is measured
- 0 The characteristic amplitude is the maximum displacement in the structure
- IP The characteristic value is the maximum displacement on plate strip # IP
- IPDFL IPDFL and IYDFL control the transverse location where a characteristic displacement is computed and reported during the nonlinear analysis. The displacement (normalized by HREF) is printed in 'nlpan.out' for each equilibrium solution, labeled as WCN. This feature serves only as a user convenience.
- IP Deflection is measured on plate strip # IP
- IYDFL Determines the location on plate strip # IPDFL where the characteristic deflection is computed. Where B is the width of plate strip # IPDFL:
- 1 Compute deflection at $Y=0$, $X=L/2$, plate strip # IPDFL
- 0 Compute deflection at $Y=B/2$, $X=L/2$, plate strip # IPDFL
- 1 Compute deflection at $Y=B$, $X=L/2$, plate strip # IPDFL

Comment line - not used for data.

**** LOADING AND MODELLING OPTIONS ****

CONTRL	COMPAT
C*1	C*1

- CONTRL Specifies the type of control used for the generalized in-plane loads.
- Note: for simple rectangular plates, both types of control yield the same load/end-shortening relationship, but for more complex configurations, a discrepancy arises between the two methods. A correction is under development to fix this discrepancy, but currently CONTRL='D' is believed to provide greater accuracy.
- 'D' Displacement control
- 'L' Load control
- COMPAT Specifies whether displacement compatibility is enforced in the linear solution for multiply connected cross sections. See the discussion in the section "NLPAN Modes of Operation."
- 'Y' Displacement compatibility is enforced. In general, NLPAN must be run first in a pre-processor mode (ILNPRT=2) to compute values NX(1), NY(1), FNY(IP) to put in file 'pasco.in'. These are printed in file 'nlpan.out'.
- 'N' Displacement compatibility is either not enforced, or is not applicable.

<hr/> ILSET	NXGL	NYGL	EPXL	EPYLG
I	R	R	R	R

Note: This input set must be present, but values are used only if ILNPRT=2 (pre-processor mode). If ILNPRT=0 then ILSET=1 is assumed, and NXGL and NYGL (NX(1), NY(1)) are taken from file 'pasco.in'.

ILSET Determines which two parameters define the unit in-plane load system. All loads and strains defined positive for tension/extension. Unit in-plane loading must generally be tensile, because buckling eigenvalues are assumed to be negative.

- 1 NXGL, NYGL
- 2 NXGL, EPYLG
- 3 EPXL, EPYLG
- 4 EPXL, NYGL

NXGL Positive unit value for global X-normal axial load per unit width based on global width B. Equivalent to NX(1) in PASCO input.

NYGL Unit value for global Y-normal axial load per unit length based on length L. Equivalent to NY(1) in PASCO input.

EPXL Unit value for axial strain in X-direction

EPYLG Unit value for mean Y-normal strain in skin (change in panel width per unit width)

PRUNIT
R

PRUNIT Unit pressure load, force per unit area. See the description of parameter BETAA in input file 'nlpan.in2'.

LOCGL
C*1

LOCGL 'Y'/'N' Used to control modifications to the second-order displacement fields necessary to improve the solution accuracy, particularly in cases of local-global mode interaction. In general, set LOCGL='Y' unless INDPLT=1 (simple plate analysis).

INDPLT

I

- INDPLT 1 Configuration is a rectangular plate with a single reference plane (may be constructed from several linked plate strips if no node-line offsets are used). Implies that $u_i=v_i=w_{ij}=0$. This reduces the cost of the analysis by avoiding unneeded calculations and data storage.
- 2 Complex configuration with multiple reference planes. Implies that u_i, v_i, w_{ij} are in general not zero.

Comment line - not used for data.

**** LOAD, WIDTH, WALL INDEXING ****

ILBWAL(1)

I

ILBWAL(2) ...

I

ILBWAL(NPLATE)

I

ILBWAL(IP) See the discussion in the section "General Aspects of Specifying Geometry." ILBWAL(IP) is an integer in the interval 1 to NLBWAL, where NLBWAL is the number of unique combination of:

- i) wall properties,
- ii) width B, and
- iii) unit in-plane loads,

among all plate strips in the structure. ILBWAL(IP) specifies which set of characteristics plate strip # IP has. These indices must match the values assigned by PASCO. NLBWAL is passed to NLPAN via file 'modes.in' created by PASCO.

NKWALL

I

NKWALL Number of different laminates defined in input file 'pasco.in'.

--- End of file 'nlpan.in1' ---

File 'nlpan.in2' input lines. (This file contains the control parameters for the nonlinear analysis, the control parameters for post-processing, and the modal-imperfection amplitudes. File 'nlpan.in2' is read every time NLPAN is run, including runs in the RESTART mode.)

NIMP	IZCIP	SWITCH
I	I	Logical

NIMP Number of sets of modal imperfection amplitudes for use in an equal number of consecutive nonlinear analysis run. NIMP lies in the range 1 to 30

IZCIP Controls the zeroing of coefficients CIP(I) (in the nonlinear algebraic equations) which, when non-zero, cause the initial response to in-plane loading to be nonlinear. Each coefficient CIP(I) corresponds to a particular VIPASA buckling mode incorporated in the NLPAN analysis. CIP(I) may be non-zero either for physical reasons, indicating that the initial response is truly nonlinear, or may be non-zero due to approximations used in the method of analysis. One application is to set IZCIP=1 to eliminate an initial bowing response characteristic of bowing imperfections.

0 Do not zero the coefficients CIP(I).

-1 Set CIP(I) to zero for all modes.

M Set CIP(I) to zero if NWAVEA(I) <= M, where NWAVEA(I) is the longitudinal halfwave number for the VIPASA buckling mode

SWITCH Flag used in an investigation of compound solution branching. Set to .FALSE.. (If set to .TRUE., then at points of near-simultaneous solution branching in two modes, the initial branch-switching step will be controlled by a specified increment to the non-critical mode rather than by a specified increment to the critical mode.)

Q0(1)	Q0(2) ...	Q0(NEIG)	(IIM=1)
Q0(1)	Q0(2) ...	Q0(NEIG)	(IIM=2)
...
Q0(1)	Q0(2) ...	Q0(NEIG)	(IIM=NIMP)
R	R	R	

Q0(I) Modal imperfection amplitude for VIPASA buckling mode number I, where I varies from 1 to NEIG, where NEIG is the number of modes incorporated in the analysis. Modal amplitudes are normalized based on a maximum deflection equal to the reference thickness value HREF (listed in 'nlpan.out'). Characteristics of the modes including critical load level, halfwave number, symmetry, and total number NEIG are listed in the output file 'nlpan.out'.

QF(1)	QF(2) ...	QF(NEIG)
R	R	R

QF(I) Modal amplitudes used to specify forced end displacements or end rotations. QF input must be present, but is used only when displacement constraints are used ($NCU \geq 2$ or $NCW \geq 1$). These values differ from imperfection amplitudes Q0(I) in that they are stress-producing. Amplitudes QF are significant only in terms of the associated generalized displacements at the longitudinal ends. They are intended for use in simulating a forced initial rotation of the panel ends.

NRANGE

I

NRANGE Number of load ranges specified. Intended for use in modelling asynchronous application of multiple load types. Within each load range, the in-plane, pressure, and thermal load parameters all vary linearly with a single generalized load parameter. All generalized loads are continuous from one range to the next, but the load rates are discontinuous. NRANGE must be in the range 1 to 5.

LAMDAA(IR)	BETAA(IR)	HEATA(IR)	(IR=1)
LAMDAA(IR)	BETAA(IR)	HEATA(IR)	(IR=2)
...
LAMDAA(IR)	BETAA(IR)	HEATA(IR)	(IR=NRANGE)
R	R	R	

These are the target values for the three load parameters, used to define the NRANGE load ranges. All three parameters are assumed to be zero initially.

LAMDAA In-plane load parameter. This is a normalized value, where the reference value REFLAM is listed in output file 'nlpan.out'. LAMDAA=1.0 corresponds to the critical buckling load for the case of pure in-plane loading.

BETAA Load multiplier for transverse pressure. The applied pressure P is given by $P=BETAA*PRUNIT$, where PRUNIT is the unit pressure specified in file 'nlpan.in1'.

HEATA Load parameter for thermal loading. In a given plate strip, the thermal load T is given by $T=HEATA*TUA(IP)$, where TUA(IP) is the unit temperature specified in file 'nlpan.in1'.

TOL	ITMAX	UU	VV
R	I	R	R

These are input parameters for subroutine ZROOT, which uses Barstow's method to find the roots of a polynomial with real coefficients. The polynomial equation arises when applying Thurston's method for negotiating solution branching. The default values provided generally work well, and need to be changed only if a warning message is issued.

TOL Tolerance to measure convergence. Default = 1.E-12
0. Use default value.

ITMAX Maximum number of iterations allowed. Default = 20
0 Use default value

UU, VV Starting values used in iterative solution procedure. The starting values are automatically varied in NLPAN if convergence problems are indicated. Defaults: UU=-1., VV=2.
0. Use default value.

ILSTM	CCRIT	MAXIT
I	R	I

ILSTM Positive integer giving the maximum permitted number of load steps.

CCRIT Tolerance to measure convergence of the iterative procedures for solving the nonlinear equilibrium equations. Suggested value: 1.E-5

MAXIT Maximum number of iterations allowed in the iterative solutions procedures. With the methods used, convergence is usually rapid. Suggested value: 6

DSNOM	DSFACT	DSMIN	DELQ	EVCUT	DSQUIT
R	R	R	R	R	R

These parameters control the solution step sizes, and specify cutoff and decision values in the nonlinear solution strategies. DS refers to the arc-length increment used from one solution to the next in a Riks-type approach of arc-length control. The modal amplitudes, load parameters, and Lagrange multipliers (when needed) are all normalized to take on values with order of magnitude unity, so DS should be interpreted accordingly. For all six parameters, an input value 0.0 forces the use of the default value.

DSNOM Nominal value used for DS. DS will never exceed this value. Default: 0.3

DSFACT Factor for reducing DS compared to DSCRIT, where the latter is the arc-length increment predicted (based on extrapolation) to lead to a critical stability point. If (DSFACT*DSCRIT)<DSNOM then DS=DSFACT*DSCRIT. Default: 0.6

DSMIN Minimum value permitted for DS before a solution at the critical point solution is attempted. Default: 0.002

DELQ	Step size used for initiating a solution along a new path at a branch point. Approximately equivalent to an increment in a modal amplitude. Default: 0.005
EVCUT	If a solution branch point is detected, EVCUT is used to select between a one-mode and two-mode solution branching analysis. If the first two eigenvalues of the tangent stiffness matrix are separated by more than EVCUT, a single-mode branching analysis is performed, otherwise a two-mode branching analysis is performed. Setting EVCUT small tends to force a single-mode branching analysis, in which case DELQ must also be small to avoid stepping past secondary branch points. Default: 0.01
DSQUIT	Minimum permitted value for DS. If DS is less than DSQUIT and solution convergence is not achieved, execution is halted. Default: 0.24*DSMIN

IFREQ

I

IFREQ	≥1	Postprocessing requests are processed at every IFREQ'th load step.
	0	No post-processing

(Note: This and all following input records are required only if IFREQ>0)

IPDISP	IPSTRN	IPSS	IPSRES	IPQY	IPPROF
I	I	I	I	I	I
<p>Post-processing control parameters. (Results are computed at model locations which are specified in following input records.) Each parameter may be specified as 0 or 1, with the following effect:</p> <p>1 Output is requested.</p> <p>0 No output is requested</p>					
IPDISP	Print displacement values to file 'displ.out'				
IPSTRN	Print mid-surface strains and curvatures to file 'strain.out'				
IPSS	Print surface strains EPSx and EPSy to file 'strain.out'				
IPSRES	Print stress resultant values to file 'sres.out'				
IPQY	Print force resultant QY which acts in the Z-direction on the Y-normal face in a plate strip, to file 'sres.out'				
IPPROF	<p>If ICOORP≠2: print the displacement profile (referred to local plate-strip coordinate directions) at a constant X-station to file 'displ.out'.</p> <p>If ICOORP=2: print a PATRAN-readable displacement-results file 'nlpanNNN.dis', where NNN is the corresponding load step number. The displacements are computed at locations determined by parameters NXINT and NEY(IP) of input file 'nlpan.in1'.</p>				

NINTX	NXLOC
I	I

NINTX ≥1 If NINTX≥1 then NINTX is the number of uniform intervals in the X-direction determining where postprocessing results are computed. NINTX may be up to 100 for displacements, and up to 50 for strains and stress resultants. If NINTX≥1 then NXLOC is forced to NINTX+1.

 0 Use NXLOC and XLOCN input to specify X locations.

NXLOC ≥1 Number of specific X values used for post-processing. Ignored if NINTX≥1.

Conditional - include only if NINTX=0 and NXLOC>0:

XLOCN(IX) (IX=1)

XLOCN(IX) (IX=2)

...

XLOCN(IX) (IX=NXLOC)

R

XLOCN(IX) Value of X, as a fraction of length L, where results are to be computed. $0.0 \leq XLOCN(IX) \leq 1.0$

NYLOC

I

NYLOC Number of cross-sectional stations where results are computed. Maximum allowable: 100

IP(IY) ID(IY) (IY=1)

IP(IY) ID(IY) (IY=2)

...

IP(IY) ID(IY) (IY=NYLOC)

I

I

IP(IY) Index number of the plate strip where results are to be computed.

ID(IY) Index number of the discretization point in the Y-domain of plate strip # IP(IY) where results are to be computed. Index ID(IY) lies in the range 1 to (NINT(IP)+1). Values NINT(IP) (IP=1,2, ..., NPLATE) are listed in the output file 'nlpan.out', and can be specified directly for each plate strip in input file 'nlpan.in1'.

--- End of file 'input.in2' ---

Example Input Files

Unit cell representation of a T-stiffened panel. The input files for a test case designated UNITA are listed below. UNITA refers to a unit-cell representation of a T-stiffened panel. The general configuration is that shown in Figure E1(a). This model was used to analyze a panel which was tested experimentally. A comparison of analytical and experimental results is presented in [E2]. The test panel had three evenly spaced T-stiffeners. The analytical model includes only a single stiffener with a half-bay of skin on each side, with symmetry conditions imposed at the side edges of the skin. Three different laminates were defined to model the skin, the stiffener flange, and the stiffener blade, respectively, and the mean values of lamina thickness measured for the test panel were used in the analysis. The thickness of the adhesive used to bond the stiffeners to the skin is represented in file 'pasco.in' by T(10); the in-plane stiffness of the adhesive is neglected. Thickness T(11) is used to specify the offset between the mid-surface of the stiffener flanges and the mid-surface of the skin. Thickness T(11) is defined in 'pasco.in' in terms of the other thicknesses using a constraint equation established by parameters AT and AC. The offset values are assigned using the first two HCARD records in file 'pasco.in', and using the IECVZ parameters in file 'nlpan.in1'.

Input file 'nlpan.in1' features axial displacement constraints at the longitudinal ends at node-line numbers 3 and 4 (see Figure E1(a)) in order to simulate clamping of the panel ends. The constraint locations are specified in terms of locations on plate strips 3 and 7 using IPCU and YCU input. The following modes, specified by input parameters NMUSE, NSOL, MHIN, and ISOL, are used in the analysis: (1,1), (1,3), (3,2), (3,3), (5,2), (5,3), (7,2), and (7,4). All of these modes have symmetric cross-sections. The symmetry of the modes is indicated in the output file 'nlpan.out', and is determined by comparing the deflections of node-line numbers 2 and 5 (see the NODSYM input in 'nlpan.in1').

In input file 'input.in2', an imperfection amplitude $Q0(5)=0.02$ is specified ($Q(5)$ corresponds to mode (5,2), the designated critical local mode), and forced end rotation is imposed through input $QF(1)=1.79$. Mode 1 (mode (1,1)) is a bowing type mode. The longitudinal variation of displacements for mode 1 is given approximately by $[HREF \sin(\pi X / L)]$, where $HREF=0.0435$ in. (the skin thickness) and $L=20$ in. (the panel length). Using these values, it can be shown that $QF(1)=1.79$ corresponds to an end rotation of 0.7 degrees, which is the value of end rotation imposed on each end of the test panel during one experiment. Additional discussion of the analysis and tests is found in [E2]. The PATRAN-generated image of a deformed panel presented in Figure E2 corresponds to this NLPAN model. The deformation state of the panel was computed for an equilibrium solution at the theoretical elastic limit-load point; the displacements have been amplified for clarity.

In the listings of files 'nlpan.in1' and 'nlpan.in2', comments are set apart from input data using exclamation points (!). The exclamation points are used only for visual purposes, and serve no other function in the input files.

File 'pasco.in' for the UNITA example.

```
UNITA - TEST PANEL A - UNIT-CELL REPRESENTATION
&CONDAT
&END
&PANEL
B=1.43,.49,.49,1.43,.49,.49,.49,
EL=20.,
CONV1=50000.,
FREQ=0.,
IP=0,
MAXJJJ=0,
MAT(1,1)=1,1,1,2,2,2,3,3,3,
T(1)=.00544,.00544,.00544,.00563,.00563,.00563,
.00483,.00483,.00483,.0045,1.E30,
AT(1,1)=4.,0.,0.,4.,0.,0.,0.,0.,1.,-1.,
AC(1)=0.,
THET(1)=0,50,90,0,15,90,0,15,90,0,
KWALL(1,1)=2,-2,1,3,
KWALL(1,2)=5,-5,4,6,
KWALL(1,3)=8,-8,7,9,
IWALL(1)=1,1,1,1,2,2,3,
FSTIFF=10.,
HCARD=6,-8,-5,0,-11,0,-11,
        6,-9,-6,0,-11,0,-11,
        4,-10,7,90,0,
        2,121,10,
        13,11,1,-990,9000,2,-8,3,-9,-121,4,0,-990,9000,
ICARD=5,1,2,1,-990,9000,
        5,2,4,2,4,8,
        3,3,4,10,
        5,4,5,3,5,9,
        3,5,6,4,
        3,6,-990,9000,
ICREP=1,
NOBAY=1,
NX(1)=500.,
&END
&MATER
E1(1)=17.02E6, E2(1)=1.64E6, E12(1)=.80E6, ANU1(1)=.30,
RHO(1)=1.477E-4, ALFA1(1)=0.25E-6, ALFA2(1)=16.2E-6,
ALLOW(1,1)=2.,011,-0.011,0.01,-0.013,0.0155,
E1(2)=16.44E6, E2(2)=1.64E6, E12(2)=.77E6, ANU1(2)=.30,
RHO(2)=1.477E-4, ALFA1(2)=0., ALFA2(2)=0.,
ALLOW(1,2)=2.,011,-0.011,0.01,-0.013,0.0155,
E1(3)=19.17E6, E2(3)=1.64E6, E12(3)=.90E6, ANU1(3)=.30,
RHO(3)=1.477E-4, ALFA1(3)=0., ALFA2(3)=0.,
ALLOW(1,3)=2.,011,-0.011,0.01,-0.013,0.0155,
&END
-- End of file 'pasco.in' --
```

File 'nlpan.in1' for the UNITA example.

```

UNITA - TEST PANEL A - UNIT-CELL REPRESENTATION
0 0 0 0      !ICOORP,ILNPRT,IEFPRT,IQUPRT
0 0 0 0      !INGPRT,ICOPRT,IPRINT,IPBUG
'STOLL' 0 0  !USER, IHALT, MSRCH
'Y' 2 5      !SYMSTR, NODSYM(1), NODSYM(2)
4 'Y'        !NMUSE, FORCE
2 2 2 2      !NSOL(I), I=1,NMUSE
1 3 5 7      !MHIN(I), I=1,NMUSE
1 3          !ISOL(1,J), J=1,NSOL(I), I=1
2 3          !                      I=2
2 3          !                      I=3
2 4          !                      I=4
7 6          !NPLATE NNODE
2            !NPOFFS
5 0 -11 0 -11 !IP,IECVY(IP,1),IECVZ(IP,1),IECVY(IP,2),IECVZ(IP,2) IPOFFS=1
6 0 -11 0 -11 !                      IPOFFS=2
0. 1 1 0.     !MU(IP), SKVEC(IP), PRVEC(IP) TUA(IP), IP=1
0. 1 1 0.     !                      IP=2
0. 1 1 0.     !                      IP=3
0. 1 1 0.     !                      IP=4
0. 0 0 0.     !                      IP=5
0. 0 0 0.     !                      IP=6
90. 0 0 0.    !                      IP=7
1 2          !NOD(IP,IE), IP=1
2 4          !                      IP=2
4 5          !                      IP=3
5 6          !                      IP=4
2 4          !                      IP=5
4 5          !                      IP=6
3 4          !                      IP=7
1 6          !BNODE(IB), IB=1,2
2 3 2 1      !BCVEC(IC,IB), IC=1 to 4, IB=1
2 3 2 1      !                      IB=2
2 0          !NCU, NCW
3 0.         !PCU(ICU), YCU(ICU), ICU=1
7 0.         !                      ICU=2
0 0          !NSPU, NSPW
**** DESCRETIZATION AND REFERENCE VALUES ****
12          !NINTN
1 0 2 1      !PHREF, IPWDET, IPDFL, IYDFL
**** LOADING AND MODELLING OPTIONS ****
'D' 'N'      !CONTRL, COMPAT
1 500. 0. 0. 0. !ILSET,NXGL,NYGL,EPXL,EPYLG
0.0          !PRUNIT
'Y'          !LOGLO
2            !INDPLT
**** LOAD, WIDTH, WALL INDEXING ****
1 2 2 1 3 3 4 !LBWAL(IP),IP=1,NPLATE
3            !NKWALL
-- End of file 'nlpan.in1' --

```

File 'nlpan.in2' for the UNITA example.

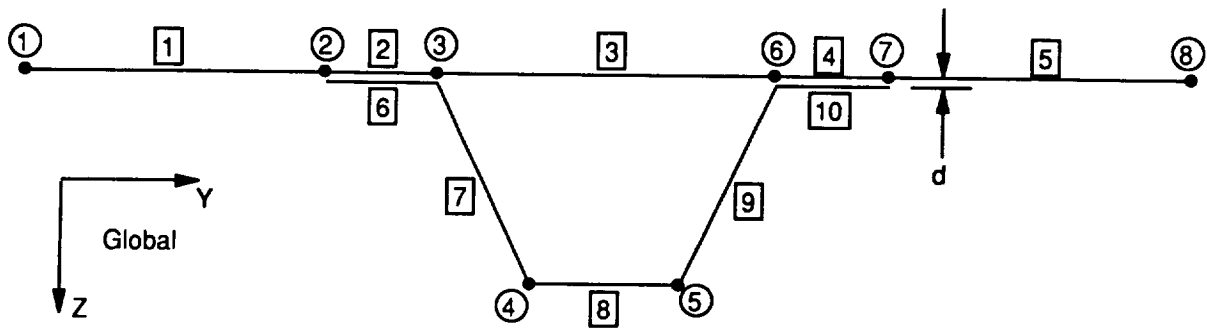
```

1 0 .FALSE.          !NIMP, IZCIP, SWITCH
0. 0 0 0 0.02 0. 0. 0. !QONST(IE,IIMP),IE=1,NEIG)
1.79 0. 0. 0. 0. 0. 0. !QF(IE),IE=1,NEIG
1          !NRANGE
20. 0. 0.          !LAMDAA(1), BETAA(1), HEATA(1)
0. 0 0 0.          !TOL ITMAX UU VV
30 0.00001 6       !ILSTM, CCRIT, MAXIT
.25 .6 .001 .005 .05 0. !DSNOM,DSFACT,DSMIN,DELQ,EVCUT,DSQUIT
0          !IFREQ
0 1 0 0 0 0       !IPDISP, IPSTRN, IPSS, IPSRES, IPQY, IPPROF
0 3          !NINTX,NXLOC
0.094        !XLOCN(IX), IX=1
0.406        !      IX=2
0.5          !      IX=3
2          !NYLOC
1 1          !IP(IY), ID(IY), IY=1
7 3          !      IY=12
-- End of file 'nlpan.in2' --

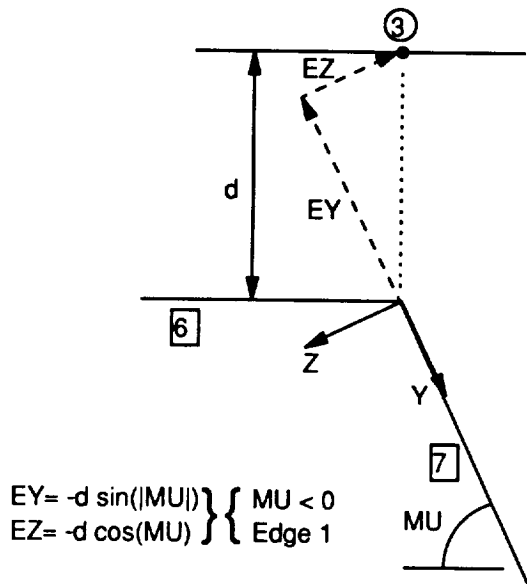
```

Unit cell representation of a hat-stiffened panel. Input files 'pasco.in' and 'nlpan.in1' are listed below for a unit-cell representation of a hat-stiffened laminated composite panel. The hat stiffener includes mounting flanges. The cross-sectional representation is shown in Figure E3. The slope of the webs of the hat stiffener (plate strip numbers 7 and 9) relative to the skin is 65 degrees for the configuration described in the input files. The mid-surfaces of the stiffener flanges are offset from the mid-surface of the skin by a distance d . Formulas for computing the offset measures EY and EZ between the edges of plate strips 7 and 9 and the mid-surface of the skin are included in Figure E3, along with sketches which show the geometric details. The cross-sectional proportions and laminate configurations used in the input files were chosen arbitrarily.

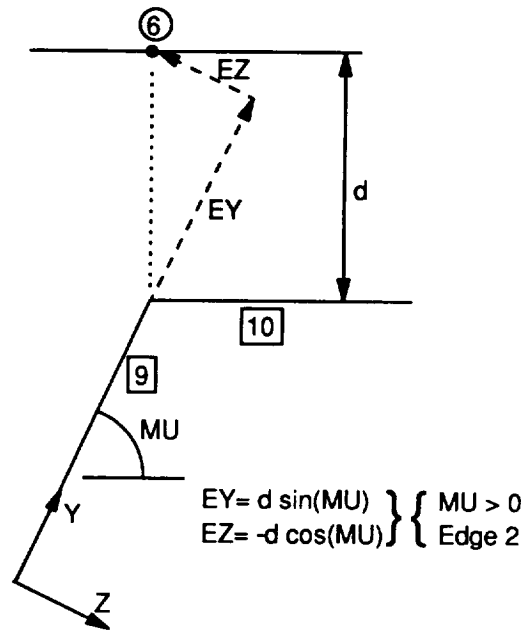
There are six thickness values $T(I)$ included in input file 'pasco.in'. The first three values are lamina thicknesses. $T(4)$ is the offset between the reference surfaces of the skin and the stiffener flanges. $T(5)$ and $T(6)$ are the amplitudes of the eccentricity measures EY and EZ , respectively, for plate strip numbers 7 and 9, which are defined as illustrated in Figure E3.



Cross Sectional Representation



**Node-Line Offset for
Plate Strip No. 7**



**Node-Line Offset for
Plate Strip No. 9**

Figure E3. Unit-cell cross-sectional representation of a hat-stiffened panel, including the geometric details of the node-line offsets.

File 'pasco.in' for a hat-stiffened panel.

```
HAT - UNIT-CELL REPRESENTATION OF A HAT-STIFFENED PANEL
&CONDAT
&END
&PANEL
B=2.,.75,2.267855,.75,2.,.75,1.5,1.,1.5,.75,
EL=15.,
CONV1=50000.,
FREQ=0.,
IP=0,
MAXJJJ=0,
MAT(1,1)=1,1,1,
T(1)=.005,.005,.005,.07,.0634,.0296,
THET(1)=0,45,90,
KWALL(1,1)=2,-2,2,-2,1,3,
KWALL(1,2)=2,-2,1,3,2,-2,1,3,
KWALL(1,3)=2,-2,1,3,2,-2,1,3,
KWALL(1,4)=2,-2,1,3,1,1,2,-2,1,3,
IWALL(1)=1,1,1,1,1,2,3,4,3,2,
FSTIFF=10.,
HCARD=6,-11,-6,0,-4,0,-4,
        6,-12,-7,-5,-6,0,0,
        6,-13,-9,0,0,5,-6,
        6,-14,-10,0,-4,0,-4,
        4,-15,12,-65,0,
        4,-16,13,65,0,
        4,17,15,8,16,
        14,18,1,-990,9000,2,-11,3,-17,4,-14,5,0,-990,9000,
ICARD=5,1,2,1,-990,9000,
        5,2,3,2,3,11,
        3,3,6,3,
        3,3,4,15,
        3,4,5,8,
        3,5,6,16,
        5,6,7,4,7,14,
        3,7,8,5,
        3,8,-990,9000,
ICREP=1,
NOBAY=1,
NX(1)=1.,
NY(1)=0.,
&END
&MATER
E1(1)=18.5E6, E2(1)=1.64E6, E12(1)=.87E6, ANU1(1)=.30,
RHO(1)=1.477E-4, ALFA1(1)=0.25E-6, ALFA2(1)=16.2E-6,
ALLOW(1,1)=2.,.011,-0.011,0.01,-0.013,0.0155,
&END
-- End of file 'pasco.in' --
```

File 'nlpan.in1' for a hat-stiffened panel.

```

HAT - UNIT-CELL REPRESENTATION OF A HAT-STIFFENED PANEL
0 0 0 0      !ICORP,ILNPRT,IEFPRT,IQUPRT
0 0 0 0      !INGPRT,ICOPRT,IPRINT,IPBUG
'STOLL' 1 0  !USER, IHALT, MSRCH
'Y' 1 8      !SYMSTR, NODSYM(1), NODSYM(2)
2 'Y'        !NMUSE, FORCE
1 2          !NSOL(I), I=1,NMUSE
1 5          !MHIN(I), I=1,NMUSE
1            !ISOL(1,J), J=1,NSOL(I), I=1
1 3          !      I=2
10 8         !NPLATE NNODE
4            !NPOFFS
6 0 -4 0 -4  !IP,IECVY(IP,1),IECVZ(IP,1),IECVY(IP,2),IECVZ(IP,2) IPOFFS=1
7 -5 -6 0 0  !      IPOFFS=2
9 0 0 5 -6   !      IPOFFS=3
10 0 -4 0 -4  !      IPOFFS=4
0. 1 1 0.    !MU(IP), SKVEC(IP), PRVEC(IP) TUA(IP), IP=1
0. 1 1 0.    !      IP=2
0. 1 1 0.    !      IP=3
0. 1 1 0.    !      IP=4
0. 1 1 0.    !      IP=5
0. 0 0 0.    !      IP=6
-65. 0 0 0.  !      IP=7
0. 0 0 0.    !      IP=8
65. 0 0 0.   !      IP=9
0. 0 0 0.    !      IP=10
1 2          !NOD(IP,IE), IP=1
2 3          !      IP=2
3 6          !      IP=3
6 7          !      IP=4
7 8          !      IP=5
3 4          !      IP=6
4 5          !      IP=7
5 6          !      IP=8
6 7          !      IP=9
1 8          !BNODE(IB), IB=1,2
2 3 2 1      !BCVEC(IC,IB), IC=1 to 4, IB=1
2 3 2 1      !      IB=2
0 0          !NCU, NCW
0 0          !NSPU, NSPW
**** DESCRETIZATION AND REFERENCE VALUES ****
12          !NINTN
1 0 3 0      !IPHREF, IPWDET, IPDFL, IYDFL
**** LOADING AND MODELLING OPTIONS ****
'D' 'N'      !CONTRL, COMPAT
1 1. 0. 0. 0. !ILSET,NXGL,NYGL,EPXL,EPYLG
0.0          !PRUNIT
'Y'          !LOGLO
2            !INDPLT
**** LOAD, WIDTH, WALL INDEXING ****
1 2 3 2 1 4 5 6 5 4 !ILBWAL(IP),IP=1,NPLATE
4              !INKWALL
-- End of file 'nlpan.in1' --

```

Appendix E References

- E1. Anderson, M.S., Stroud, W.J., Durling, B.J., and Hennessy, K.W., "PASCO: Structural Panel Analysis and Sizing Code, User's Manual," NASA TM-80182, Nov., 1981.
- E2. Stoll, F., "Geometrically Nonlinear Analysis of Stiffened Composite Panels with Various End-Support Conditions," paper no. AIAA-93-1615, presented at the 34'th AIAA/ASME/ASCE/AHS/ASC Structures, Structural Dynamics, and Materials Conference, La Jolla, CA, April 19-21, 1993.

REFERENCES

1. Dickson, J.N., and Biggers, S.B., "POSTOP: Postbuckled Open-Stiffener Optimum Panels - Theory and Capability," NASA-CR-172259, January 1984.
2. Bushnell, D., "PANDA2 - Program for Minimum Weight Design of Stiffened, Composite, Locally Buckled Panels," *Computers & Structures*, Vol 25, No. 4, 1987, pp. 469-605.
3. Ali, M.A., and Sridharan, S., "A Versatile Model for Interactive Buckling of Columns and Beam-Columns," *Int. J. Solids and Structures*, Vol. 24, No. 5, 1988, pp. 481-496.
4. Sridharan, S., and Peng, M.-H., "Performance of Axially Compressed Stiffened Panels," *Int. J. Solids and Structures*, Vol. 25, No. 8, 1989, pp. 879-899.
5. Hancock, G.J., Davids, A.J., Key, P.W., Lau, S.C.W., and Rasmussen, K.J.R., "Recent Developments in the Buckling and Nonlinear Analysis of Thin-Walled Structural Members," *Thin-Walled Structures*, Vol. 9, 1990, pp. 309-338.
6. Kakol, W., "Stability Analysis of Stiffened Plates by Finite Strips," *Thin-Walled Structures*, Vol. 10, 1990, pp. 277-297.
7. Stoll, F., Gurdal, Z., and Starnes, J.H. Jr., "A Method for the Geometrically Nonlinear Analysis of Compressively Loaded Prismatic Composite Structures," Rept. No. CCMS-91-03, Center for Composite Materials and Structures, Virginia Polytechnic Institute and State University, Blacksburg, VA, 1991.
8. Kwon, Y.B., and Hancock, G.J., "A Nonlinear Elastic Spline Finite Strip Analysis for Thin-Walled Sections," *Thin-Walled Structures*, Vol. 12, 1991, pp. 295-319.
9. Sheinman, I., Frostig, Y., and Segal, A., "PBCOMP Program for Buckling and Postbuckling of Stiffened Laminated Curved Panels," *Computers and Structures*, Vol. 42, 1992, pp. 87-95.
10. Sridharan, S., Zeggane, M., and Starnes, J.H. Jr., "Postbuckling Response of Stiffened Composite Cylindrical Shells," *AIAA Journal*, Vol. 30, No. 12, 1992, pp. 2890-2905.
11. Yoda, T., and Atluri, S.N., "Postbuckling Analysis of Stiffened Composite Panels, Using a Higher-Order Shear Deformation Theory," *Computational Mechanics*, Vol. 9, 1992, pp. 390-404.
12. Wittrick, W.H., and Williams, F.W., "Buckling and Vibration of Anisotropic or Isotropic Plate Assemblies under Combined Loadings," *Int. J. Mechanical Science*, Vol. 16, 1973, pp. 209-239.
13. Stroud, W.J., and Anderson, M.S., "PASCO: Structural Panel Analysis and Sizing Code, Capability and Analytical Foundations," NASA-TM-80181, November, 1981.
14. Anderson, M.S., Stroud, W.J., Durling, B.J., and Hennessey, K.W., "PASCO: Structural Panel Analysis and Sizing Code, User's Manual," NASA TM-80182, 1981.
15. Sridharan, S., "Doubly Symmetric Interactive Buckling of Plate Structures," *Int. J. of Solids and Structures*, Vol. 19, No. 7, 1983, pp. 625-641.
16. Stoll, F., "Analysis of the Snap Phenomenon in Buckled Plates," accepted for publication in *Int. J. Non-Linear Mechanics*.
17. Riks, E., "An Incremental Approach to the Solution of Snapping and Buckling Problems," *Int. J. Solids and Structures*, Vol. 15, 1979, pp. 529-551.
18. Thurston, G.A., "Continuation of Newton's Method Through Bifurcation Points," *Journal of Applied Mechanics*, Vol. 36, 1969, pp. 425-430.

19. Nakamura, T., and Uetani, K., "The Secondary Buckling and Post-Secondary-Buckling Behaviors of Rectangular Plates," *Int. J. Mech. Sci.*, Vol 21, 1979, pp. 265-286.
20. Meirovitch, L., *Computational Methods in Structural Dynamics*, Sijthoff & Noordhoff, Rockville, Maryland, 1980, Section 7.2.
21. Reddy, J.N., *An Introduction to the Finite Element Method*, McGraw-Hill Book Company, New York, 1984, pp. 54-56.
22. Budiansky, B., "Dynamic Buckling of Elastic Structures: Criteria and Estimates," in *Dynamic Stability of Structures, Proceedings of an International Conference at Northwestern University, Oct. 18-20, 1965*, Pergamon Press, New York, 1966, pp. 83-106.
23. Stoll, F., "Geometrically Nonlinear Analysis of Stiffened Composite Panels with Various End-Support Conditions," paper no. AIAA-93-1615, in *Proceedings of the 34th AIAA/ASME/ASCE/AHS/ASC Structures, Structural Dynamics and Materials Conference*, 1993.
24. Stoll, F., "An Implementation of Solution Strategies for the Analysis of Complex Equilibrium Behavior," accepted for publication in *Int. J. Non-Linear Mechanics*.
25. Starnes, J.H. Jr., Knight, N.F. Jr., and Rouse, M., "Postbuckling Behavior of Selected Flat Stiffened Graphite-Epoxy Panels Loaded in Compression," *AIAA Journal*, Vol. 23, No. 8, August, 1985, pp.1236-1246.
26. Thompson, J.M.T., Tulk, J.D., and Walker, A.C., "An Experimental Study of Imperfection-Sensitivity in the Interactive Buckling of Stiffened Plates," in *Buckling of Structures*, ed., B. Budiansky, Springer-Verlag, Berlin, 1976, pp. 149-159.
27. Hyer, M.W., Loup, D.C., and Starnes, J.H. Jr., "Stiffener/Skin Interactions in Pressure-Loaded Composite Panels," *AIAA Journal*, Vol. 28, No. 3, 1990, pp. 532-537.
28. Meyers, C.A., and Hyer, M.W., "Thermally-Induced, Geometrically Nonlinear Response of Symmetrically Laminated Composite Plates," paper no. AIAA-92-2539-CP, in *Proceedings of the 34th AIAA/ASME/ASCE/AHS/ASC Structures, Structural Dynamics and Materials Conference*, 1993, pp. 1027-1037.

Type of Load Control	Load Axis 1	Load Axis 2	
		Option 1 (BCVEC(2,IB)=1, IB=1,2)	Option 2 (BCVEC(2,IB)=2 or 3, IB=1 or IB=2)
Displacement Control (CONTRL='D')	$\Delta u = \lambda \Delta u_L$	$\overline{\Delta v} = \lambda \Delta v_L$	$N_{yG} = 0$
Load Control (CONTRL='L')	$N_{xG} = \lambda N_{xGL}$	$\overline{\Delta v} = 0$	$N_{yG} = \lambda N_{yGL}$

Table 1. Options for Control of the In-Plane Loading. IB = boundary index number (1 or 2).

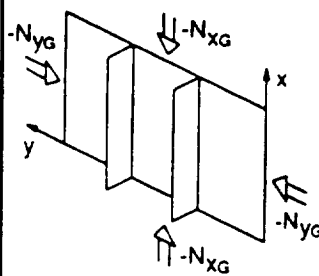
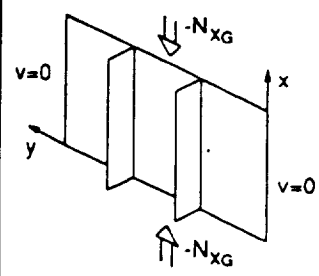
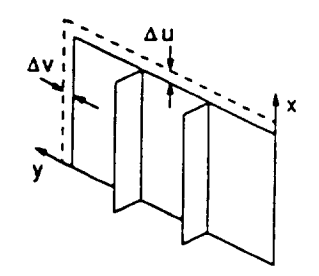
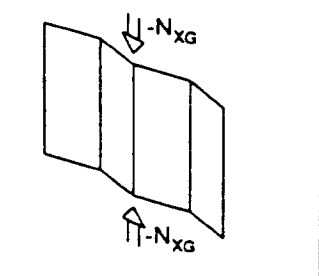
Load Case	Flat Skin?	In-Plane Loading Characteristics		Control Param. (CTRL in Table 1)	Option for Load Axis 2 in Table 1
A	Yes	Constant ratio: $N_{yG} : N_{xG}$		'D' / 'L' if $N_{yG} = 0$ 'L' if $N_{yG} \neq 0$	2
B	Yes	$\Delta v = 0$		'D' / 'L'	1
C	Yes	Constant ratio: $\Delta v : \Delta u$		'D'	1
D	No	Nominal uniaxial loading		'D' / 'L'	1* / 2
* $N_{yG} = 0$ in prebuckling; nonlinear contributions to Δv are zero.					

Table 2. Input Parameters Corresponding to Several Different Cases for In-Plane Loading.

Component (IC)	Option 1 (BCVEC(IC,IB)=1)	Option 2 (BCVEC(IC,IB)=2)	Option 3 (BCVEC(IC,IB)=3)
1: U^n, F_z^n	$U^n_{,xx} = 0$	$F_x^n = 0$	-
2: V^n, F_y^n	$V^n = \lambda V_L^n$	$F_y^n = n_y N_{yG}$	$V_{,x}^n = 0$ $\bar{F}_y^n = n_y N_{yG}$
3: W^n, F_z^n	$W^n = 0$	$F_z^n = 0$	-
4: Ψ^n, M^n	$\Psi^n = 0$	$M^n = 0$	-

Table 3. Options Available for Specifying Conditions Along the Boundary Node-Lines. IB = boundary index number (1 or 2).

Case	Simplification
CTRL = 'D'	$A_{ij} \equiv 0 \quad (i, j = 1, 2, \dots)$ $\{u_A\} \equiv 0$
$N_{yG} = 0$ -or- BCVEC(2,IB)=1, (IB=1,2)	$\{u_A\} \equiv 0$
BCVEC(2,IB) \neq 3 (IB=1 or 2)	$B_i \equiv 0 \quad (i = 1, 2, \dots)$ $\{u_B\} \equiv 0$

Table 4. Simplifications to the General Displacement Form for Special Cases.

	Symmetrical Structure	Unsymmetrical Structure
Local Postbuckling ^a	1. $(m_i, 1)$ 2. (m_i, i_2) $(3m_i, i_1) (3m_i, i_2)$ 3. (m_i, i_3) $(5m_i, i_1)$	1. $(m_i, 1) (m_i, 2)^b \dots$ 2. $(3m_i, 1) (3m_i, 2) \dots$ 3. $(5m_i, 1) (5m_i, 2) \dots$
Global Postbuckling, s.s. ends	1. $(1, 1)$ 2. $(3, s_1) (3, s_2)$	1. $(1, 1) (1, 2)^b$ 2. $(3, 1) (3, 2) \dots$
Global Postbuckling, clamped ends	1. $(1, 1)$ $(3, s_1) (3, s_2)$ 2. $(5, s_1) (5, s_2)$	1. $(1, 1) (1, 2)^b$ $(3, 1) (3, 2) \dots$ 2. $(5, 1) (5, 2) \dots$
Local/Global Mode Interaction, s.s. ends	A1. $(1, 1)$ $(m_i, u_1) (m_i, u_2)$ 2. $(m_i+2, u_1) (m_i+2, u_2)$ $(m_i-2, u_1) (m_i-2, u_2)$ B1. $(1, 1)$ $(m_i, s_1) (m_i, s_2)$ 2. $(m_i+2, s_1) (m_i+2, s_2)$ $(m_i-2, s_1) (m_i-2, s_2)$	1. $(1, 1) (1, 2)^b$ $(m_i, 1) (m_i, 2) \dots$ 2. $(m_i+2, 1) (m_i+2, 2) \dots$ $(m_i-2, 1) (m_i-2, 2) \dots$
Local/Global Mode Interaction, clamped ends	A1. $(1, 1)$ $(3, s_1) (3, s_2)$ $(m_i, u_1) (m_i, u_2)$ $(m_i+2, u_1) (m_i+2, u_2)$ $(m_i-2, u_1) (m_i-2, u_2)$ B1. $(1, 1)$ $(3, s_1) (3, s_2)$ $(m_i, s_1) (m_i, s_2)$ $(m_i+2, s_1) (m_i+2, s_2)$ $(m_i-2, s_1) (m_i-2, s_2)$	1. $(1, 1) (1, 2)^b$ $(3, 1) (3, 2) \dots$ $(m_i, 1) (m_i, 2) \dots$ $(m_i+2, 1) (m_i+2, 2) \dots$ $(m_i-2, 1) (m_i-2, 2) \dots$
m_i - Critical halfwave number for local buckling. (m, u) - Unsymmetric mode. (m, s) - Symmetric mode. 1. - Essential modes. 2., 3. - Supplemental modes for improved accuracy. A, B - Dual mode sets which should each be used independently in separate analyses. ^a Modes $(m, i_1), (m, i_2), \dots$ match mode $(m_i, 1)$ w.r.t. transverse symmetry or lack thereof. ^b Include mode $(m, 2)$ if its eigenvalue is close to that for $(m, 1)$.		

Table 5. Suggested Mode Sets for Analyzing Various Types of Postbuckling Response.

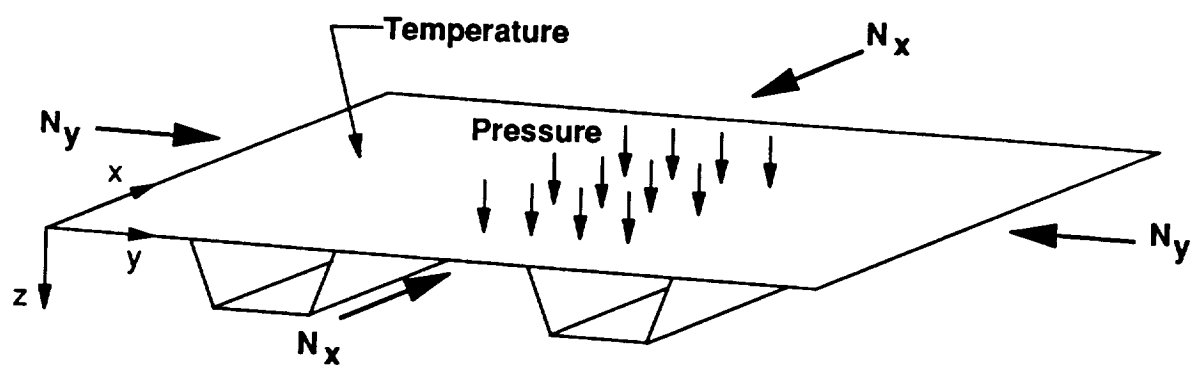


Figure 1. Generalized load types modelled by NLPAN.

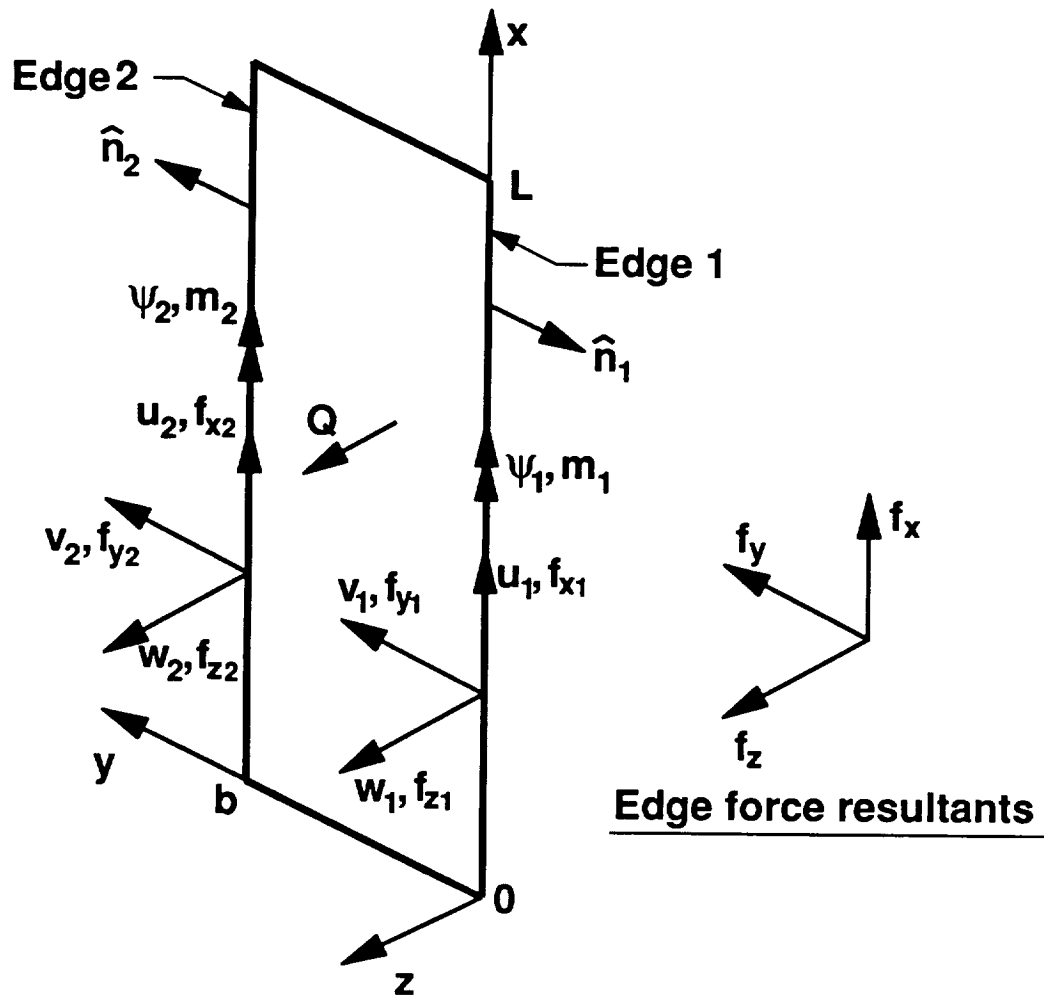


Figure 2. Labeling conventions for a representative plate strip.

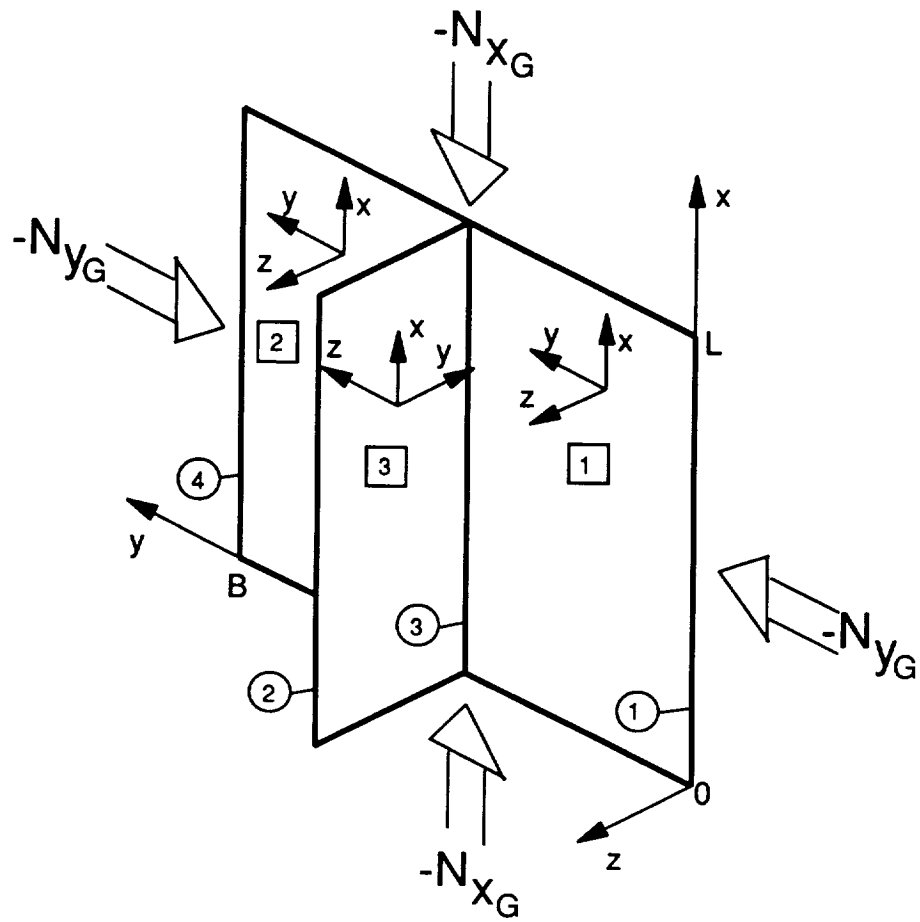
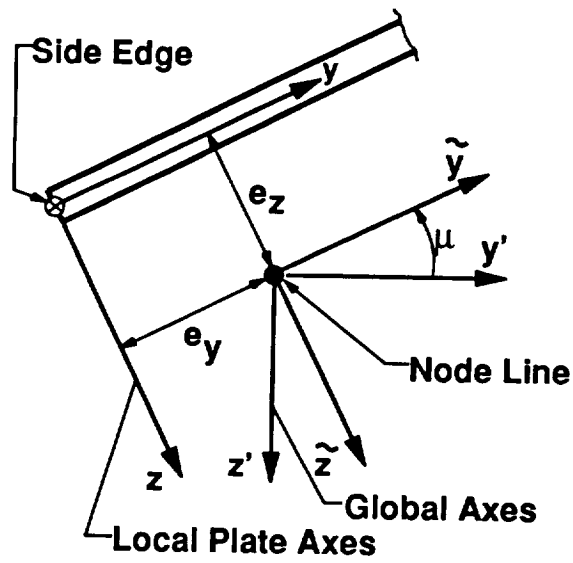
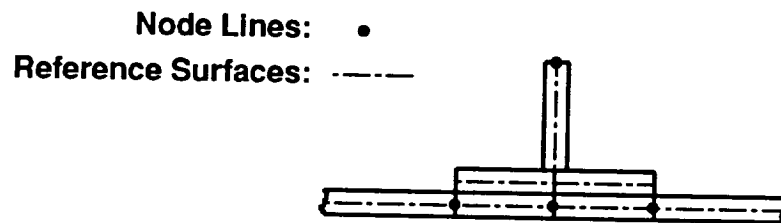


Figure 3. Labling conventions for a linked-plate analysis model.

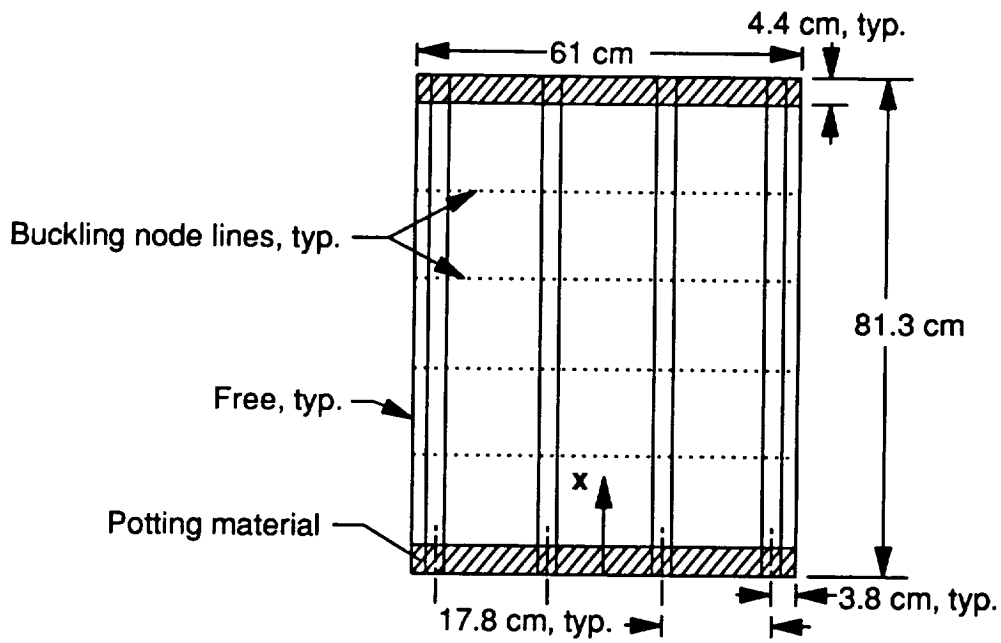


a) Symbol definitions.

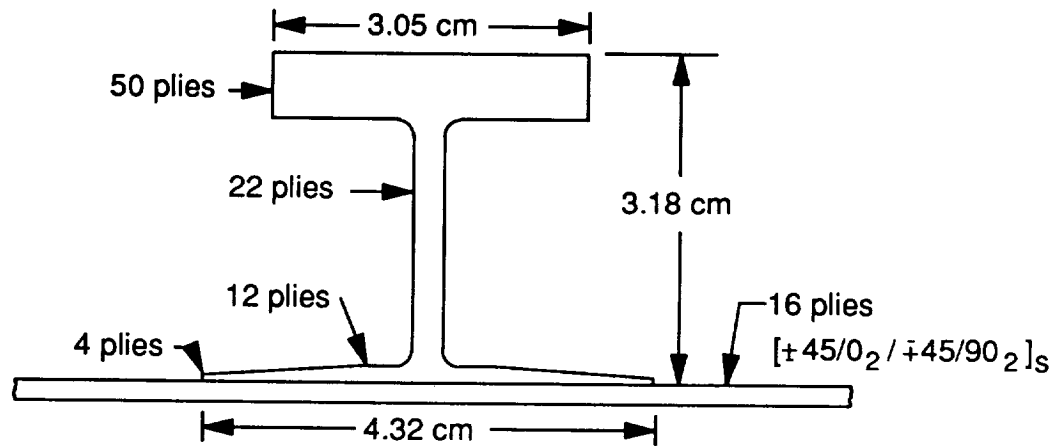


b) Example of a configuration featuring non-zero offsets.

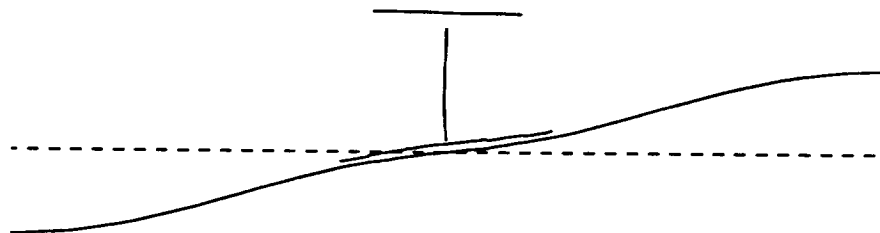
Figure 4. Relative orientation of the side-edge of a plate strip and its associated node line.



a) Test configuration.

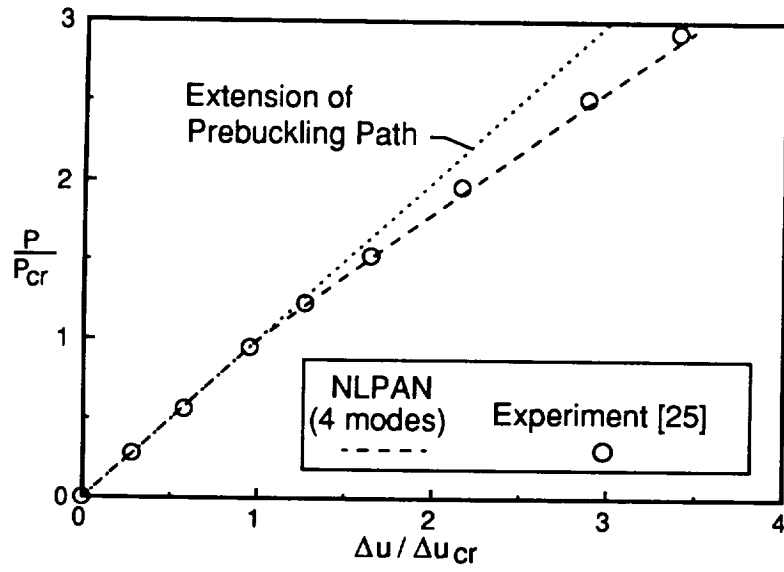


b) Stiffener details.

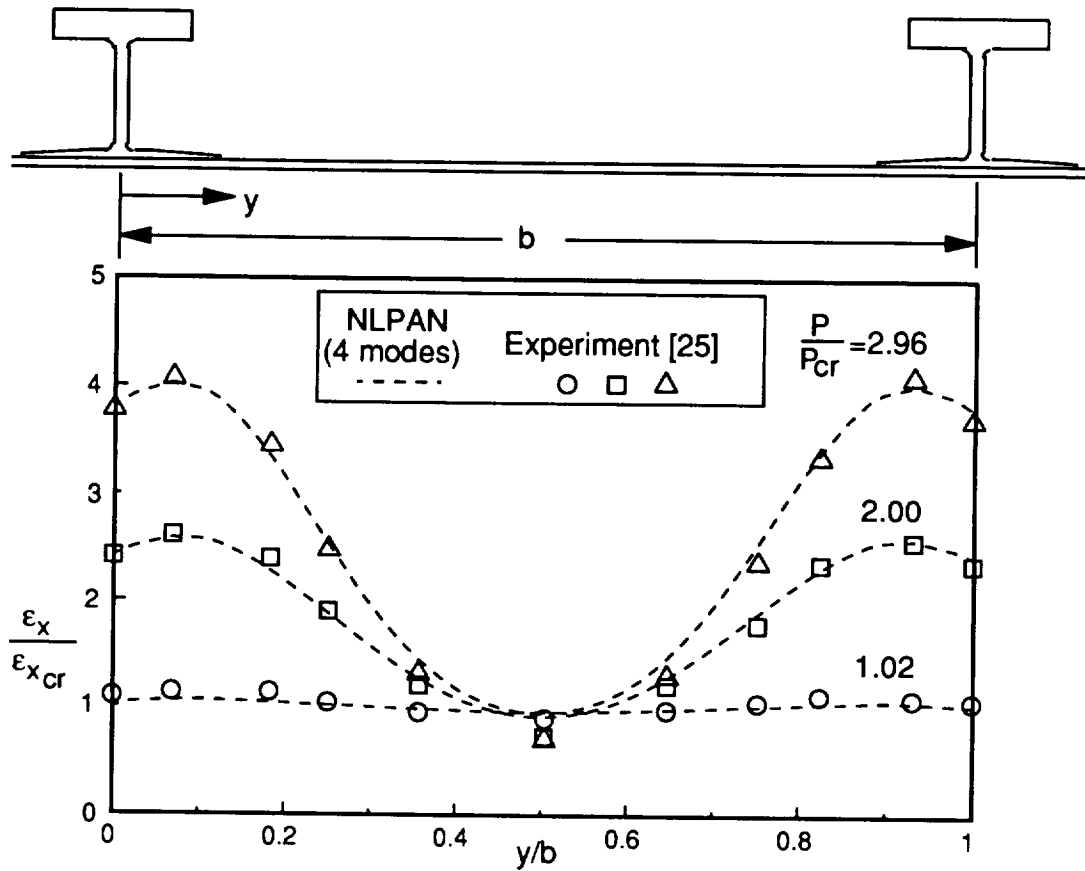


c) Profile of the theoretical buckling mode for a unit cell representation with 17 plate strips and 12 node lines (buckling mode has 5 longitudinal halfwaves).

Figure 5. I-stiffened graphite/epoxy panel configuration.

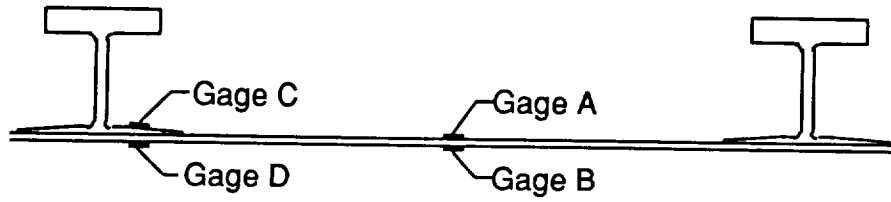


a) Normalized end load versus normalized end shortening.

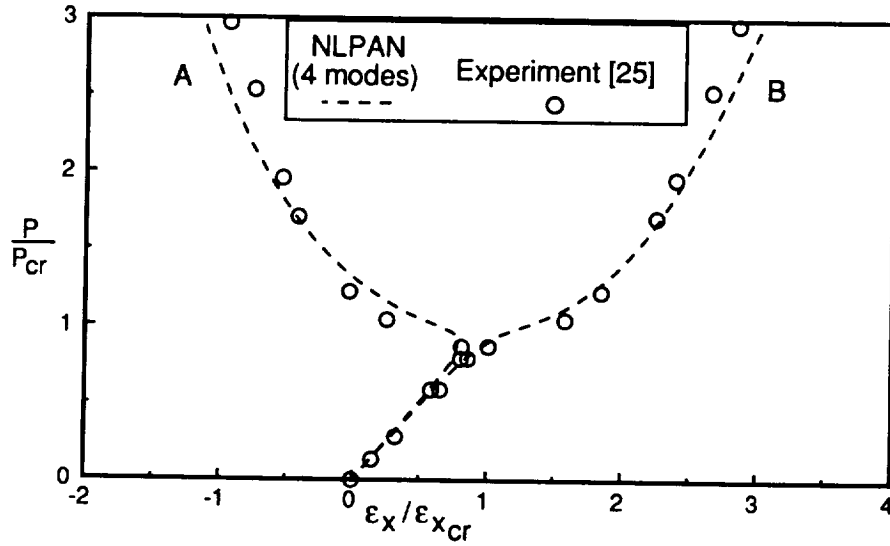


b) Normalized membrane strains in the skin, mid-length, center bay.

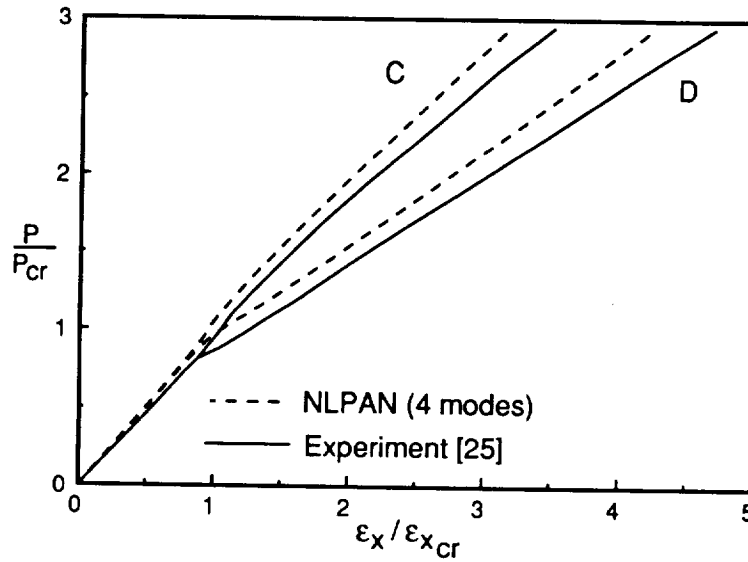
Figure 6. Analytical and experimental results for an I-stiffened panel.



a) Strain gage placement, mid-length, center bay.

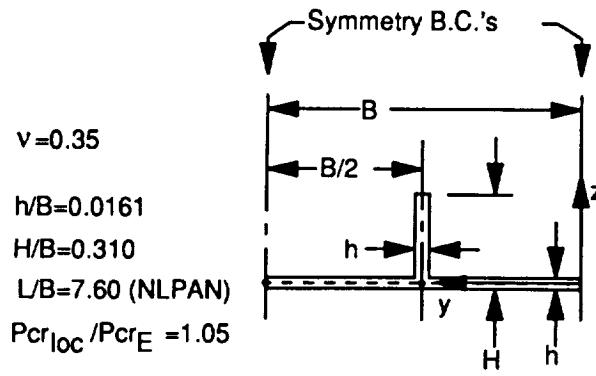


b) Skin strains, mid-bay.

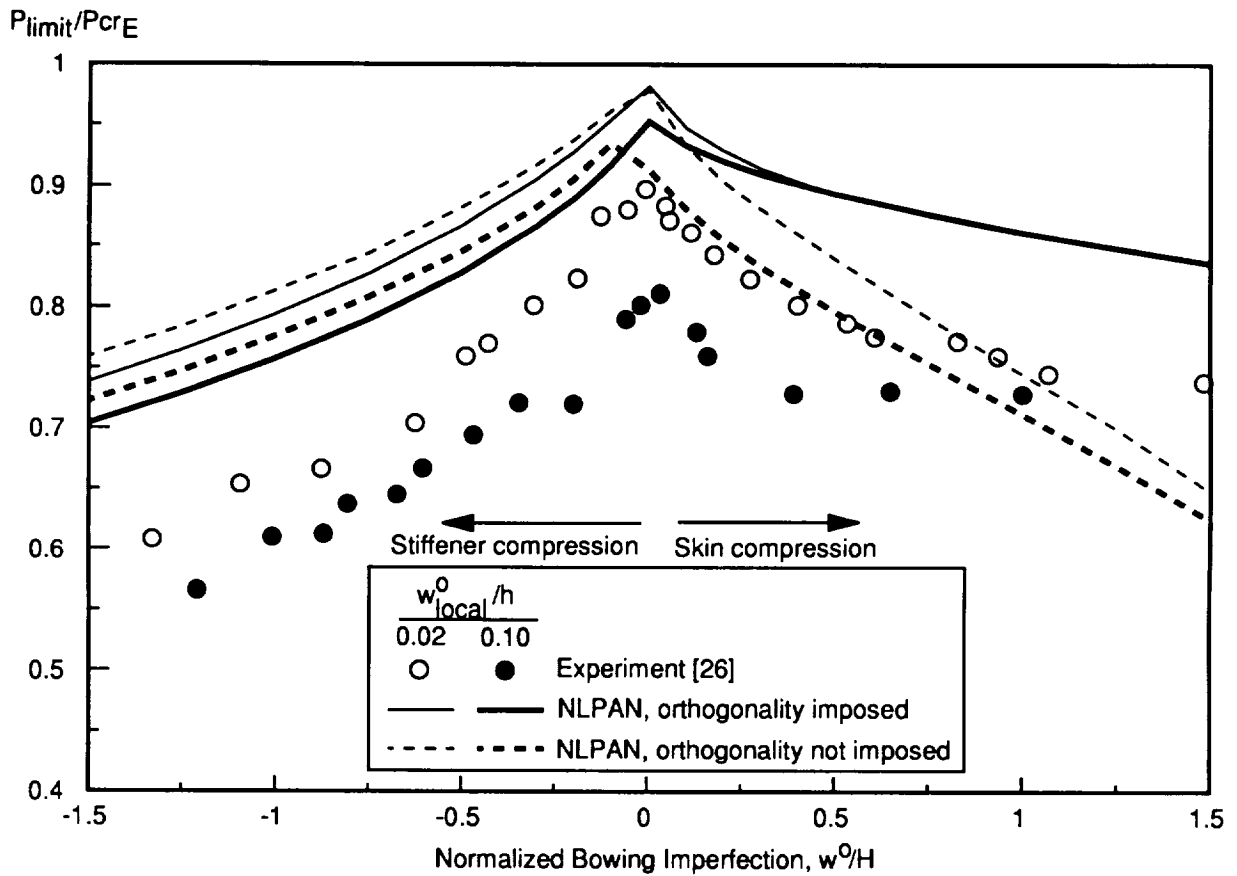


c) Strains at a stiffener flange.

Figure 7. Longitudinal surface strains on an I-stiffened panel.



a) Unit-stiffener-cell analysis model.



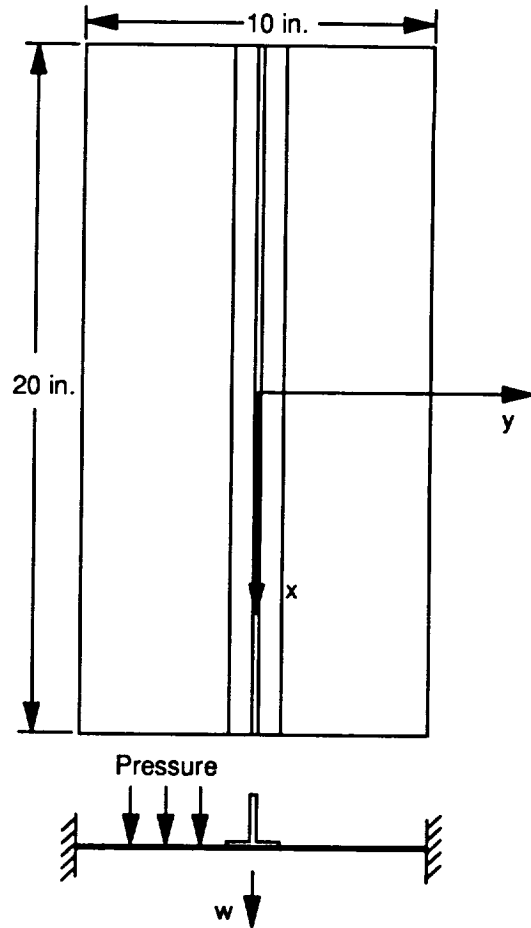
b) Limit loads from experiments, and from analysis with and without orthogonality imposed between $\{u_{ij}\}$ and $\{u_i\}$.

Figure 8. Results for an imperfection-sensitive thin-blade-stiffened isotropic panel loaded in uniaxial compression.

Boundary conditions common to all analyses:

$x=-10, 10: u=0, N_{xy}=0, w=0$

$y=-5, 5: u=0, v=0, w=0, w,y=0$



a) Test section and boundary conditions

Lamina properties used in analysis:

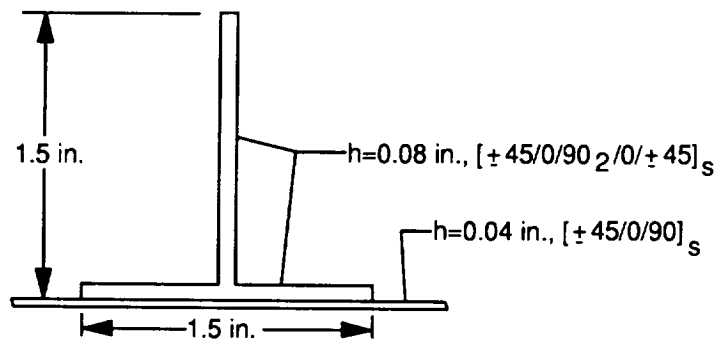
$E1 = 18.5 \text{ Msi}$

$E2 = 1.64 \text{ Msi}$

$G12 = 0.87 \text{ Msi}$

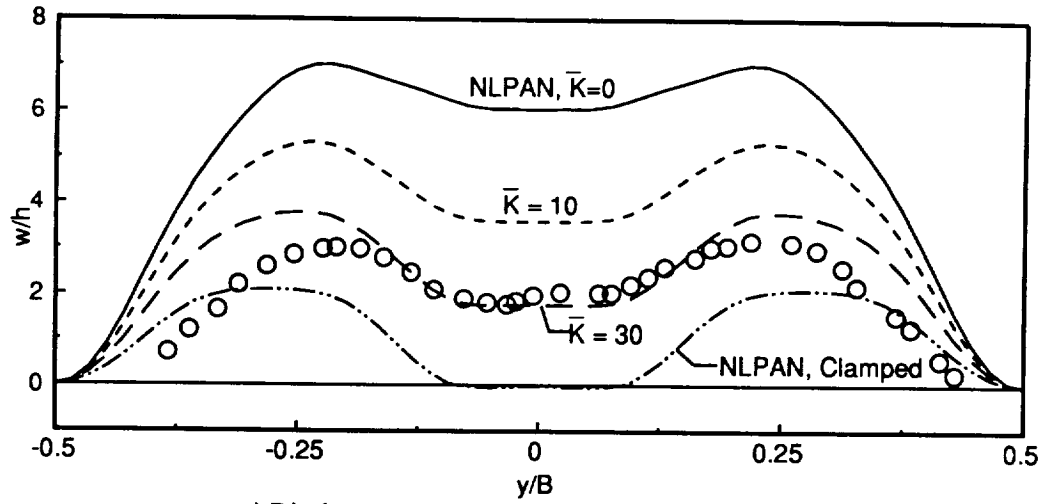
$\nu_{12} = 0.3$

$h_{\text{ply}} = 0.005 \text{ in.}$

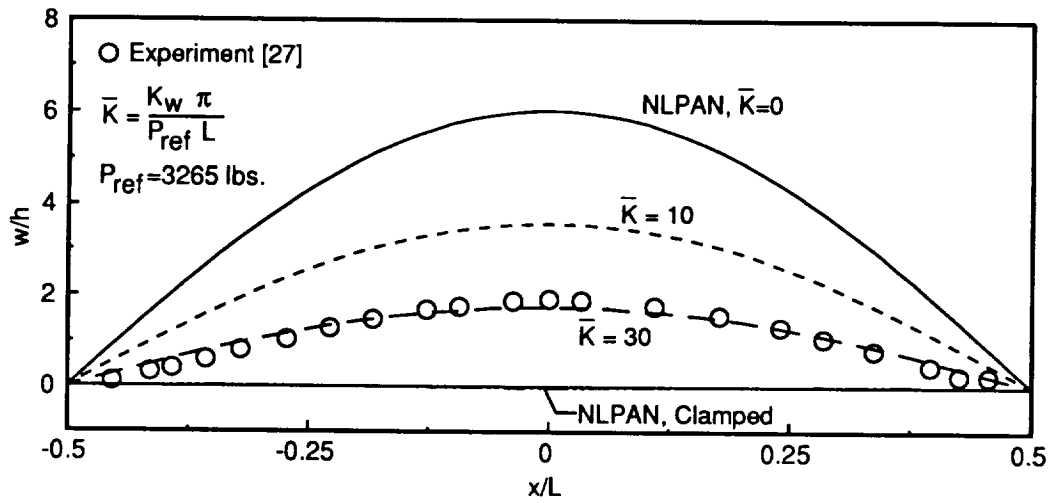


b) Stiffener and laminate details.

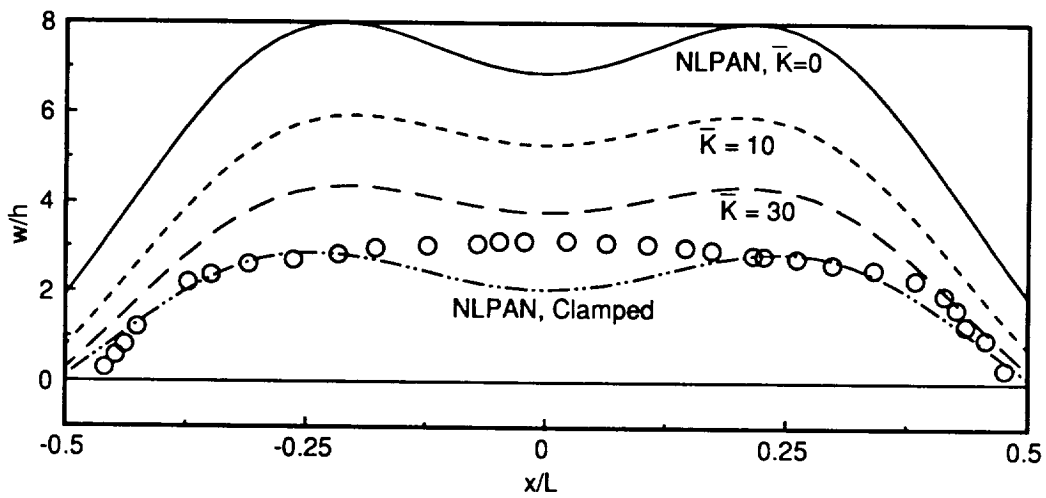
Figure 9. Pressure-loaded panel configuration.



a) Displacements across the width at the mid-length.



b) Displacements along the length under the stiffener ($y=0$).



c) Displacements along the length on the skin ($y/B=0.25$)

Figure 10. Skin displacements with one atmosphere pressure (14.7 psi).

Lamina properties:

$$E1 = 22.5 \text{ Msi}$$

$$E2 = 1.17 \text{ Msi}$$

$$G12 = 0.66 \text{ Msi}$$

$$\nu_{12} = 0.22$$

$$\alpha_1 = -.04 \cdot 10^{-6} \text{ per degree F}$$

$$\alpha_2 = 16.7 \cdot 10^{-6} \text{ per degree F}$$

$$h_{\text{ply}} = 0.005 \text{ in.}$$

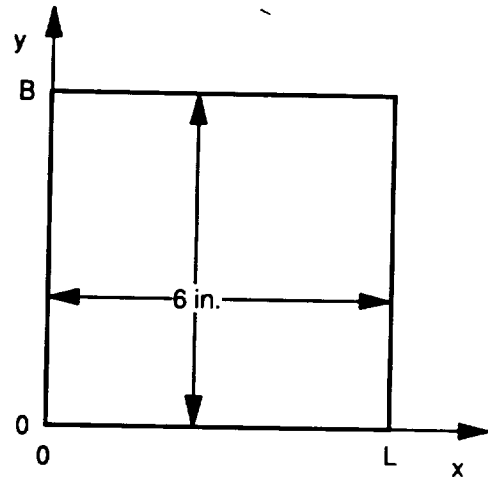
Laminate configuration: $[+45/-45/0/0]_s$

Boundary conditions: $x=0, L: u=0, w=0, M_x=0, N_{xy}=0$

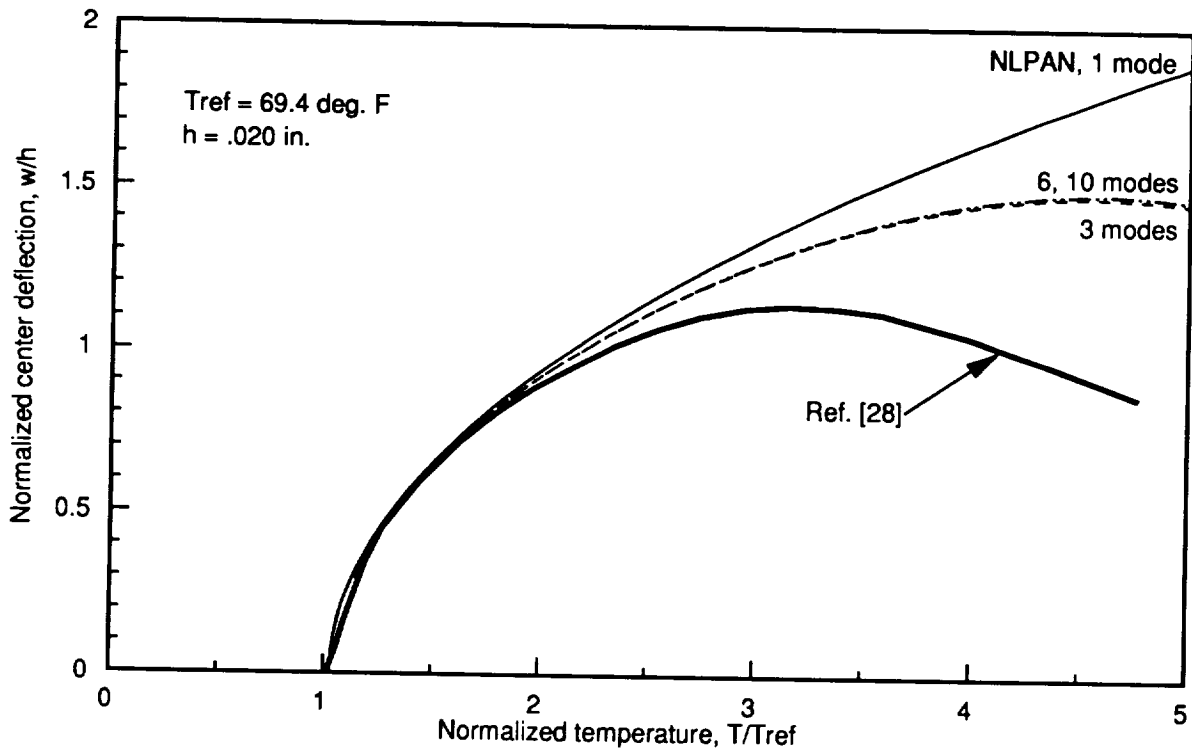
$y=0, B: v=0, w=0, M_y=0, N_{xy}=0$

Buckling temperature: $T_{\text{crit}} = 69.4 \text{ deg. F}$ (Ref. [28])

$T_{\text{crit}} = 71.4 \text{ deg. F}$ (NLPAN)



a) Plate configuration and properties.



b) Center deflection versus temperature.

Figure 11. Laminated composite plate subjected to thermal loading.